# Studies on Characterization of Discoidal Phospholipid Membrane and Its Application to Design of Membranous Functional Materials

**Shogo Taguchi**

**MARCH 2019**

# Studies on Characterization of Discoidal Phospholipid Membrane and Its Application to Design of Membranous Functional Materials

**A dissertation submitted to**

**THE GRADUATE SCHOOL OF ENGINEERING SCIENCE**

**OSAKA UNIVERSITY**

**in partial fulfillment of the requirements for the degree of**

**DOCTOR OF PHILOSOPHY IN ENGINEERING**

**BY**

**Shogo Taguchi**

**MARCH 2019**

# PREFACE

This dissertation work was conducted under the supervision of Professor Hiroshi Umakoshi at Division of Chemical Engineering, Graduate School of Engineering Science, Osaka University from 2014 to 2019.

The objective of this thesis is to establish the methodology to prepare the vesicles or planer membrane such as supported lipid bilayer (SLB) for application to membranous functional materials by using a discoidal phospholipid membrane as a resource material. The morphological change of the discoidal assembly upon its dilution step indicates that short-chained lipid (DHPC) concentration and the size of the assembly are important factors to prepare the membranous functional materials.

The author hopes that this research would contribute to the design and development of a variety of "*soft*" membranous materials. The methodology established in this study is expected to contribute to its application to the continuous preparation method of bicellar, vesicular or planar membranous materials that possess the heterogeneous texture at their surface.

Shogo Taguchi

Division of Chemical Engineering

Graduate School of Engineering Science

Osaka University

Toyonaka, Osaka, 560-8531, Japan

**Abstract**

Bicelles consisting of short-chain phospholipids and long-chain phospholipids are important materials for developing functional "*membranous*" materials. In this study, a strategy to design and to develop various membranous materials by utilizing bicelle as a key material was established. In chapter 1, there are the general features of the membranous materials, such as liposomes, planer membranes, and bicelles, from both viewpoints of fundamental and applied aspect. A possible advantage of a bicelle for its utilization as functional materials is discussed.

In chapter 2, the behaviors of self-assemblies of the DMPC/DHPC mixtures were evaluated based on the physicochemical properties of the membranes. The morphologies were systematically classified into the dominant states; large vesicle (> 30 nm, "*ordered*" bilayer), gel-bicelle (< 30 nm, "*ordered*"), and micelle (< 30 nm, "*disordered*"). Furthermore, the bicelle structure is transformed from bicelles to vesicles in dilution. The results are summarized in the "*bicelle*" diagram. Based on the "*bicelle*" diagram, a strategy to prepare various membranous materials was finally proposed.

In chapter 3, the functional "*discoidal*" bicelle shown highly-ordered orientation of the functional molecule. Photo-functional molecule chlorophyll *a* (Chl*a*) was mixed in the membranes. The aggregation of Chl*a* was achieved on a bicelle. The aggregate was maintained in dilution process with the morphological disruption from bicelles to vesicles. The condensed functional molecules on a bicelle membrane can be apply to functional membrane materials.

In chapter 4, the vesicle-like material was prepared by using the flow devices according to the "*bicelle*" diagram. The membrane properties of the vesicle-like assembly formed by dilution were compared with liposomes obtained by other conventional preparation methods. All of the assemblies had similar membrane properties. Manipulation of DHPC concentration is one of the important factors for controlling the shape of the bicelle for development of the membrane materials in dilution. Furthermore, vesicle was prepared continuously by dilution of bicelle suspension by flow path. The dilution ratio was found to be a key factor to control the assembled form.

In chapter 5, formation of supported lipid bilayer (SLB) was confirmed by adding and diluting of bicelles on the substrate. The formation of the SLB on the substrate by using small bicelles was promoted because of the instability of the edge of membrane disks. The heterogeneity of the SLBs were evaluated by observation with a fluorescence microscope and a spectrum observation using fluorescent probes. It was found that the addition of a DMPC/DHPC bicelle and a DPPC/DHPC bicelle together induce the formation of heterogeneous membrane of the SLB. Continuous preparation of SLB by using bicelles in flow dilution was able to create a phase separation system like a biological membrane.

General conclusion in chapter 6, based on a "*bicelle*" diagram, a strategy to form various kinds of membranous functional materials (i.e., (i) chlorophyll a-bicelle, (ii) vesicle, and (iii) heterogeneous SLB) was finally proposed.

## CONTENTS

# Chapter 1

## General introduction

Bicelles consist of short-chain phospholipids and long-chain phospholipids. It acts as important materials for developing functional "*membranous*" materials. In this chapter, I describe the general features of the membranous materials, such as vesicles (liposomes), supported bilayer membrane (SLB), and bicelles, from both viewpoints of fundamental and applied aspect. A possible advantage of a discoidal membrane (bicelle) for its utilization for functional materials is discussed, followed by the review of some researches relating to this research.

### General aspect of lipid self-assembly

Biological membranes embedding various kinds of membrane proteins are known to support various kinds of functions, such as signal transduction [Simons *et al.*, 2000, Nagafuku *et al.*, 2003], substance transportation [Bell, 1978, Théry *et al.*, 2009], and energy storage source [Haagsman *et al.*, 1984, Farese *et al.*, 2009]. The major components of the biomembranes are lipids. Lipids are known to be assembled with other molecules, such as nucleic acids, proteins, and carbohydrates via the hydrophobic interaction or binding, resulting in the construction of variety of constructing unique membranous structures [Dowhan, 1997]. The membrane structure may play an important role as a platform for various kinds of "*life*" activities by providing heterogeneous sites and a dynamically-modulating ones, as well as a physical barrier to partition the inside and outside on cells or organelles [Vigh *et al.*, 2005]. In addition, some of the lipid molecules have reported to function after being converted into physiologically active molecules or signaling molecules, and they play an essential role in many life phenomena [Lee, 2004, Smith, 2012]. The heterogeneity in the biomembrane often comes from the molecular structure of lipids. Amphiphilic lipids calling phospholipids have phosphate choline groups that bound to the glycerol basic structure with two acyl chains. They are easy to form a bilayer membrane structure that are spontaneously assembled in an aqueous solution [Johnson *et al.*, 1971]. The bilayer of phospholipids is known to show different phase states on the surface of the self-assemblies, depending on the length of hydrophobic chains and

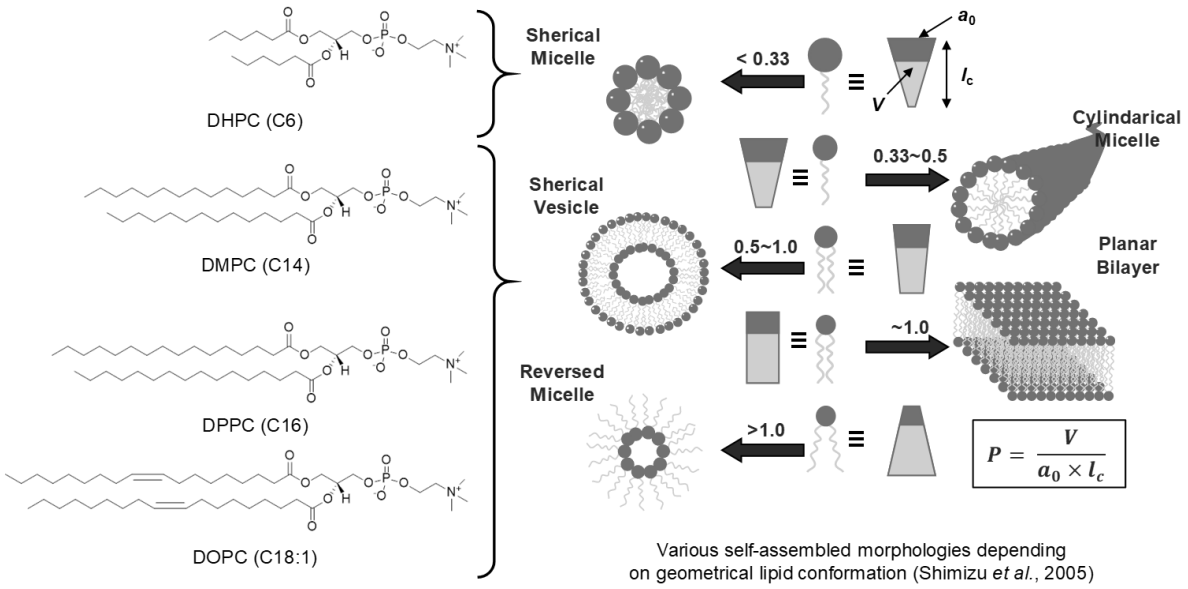


**Figure 1-1.** Species of lipids and morphology of those assemblies [Shimizu *et al.*, 2005].

the presence or absence of unsaturated chains [Nagle *et al.*, 2000, Shimizu *et al.*, 2005] (**Figure 1-1**). For example, the long chain phospholipid, such as 1,2-dipalmitoyl-*sn*-glycero-3-phosphocholine (DPPC), forms a spherical vesicle having a bilayer membrane structure by dispersing the lipids in water. The membrane of the DPPC vesicle shows an ordered gel phase at room temperature (the main phase transition temperature ($T_{m,\,DPPC}$): 41.3 ºC) [Mabrey *et al.*, 1976]. Unsaturated phospholipids, such as 1,2-dioleoyl-*sn*-glycero-3-phosphocholine (DOPC), form a disordered liquid-crystalline (LC) phase at the same temperature ($T_{m,\,DOPC}$: -40.3 ºC). It is due to the bulkiness of the packing of hydrophobic chains [Simons *et al.*, 2004]. In the DOPC/DPPC/cholesterol mixed system, micro-domains are formed on the vesicle membrane surface, depending on the composition ratio [Feigenson, 2009, Lingwood *et al.*, 2010] (**Figure 1-2**). The interaction among the ordered and rigid DPPC molecules is stronger than that among non-ordered DOPC molecules. In addition, presence of cholesterol molecules is known to affect the formation of the micro-domains [Sullan *et al.*, 2010, Suga *et al.*, 2013]. Interaction of the phospholipid molecules with cholesterol also forces neighboring acyl chains into more extended conformations, resulting in the further segregation via hydrophobic mismatch [García-Sáez *et al.*, 2007]. Biological membranes interact with proteins, especially, on the heterogeneous membranes, called as “rafts” and “micro-domains”, and the raft structures are

known to play important roles of in signal transduction and substance transport [Sezgin *et al.*, 2017].

An artificial lipid membrane forming the micro-domains is expected to be utilized for an elucidation of the function of membrane proteins and biological membranes if the micro-domain structure could be prepared stability in an aggregation. One of the possible materials is the "*bicelle*" or "*discoidal membrane*" that are formation different lipids with both long and short acyl chains [van Dam *et al.*, 2004]. Because a short-chain phospholipid such as 1,2-dihexanoyl-*sn*-glycero-3-phosphocholine (DHPC) has high critical micelle concentration ($CMC_{DHPC}$: 16 mM), high concentration is required to form a micelle assembly. Since DHPC is known to act as a surfactant against long-chain lipid bilayers, it is also used for membrane protein extraction [De Angelis *et al.*, 2007, Ujwal *et al.*, 2011]. In the DMPC/DHPC mixture system with extremely different lengths of hydrophobic acyl chains, the discoidal assembly (bicelle) can be seen in a high total lipid concentration [van Dam *et al.*, 2004] (**Figure 1-3**). This can be considered as phase separation between ordered DMPC dispersed phase and DHPC continuous phase in aqueous solution. Those assemblies are bilayer-micelle, called bicelle, and are expected to be applied to a membrane material [Prosser *et al.*, 2006, Kolahdouzan *et al.*, 2017].

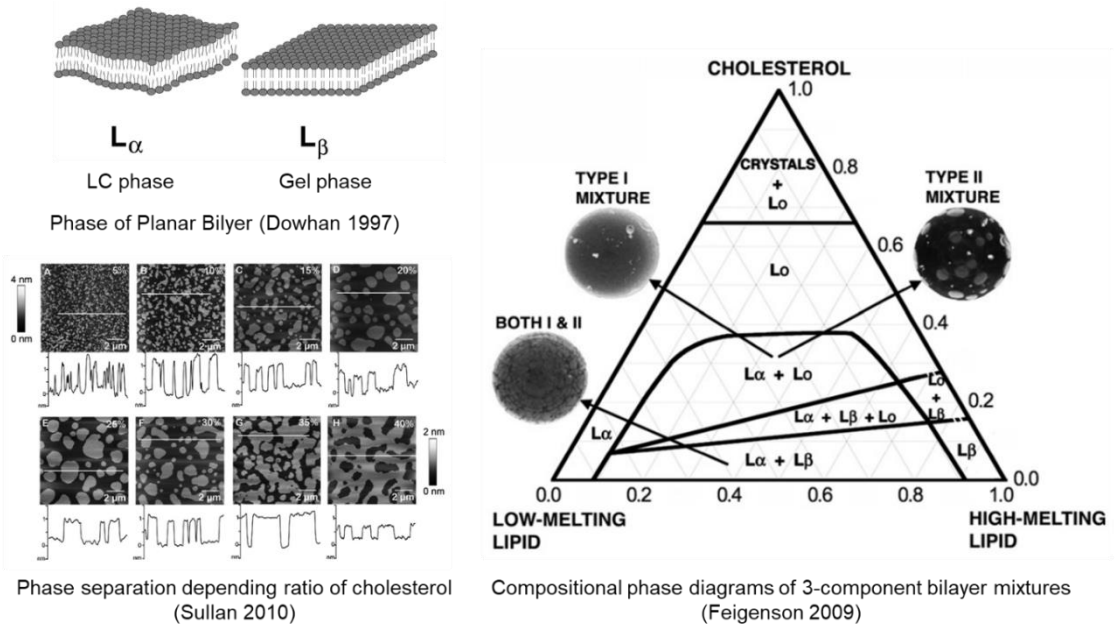


**Figure 1-2.** Phase state of artificial lipid bilayer and phase separation of model biomembrane [Feigenson *et al.*, 2009, Sullan *et al.*, 2010].

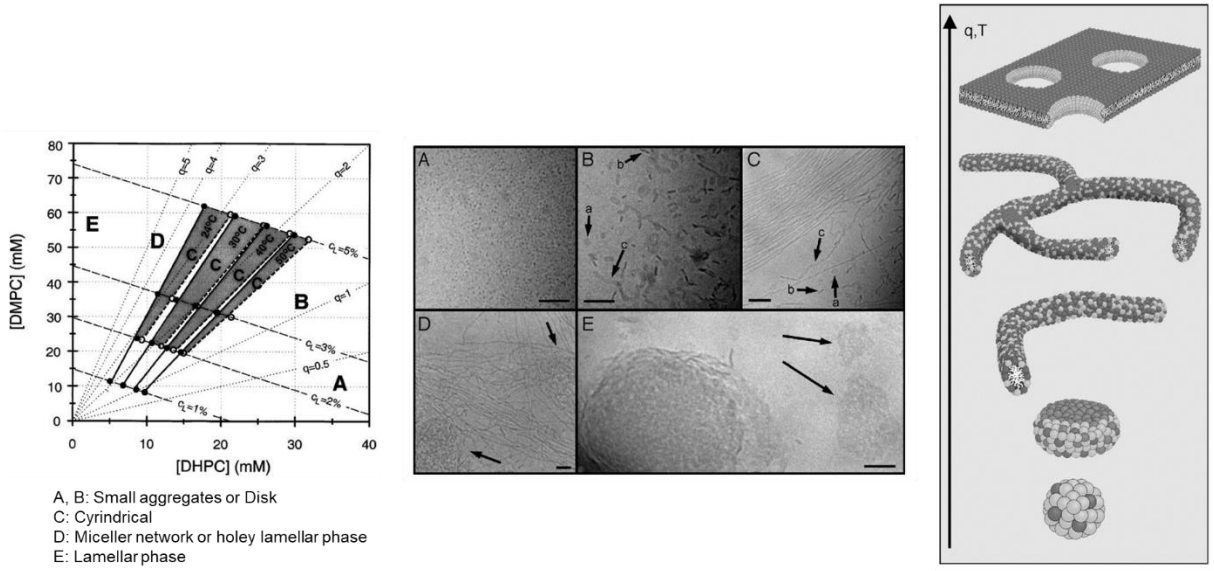


**Figure 1-3.** Structure of DMPC/DHPC mixture at high concentration of lipids ($C_{lipid}$: 1-5%) [van Dam *et al.*, 2004].

**Application of functional membranous materials**

There are many examples of the utilization of the lipid membranes; as the functional materials, that elucidate the biological reactions [Green *et al.*, 2004, Klymchenko *et al.*, 2014], and development of transport carriers [Torchilin, 2005], and substrate materials [Nanga *et al.*, 2011, Juhaniewicz *et al.*, 2015] (**Figure 1-4**). The research on the self-assembling lipid systems has been continuing since the 1970s [Ottava *et al.*, 1997], aiming at their applications as biochemical analysis, biosensors, and molecular devices [Simons *et al.*, 2000]. Long chain phospholipids form spherical vesicles (liposomes) in aqueous solution. Because a liposome has the qualities that are equivalent to a cell membrane, such as a fluid membrane surface and an internal aqueous phase, many researchers have been reported to utilize it as the models of artificial membranes [Klymchenko *et al.*, 2014] (**Figure 1-4**). Their results showed that various catalysts and enzymes embedded in artificial liposomal bilayers were active like *in vivo* systems [Titorenko *et al.*, 2000]. When a liposome is employed as a carrier, the system has been devised that can release drugs inner the assemblies at an arbitrary point due to external environmental changes, such as light, heat, voltage, pH and so on [Torchilin, 2004]. Torchilin has confirmed that the development of pharmaceutical liposomes is currently a growth area. For we need some progresses in both simple production processes and, also, a variety of membrane quality control

the increasing variety of suggested applications of liposomes and such trials could expand a mew model in clinical applications of different liposomal drugs.

Recently, other kinds of carrier molecules, such as surfactants [Baillie *et al.*, 1985, Mandal *et al.*, 2018] and polymers have been reported to be proposed [Uchegbu *et al.*, 1998, Tanner *et al.*, 2011]. These carriers can be obtained by a material design conceived from the features of amphiphilic molecules in water. The amphiphilic block copolymers are formed polymer vesicles with similar assembled morphology to liposomes. Polymer vesicles can be inserted membrane proteins which are expected to design and development of nanoreactors [Tanner *et al.*, 2011]. Furthermore, based on the asymmetric selectivity of phospholipid membranes, there are some reports that lipid membranes are used as separation sites [Ishigami *et al.*, 2015]. The liposomes enabled effective oligomerization of a chiral amino acid, such as L-histidine, on or in the liposome membrane. It is also known to be applicable as an asymmetric alkylation reaction site [Iwasaki *et al.*, 2017]. By understanding the structure and properties of liposomes, they have achieved highly selective reactions in surfactants, DDAB system as cationic double-chained surfactant. In contrast, a membrane film in which a bilayer membrane is immobilized on a glass or an electrode substrate has been studied as a material for observing

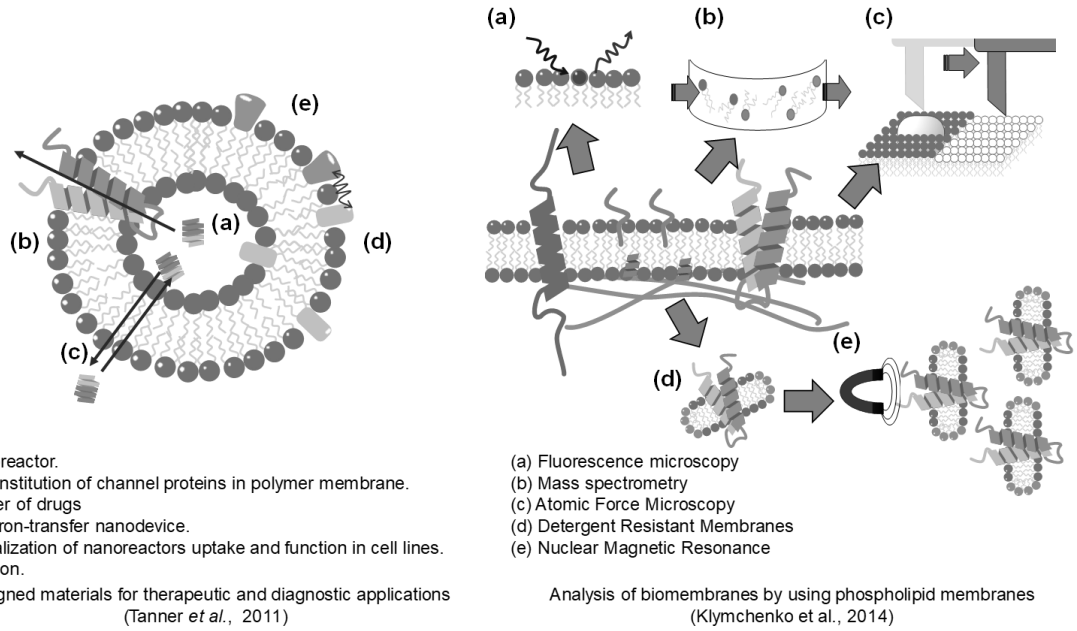


**Figure 1-4.** Applications of amphiphilic membranes to analytical using and materials developments [Tanner *et al.*, 2011, Klychenko *et al.*, 2014].

the permeability of ions and molecules in a biological membrane [Watts, 1995, Juhaniewicz *et al.*, 2015]. Watts successfully reconstructed the structure of the integral membrane protein, which the bacteriorhodopsin is a light-driven proton pump of the extremely halophilic bacterium, on an artificial membrane [Watts, 1995]. He has reported that the protein array formation is driven by specific interaction of the protein with the charged phospholipid, such as glycerol phosphate or the sulphate derivative. Membrane protein complexes such as channels and transporters in the biological membrane locally combine with charged lipids such as phosphatidylserine (PS) and sterols such as cholesterol and ergosterol and maintain a metastable structure [Lee, 2004]. It has been reported that a water channel (gramicidin A) on supported lipid bilayer (SLB) was used to a biomimetic reverse osmosis membrane [Saeki *et al.*, 2015]. The formed SLB showed high hydraulic pressure resistance and salt rejection. In their report, the water channel was stabilized by the interaction between the peptide and ergosterol on the membrane. Amphiphilic molecules including phospholipid membranes are expected to utilize active roles as membrane materials in various fields (e.g. treatment materials for any molecules such as water).

**Membrane preparation methods**

The preparation methods of membrane materials have been developed for various purposes. Representative methods were summarized in **Table 1-1**. The thin film hydration is one of the popular vesicle preparation method [LeBerre *et al*. 2008]. The assembly mainly has a multilamellar vesicle, and that morphology is arranged by filtration or ultrasonication. Small lamellar vesicles (SLVs) of about 100 nm diameter is used as a drug carrier [Hossann *et al*., 2012]. On the other hand, the ethanol injection [Kremer *et al*., 1977] and the reverse phase

**Table 1-1** List of the bitch-wise membrane preparation methods.

| | Organic solvent | System | Assembly | Residual solvent | References |
|---|---|---|---|---|---|
| Thin film hydration | Use | Batch (non-continuous) | MLVs | No | LeBerre *et al*. 2008 |
| Ethanol injection | Use | Semi-batch (stepwise) | GUVs | Yes | Pons *et al*. 1993 |
| Reverse phase evaporation | Use | Semi-batch (stepwise) | LUVs-GUVs | Yes | Szoka *et al*. 1978 |
| Supercritical reverse phase evaporation method (Semi-batch system) | Use | Semi-batch (stepwise) | LUVs | Yes | Imura *et al*. 2003 |

evaporation [Szoka *et al.*, 1978] are available for the preparation of larger vesicles, such as large unilamellar vesicles (LUVs) and giant unilamellar vesicles (GUVs) that can be uses as a biological membrane model. Imura *et al*. have demonstrated that the vesicle preparation in an interface between high-pressure carbon dioxide ($CO_2$) and water was effective as an evolutionary application of a reverse phase evaporation method. Imura *et al*. were prepared LUVs (0.2-1.2 μm) with high trapping efficiency by injecting water into ethanol (6.5wt%)/soy lecithin (0.28wt%)/liquid- or supercritical-$CO_2$ (93.2wt%). They used ethanol as cosolvent because very low polarity of $CO_2$ is not suitable to dissolve the lecithin. The reverse phase evaporation method is also applied to a continuous system for industrial use. In the continuous preparation method using the flow system, bilayer membrane assemblies can be continuously obtained by injecting lipid molecules dispersed in an organic solvent into an aqueous phase in a simple flow path [Cho *et al.*, 2015] (**Table 1-2**). Cho *et al.* achieved continuous preparation of w/o/w emulsion by mixing phospholipids dispersing isopropanol and water with the flow. They optimized the size of the obtained emulsions (diameter: 100-250 nm) by setting a pore filter (pore size: 5 μm) in the flow path and manipulating the flow velocity. Continuous preparations of GUVs have also been studied and Sugiura *et al.* developed the ice droplet technique [Sugiura *et al.*, 2008]. The ice droplet as vesicle core is mixed with the lipid dispersed solvent in flow path and leads to form an assembly with high volume inner water-phase. These preparation techniques are contributing to an improvement of batch-wise methods such as ethanol injection and reverse phase evaporation. Amphiphilic molecules at the interface between hydrophilic and hydrophobic solutions disperse in a continuous system.

**Table 1-2** List of the continuous membrane preparation methods.

| | Organic solvent | System | Assembly | Residual solvent | References |
|---|---|---|---|---|---|
| Pulsed jetting | Use | Continuous | GUV | Yes | Funakoshi *et al*. (2007) |
| Droplet emulsion | Use | Continuous | GUV | Yes | Hamada *et al*. (2008) |
| Ice droplet | Use | Continuous | LUV-GUV | Yes | Sugiura *et al*. (2008) |
| Microchannel | Use | Continuous | GUV (asymmetric) | Yes | Li *et al*. (2015) |
| Microfluidic platform | Use | Continuous | Nanodiscs | Yes | Wade *et al*. (2017) |

**Preparation of membranous material by continuous method**

Recently, the formation of asymmetric vesicles that mimic biological membranes by the more complicated microfluidic channel has been reported [Lu *et al.*, 2015]. Lu *et al.* have confirmed that the membrane asymmetry is maintained for over 30 hours. The asymmetric vesicles hold the potential to be used as model systems in membrane biology or as drug delivery. The vesicle preparations by flow systems have the possibility of continuation and the potential to continuously control the size, though there is a problem of remaining of organic solvents in those products. The organic solvent remaining in the hydrophilic phase of a bimolecular membrane is expected to weaken the packing of the bilayer membrane. In order to obtain a heterogeneous phase separation system such as a biological membrane, it is necessary to prepare the environment of bulk solutions such as pH, polarity, salt concentration etc. on the surface of the membrane material.

On the other hand, a supported lipid bilayer (SLB) is utilized to the platforms of biology, biochemistry and biomimetic technologies [Juhaniewicz *et al.*, 2015] (**Table 1-3**). Vesicular fusion is popular method for SLB formation [Abraham *et al.,* 2018]. The vesicle suspension added to the hydrophilization treatment glass substrate adsorbs to the substrate by electrostatic interaction ("vesicle adsorption"), and the vesicles collapse to obtain a planar film ("vesicle rupture"). For the adsorption of vesicles, a hydrophilic glass substrate containing silicon dioxide and mica are often used [Biswas *et al*., 2018]. In addition, for the rupture of vesicles, lipid membranes with high fluidity, such as LC phase, can easily form SLB. However, the SLB formation by vesicle fusion has limitation on the phase state of membranes.

Tabaei *et al.* reported the solvent-assisted lipid bilayer (SALB) as an SLB preparation method without using vesicles [Tabaei *et al.*, 2014] (**Figure 1-5**). This method is inspired by reverse-phase evaporation in batch-wise to make a unilamellar bilayer. The lipid molecules dissolved in the water/isopropanol solution assemble to the formation of a planar bilayer upon a gradual increase in the solvent water fraction. The DOPC bilayer film was formed on the substrate by continuously adding the DOPC solution. This method can be employed materials besides silicon dioxide such as alumina, gold, titanium, and silica. It is noted that, the water/oil flow ratio and the total lipid concentration inside the flow must be operated to form a bilayer film. In their experimental system, it is necessary to maintain a lipid concentration, at least 0.1 mg/mL, in the organic solvent.

Recently, Kawasaki *et al.* reported planar membranes using POPC/DHPC mixtures to solubilize and reconstitute membrane proteins on planar membranes at continuous system [Kawasaki *et al.*, 2012]. Below the $CMC_{DHPC}$, the lipid membrane adsorbed on the substrate was not peeled off by rinsing. They evaluate the membrane properties of the SLB from the lateral diffusivity of lipid molecules by fluorescence recovery after photobleaching and the SLB has the same characteristics as SLB prepared by the vesicle fusion method. Preparation of SLB was achieved by using bicelles in the complete aqueous condition. Kolahdouzan *et al.* observed the process of SLB formation from DOPC/DHPC bicelle by fluorescence microscopy. According to their investigation, when the total lipid concentration is low (< $CMC_{DHPC}$), the lipid aggregate in the bulk and the lipid bilayer on the substrate are mainly DOPC. Then, DHPC molecules are present as monomers in the bulk. An unstable change in the mass on the substrate surface was observed after adsorption of the bicelle to the substrate at DHPC-rich condition. Because the DHPC molecule destabilizes in the membrane, it is claimed that the control of DHPC concentration is important for the formation of SLB. Furthermore, the critical coverage, that bilayer covers the whole substrate, became faster as compared to the system with the higher ratio of DHPC than the system with the higher ratio. The adsorption of discoidal assemblies to the substrate is also expected to be influenced by the size of the assemblies. In conventional studies, bicelle containing a bilayer of a single composition was used to prepare a planar membrane. There are not many experiments in multicomponent systems for biomimetic applications. In addition, analysis of SLB is limited to observation of adsorption behavior of lipid molecules by quartz crystal microbalance with dissipation (QCM-D) monitoring and evaluation of lateral diffusivity of lipid molecules by FRAP. Membrane preparation methods have been able to imitate living cells more and to advance for industrial demand.

**Table 1-3** List of production methods of SLB.

| | Organic solvent | System | Type of substrate | Residual solvent | References |
|---|---|---|---|---|---|
| Vesicle fusion | Non-use | Non-continuous | $SiO_2$, mica, gold | No | Abraham *et al*. 2018 |
| SALB | Use | Continuous | $SiO_2$, mica, alumina, gold, titanium, and silica | Unknown | Tabaei *et al*. 2014 |
| Bicelle injection | Non-use | Continuous | $SiO_2$, gold | No | Kolahdouzan *et al*. 2017 |

**Discoidal Phospholipid Membrane (Bicelle)**

A discoidal membrane on bicelle could be effective as the membranous materials, where DMPC/DHPC system used often is known to show various morphology with different concentrations and compositions. Van Dam *et al*. estimated the lipid concentration to give a bicelle structure (higher concentration, $C_{total}$: 20-100mM) by cryo-transmission electron microscopy (cryo-TEM) and dynamic light scattering (DLS) [van Dam *et al.*, 2004]. They have reported that DMPC/DHPC mixtures vary in the assembly form, depending on its ratio and temperature. It is caused by the detergent effect of DHPC in the bilayer. In the DMPC-rich condition, vesicle, string-like, and network-like structures have been confirmed. It is because fluidization effect of DHPC is weak and it makes large aggregate. The DMPC/DHPC disk obtained under appropriate conditions (DMPC/DHPC ratio) has the bilayer membrane in the self-assembly in micelle-like size. Because DHPC molecules cover the hydrophobic acyl chains of DMPC in the bilayer disk, the disk can be dispersed in a bulk solution. Then, monomer or hydrated DHPC in the bulk is continually exchanged with one in a disk. In DHPC-rich conditions, because the fluidization of DMPC bilayer membrane is promoted by involving DHPC molecules in the bilayer, a micelle and a mixed micelle, containing DMPC, are constructed. Takajo and coworkers have reported that DHPC fluidizes DMPC bilayer membranes in a relatively low concentration system [Takajo *et al*., 2018]. They evaluate the form of assemblies in the low concentration range of lipids ($C_{total}$ < 20 mM) from differential

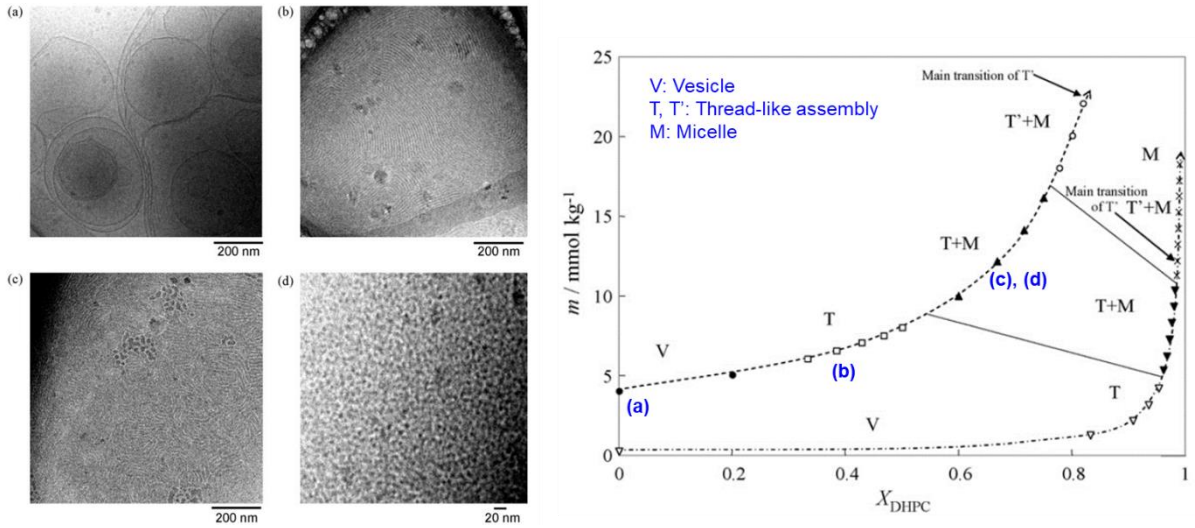


**Figure 1-5.** Structural and morphological transition of DMPC/DHPC mixture at low concentration [Takajo *et al*., 2010].

scanning calorimetry (DSC) measurement and cryo-TEM observation. They clarified that the formation of the assembly changes complicatedly depending on the DHPC concentration for the two kinds of DMPC concentrations (4 and 0.2 mM). Vesicles formed easily at DMPC-rich condition, and the assembly was small with increasing DHPC molecules. They considered that a DHPC micelle or a DMPC/DHPC mixed micelle were finally formed above the $CMC_{DHPC}$. Because DMPC/DHPC mixtures give variations of morphologies by assembling/dispersion of lipids, it can be utilized for membrane material development in step-by-step. However, physicochemical knowledge on the form of the assembly is still insufficient. To develop biomimetic membrane materials using bicelle, it is necessary to understand the behavior of assemblies at low concentration region around $CMC_{DHPC}$.

The final purpose of this thesis is to establish a strategy to design and develop various "*membranous*" materials by utilizing "*bicelle*" as a key material. DMPC and DHPC system was selected as a typical example of the bicelle. After studying the conditions to form self-assemblies, such as micelles, bicelles and vesicles, in DMPC/DHPC system, the obtained findings were summarized as a diagram along with DMPC/DHPC concentration in order to show a "*map*" of the "*membranous*" materials. Based on a "*bicelle*" diagram, a strategy to form various kinds of membranous functional materials was finally proposed. There kinds of the membranous materials (i.e., (i) chlorophyll a-bicelle, (ii) vesicle, and (iii) heterogeneous SLB) were prepared based on the bicelle diagram as case studies of the proposed strategy. The framework and the flow chart of the present study are schematically shown in **Figure 1-6** and **1-7**, respectively.

In chapter 2, the behaviors of self-assemblies of the DMPC/DHPC mixed system, focusing on the physicochemical properties of the membrane were systematically investigated at the lower total lipid concentrations less than 20 mM (< 1 wt% lipid). The properties of the assemblies at a various concentration near the $CMC_{DHPC}$ were estimated by using DLS and fluorescence probes. The assemblies were categorized as Region (i), Region (ii-1), and Region (ii-2), in which the dominant state was large vesicle (> 30 nm, "ordered" bilayer), gel-bicelle (< 30 nm, "ordered"), and micelle (< 30 nm, "disordered"), respectively. Furthermore, in the conditions at molar fractions of DHPC, $X_{DHPC}$: 0.33-0.4, the dilution was formed to lead to the transformation from bicelle to vesicle. The findings of this study are summarized in the "*bicelle*"

diagram. Based on the "*bicelle*" diagram, a strategy to prepare various membranous materials was finally proposed.

In chapter 3, the functional bicelle that has highly-ordered orientation of the functional molecule was prepared as a case study. Photo-functional molecule chlorophyll *a* (Chl*a*) was mixed in the vesicle, and the orientation behavior of Chl*a* for the phase state of the membrane was observed. Change in a polar environment of Chl*a* in a bilayer was clarified by analysis of UV-vis absorption spectrum. The possibility of operating the dispersion/association of Chl*a* in a membrane was indicated by controlling the phase state of the membrane. Furthermore, the aggregation of Chl*a* molecules was controlled on a bicelle platform. The unique absorption spectrum of Chl*a* aggregates was observed on the bicelle. The condensation of functional molecules was achieved by using bicelle with a bilayer membrane in micelle-order assembly. Moreover, the aggregate was maintained in dilution process in spite that a bicelle could be changed into a vesicle. Thus, the potential of a bicelle as the membrane materials was shown to be effective.

In chapter 4, the vesicle-like material was prepared by using the flow devices according to the "*bicelle*" diagram. Prior to its preparation, the membrane properties of bilayer membrane obtained by conventional preparation methods (thin film hydration and high-pressure $CO_2$) and the bicelle method were compared. The vesicle-like assembly obtained by dilution of bicelle suspension had the similar membrane properties as the conventional methods. Controlling DHPC concentration is an important factor for controlling the shape of the DMPC bilayer membrane for development of the membrane platform in batch dilution or in flow dilution. Furthermore, vesicle was prepared continuously by dilution of bicelle suspension by flow path. Based on the knowledge of the morphological change of the assemblies to the lipid concentrations (from chapter 2), the bicelle was changed to other morphologies by applying its suspension into the flow path with dilution. It was found that the form of the assembly obtained by the dilution route was different. The dilution ratio was found to be a key factor to control the assembled form. The membrane properties of the vesicle obtained by the flow channel have the same membrane characteristics as the vesicle prepared by the conventional method. Bicelles can be expected to be used as a membrane material for constructing membrane matters.

In chapter 5, supported lipid bilayer (SLB) was prepared by using a bicelle as its resource material. Formation of SLB was confirmed by adding/diluting of bicelles on the

substrate. The formation of the SLB on the substrate was promoted especially by using small bicelles because of the stability of the long-chain lipid bilayer edge and, also, the concentration shift of lipids after the removal of DHPC molecules. It was found that the addition of a DMPC/DHPC bicelle and a DPPC/DHPC bicelle together could induce the formation of heterogeneous SLB in the same planar membrane on the solid substrate. Phase separation on SLB was observed based on Förster resonance energy transfer (FRET). Moreover, by continuously adding the bicelle suspension to the substrate, a formation of SLB was confirmed in a short time. Continuous preparation of SLB by bicelle flow dilution was able to create a phase separation system as biological membranes.

The results obtained in this work are summarized in general conclusion. Suggestions for future works are described as extension of the present thesis.

## Meso (assemblies)

Chapter 2 Phase Separation & Morphologies of DMPC/DHPC Mixtures

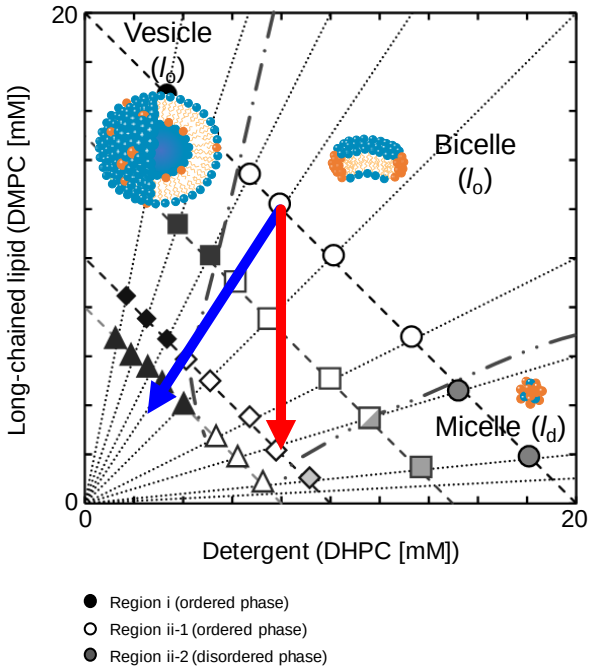


## Micro (molecules)

Chapter 3
Chlorophyll *a* (Chla) Location on Membrane

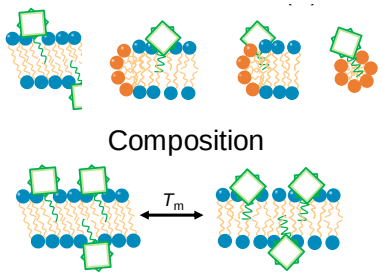


Chl*a* aggregation on Bicelle

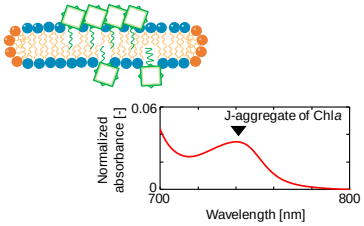


## Macro (materials)

Chapter 4 Continuous Vesicle Preparation in Flow Chip

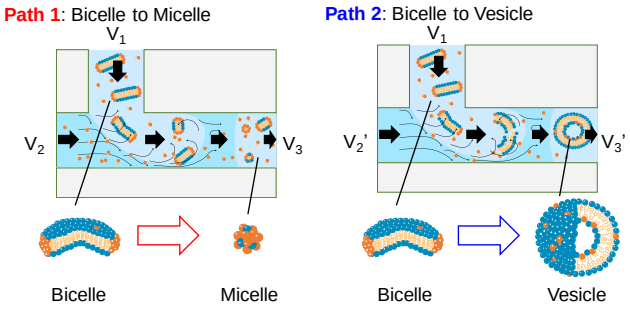


Chapter 5 Preparation of Supported Lipid Bilayer (SLB) by Using Bicelles

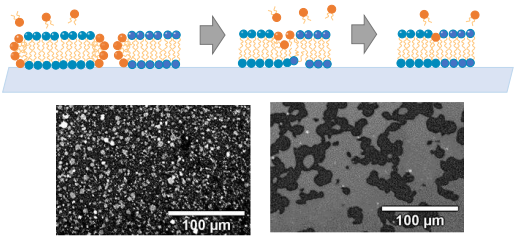


Homo-, Hetero-Planer Membranes

**Figure 1-6.** Concept of the present study.

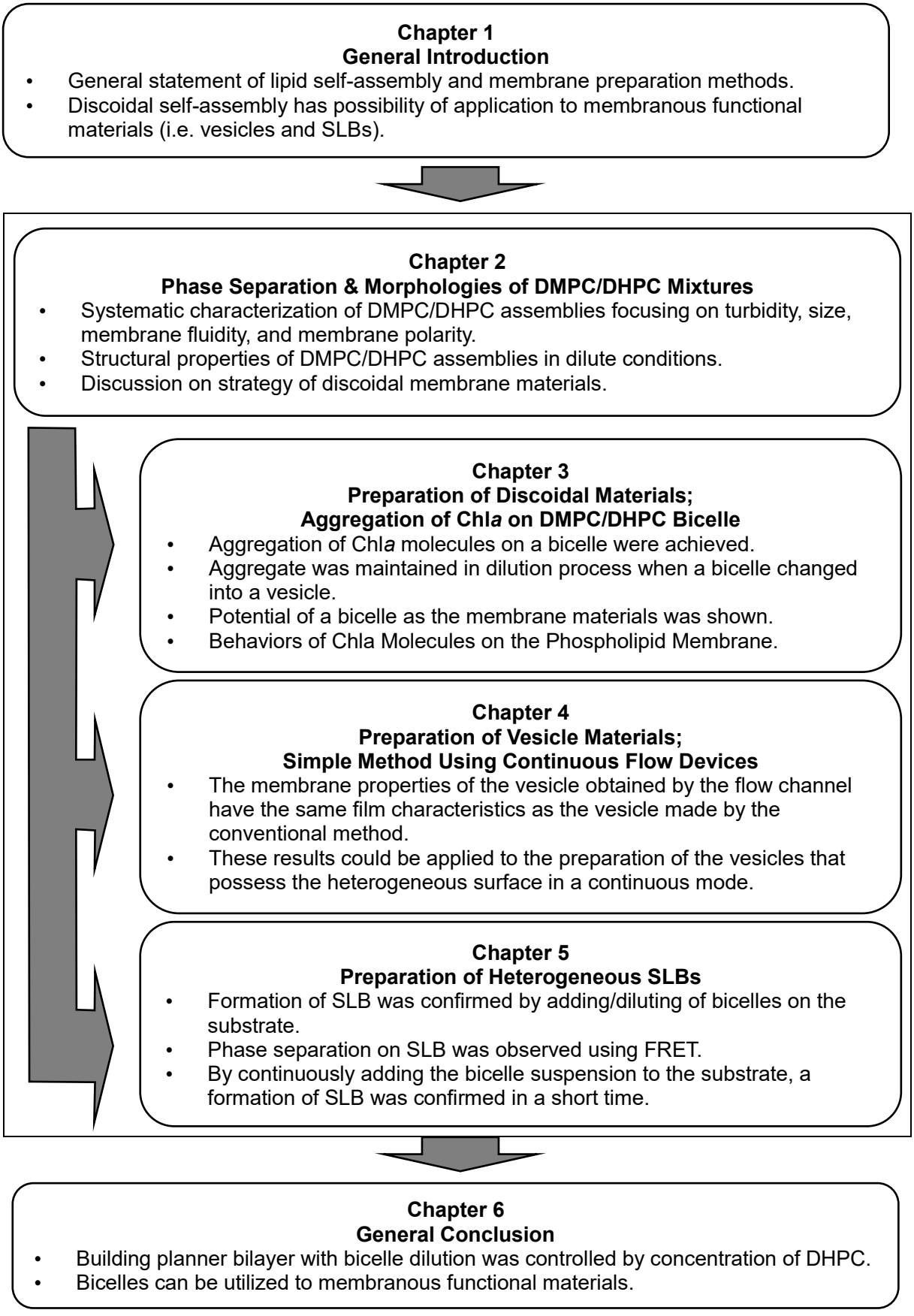


**Figure 1-7.** Framework of the present study.

# Chapter 2

## Systematic Characterization of DMPC/DHPC Self-Assemblies and Their Phase Behaviors in Aqueous Solution

### 1. Introduction

Phospholipids form a self-assembled membrane in aqueous solution to reduce the exposure of hydrophobic acyl chain groups. 1,2-Dimyristoyl-*sn*-glycero-3-phosphocholine (DMPC, C14:0) molecules form a bilayer vesicle (liposome), whereas 1,2-dihexanoyl-*sn*-glycero-3-phosphocholine (DHPC, C6:0) molecules form a micelle at a total lipid concentration higher than the critical micelle concentration (CMC: 16 mM [Burns Jr. *et al*., 1982]). Depending on the chemical structure of the phospholipids, the self-assemblies form various morphologies such as vesicle, micelle, etc. [Eytan *et al*., 1982, Ringsdorf *et al*., 1988]. In general, the self-assembly behavior of amphiphilic molecules is discussed based on the critical packing parameter, in which the head group area, length of hydrocarbon chain, and volume of molecules are dominant factors that determine the self-assembly structure. Owing to the hydrophobic region at the interior of the membrane, phospholipid assemblies are utilized as a platform to integrate various kinds of nanomaterials [Cyrus *et al*., 2012]. The lipid bilayer structure is desirable to study membrane proteins; generally, discoidal self-assemblies, called "bicelles" [Sanders *et al.*, 1992, Ottiger *et al.*, 1998], are applied to reconstruct membrane peptides and proteins [Sanders *et al*., 1995, McKibbin *et al*., 2007, Li *et al*., 2014]. Basically, a bicelle structure is composed of a mixture of lipid and detergent, as in DMPC/DHPC systems [van Dam *et al*., 2004]. Since the stability of a bicelle is sensitive to the lipid composition and temperature [Triba *et al*., 2005, Wu *et al*., 2010, Beaugrand *et al*., 2014, Mineev *et al*., 2016], it is important to investigate the thermodynamic behavior of bicelles.

The CMC value of DHPC is ca. 16 mM [van Dam *et al*., 2004], whereas the critical vesicle concentration (CVC) of DMPC is ca. 6 nM. Due to the difference in critical aggregation concentrations, the stability of a bicelle is also sensitive to the total lipid concentration [Struppe *et al*., 1998, Ye *et al*., 2014]. Upon dilution of a small bicelle assembly, the transformation from bicelle to vesicle was observed. To avoid this, a chemically modified detergent can be utilized,

making the bicelle structure stable toward heating or dilution [Ramos *et al.*, 2010, Matsui *et al.*, 2015]. To characterize bicelle properties, experiments have been carried out with high concentrations of lipid (1-10%, w/w); by employing such conditions, the structural properties of bicelles can be evaluated using cryo-electron microscopy (cryo-EM) [Ye *et al*., 2014]. Regarding the rupture of bicelles in the dilution process, a direct deposition of lipids onto a solid support, wherein the bicelles are used as carriers for lipid sources, becomes more successful [Saleem *et al*., 2015, Kolahdouzan *et al*., 2017]. Statically, the phase behavior of lipid mixture systems (e.g., DMPC/DHPC) can be controlled by focusing on parameters such as lipid composition, lipid concentration, and temperature. Then, the self-assembly morphology can be controlled in a dynamic process, such as heating/cooling and dilution, based on the phase equilibrium. However, the phase behavior of DMPC/DHPC mixture systems at low lipid concentrations (total lipid < 20 mM) has not been adequately investigated.

Interfacial membrane properties such as membrane fluidity and membrane polarity, which are evaluated using fluorescent probes, are also important factors to characterize self-assemblies [Hayashi *et al*., 2011, Nakamura *et al*., 2015]. In lipid bilayer vesicles, the interfacial properties can be used to determine the phase states [Suga *et al*., 2013, Bui *et al*., 2016]; the solid-ordered phase (gel phase) and liquid-disordered phase (liquid-crystalline phase) show quite different membrane fluidity and polarity. These properties reflect the microscopic phase state and phase separation behavior [Suga *et al*., 2013]. Saturated phospholipids are in gel phase below the phase transition temperature ($T_m$), whereas the membrane turns into liquid-crystalline phase at temperatures above the $T_m$. To date, bicelles (such as DMPC/DHPC mixture systems) have been hardly studied based on their interfacial properties, especially at low lipid concentrations (less than 1% lipids (ca. 20 mM). In fluorescent probe studies, the interfacial membrane properties can be investigated at a total lipid concentration of 100 μM [Hayashi *et al*., 2011, Suga *et al*., 2013]. Therefore, this could be suitable to evaluate the interfacial membrane properties and structural properties of DMPC/DHPC mixture systems.

The packing state of a lipid membrane is dominantly related to the function of the membrane: for example, molecular permeability and interaction of proteins [Lee, 2003, Gerebtzoff *et al*., 2004]. In previous study, significant chiral selective amino acid adsorption onto a liposome membrane was observed in a gel phase [Ishigami *et al*., 2015]. The state of a lipid bilayer can be classified as gel phase (most ordered state, like a solid), ripple-gel phase

(ordered state), and liquid-crystalline phase (disordered state). Considering the membrane fluidity and membrane polarity of micelles [Iwasaki *et al*., 2017], they can be categorized as a disordered membrane. In gel phase, the surface pressure is up to ~50 mN/m in monolayer systems (planar membrane (no curvature)), whereas it decreases to ~30 mN/m in vesicular bilayer systems [Sabatini *et al*., 2008]. This may be due to the membrane curvature of the vesicles, which could decrease lipid packing. It is hence worthwhile to investigate the interfacial properties of such a flat bilayer system.

The aim of this chapter was to clarify the self-assembly behavior of DMPC/DHPC mixtures containing various total lipid concentrations and fractions of lipids. The DMPC/DHPC assemblies were prepared with different molar fractions of DHPC ($X_{\mathrm{DHPC}}$). Analyses of the turbidity (optical density, $OD_{500}$) and size distribution (using dynamic light scattering, DLS), and of the interfacial membrane properties, using fluorescent probes, 1,6-diphenyl-1,3,5-hexatriene (DPH) and 6-dodecanoyl-*N*,*N*-dimethyl-2-naphthylamine (Laurdan), were systematically carried out. The obtained results are summarized as a diagram to show the relationship between the lipid concentrations and morphologies of the DMPC/DHPC self-assemblies. Based on the "*bicelle*" diagram, a strategy to prepare various kinds of "*membranous*" functional materials was finally proposed.

## 2. Materials and Methods

### 2.1. Materials

DHPC and DMPC ($T_m$ = 23 ºC) were purchased from Avanti Polar Lipids, Inc. (Alabaster, AL, USA). DPH and Laurdan were purchased from Sigma-Aldrich (St. Louis, MO, USA). Sodium dihydrogenphosphate (anhydrous) and disodium hydrogenphosphate were purchased from Wako Pure Chemical (Osaka Japan), and were used to prepare phosphate buffer (50 mM, pH 7.0). Ultrapure water was prepared with the Millipore Milli-Q system (EMD Millipore Co., Darmstadt, Germany). Other chemicals were used without further purification.

### 2.2. Vesicle preparation

DMPC vesicles were prepared as a reference (standard self-assembly), based on literature [Suga *et al*., 2013]. Briefly, a chloroform solution of phospholipids was dried in a round-bottom flask by rotary evaporation under vacuum. The obtained lipid films were dissolved in chloroform once more, and the solvent was evaporated. This operation was repeated at least twice. The obtained lipid thin film was kept under high vacuum for at least 3 h, and then hydrated with phosphate buffer at room temperature. The obtained DMPC suspension was frozen at −80 ºC and then thawed at 40 ºC (over the $T_m$ of DMPC); this freeze-thaw cycle was repeated five times. Notably, the DMPC vesicle suspensions were extruded through 2 layers of polycarbonate membranes with a mean pore diameter of 100 nm, using as extruding device (Liposofast; Avestin Inc., Ottawa, ON, Canada). The prepared unilamellar vesicles were kept in 4 ºC until use.

### 2.3. Preparation of DMPC/DHPC self-assembly in an aqueous solution

Lipid thin films of DMPC/DHPC mixtures were prepared by the mothed described on the above. Firstly, the self-assembly solution was prepared at the total lipid concentration of 20 mM, with various DHPC fractions, $X_{DHPC}$: 0.17-0.95. The obtained lipid thin films were hydrated with phosphate buffer at 20 ºC. No mechanical treatments (sonication, extrusion) were applied for DMPC/DHPC assemblies, to keep their spontaneous structures. In dilution of the DHPC/DMPC solution (20 mM), an aliquot amount of buffer solution was gently added to adjust the total lipid concentration, wherein the final lipid concentrations were set at 15 mM, 10 mM, 9 mM, and 8 mM. The obtained self-assembly solutions were applied for monitoring

the optical density (see section **2.4**), and dynamic light scattering (see section **2.5**). If necessary, the extrusion (see section **2.2**) was performed before fluorescent spectroscopic measurements (see sections **2.6** and **2.7**).

### 2.4. Turbidity measurements of self-assembly solution

To assess the morphological insights for DMPC/DHPC assemblies, the turbidities of DMPC/DHPC mixtures at 500 nm ($OD_{500}$) were monitored by UV-1800 Spectrophotometer (Shimadzu, Kyoto, Japan), in various total lipid concentrations. A thin quart cell (light path length: 1 mm) was employed to record the varied turbidity. An increased turbidity in the suspension could be an evidence for the growth of self-assembly in size [Walter *et al*., 1991, Guo *et al*., 2011, Craig *et al*., 2016]. Thus, the morphological transition from bicelles to vesicles could be assessed by a jump-up of the $OD_{500}$ values, in dilution.

### 2.5. Dynamic light scattering (DLS)

The apparent sizes of mixtures (total lipid concentration: 20 mM) were determined by dynamic light scattering (DLS). Measurements were performed with the particle size analyzer (Zetasizer Nano ZS, Malvern Panalytical, Grovewood Rd, UK). The average diameters were calculated based on a number-average diameter.

### 2.6. Evaluation of membrane fluidity

As interfacial properties, the membrane fluidity was investigated by using DPH, based on previously described methods [Shintzky *et al*., 1978, Hayashi *et al*., 2011]. DPH was added to DMPC/DHPC assemblies with a molar ratio of lipid/DPH = 250/1. After incubation for 30 min, the fluorescence polarization of DPH was measured using a fluorescence spectrophotometer (FP-8500, JASCO, Tokyo, Japan) (Ex. = 360 nm, Em. = 430 nm). Fluorescence polarizers were set on the excitation and emission light pathways. With the emission polarizer angle of 0º, the fluorescence intensities obtained with the emission polarizer angle 0º and 90º were defined as $I_{\parallel}$ and $I_{\perp}$, respectively. With the emission polarizer angle of 90º, the fluorescence intensities obtained with the emission polarizer angle 0º and 90º were defined as $i_{\perp}$ and $i_{\parallel}$, respectively. The polarization ($P_{DPH}$) of DPH was then calculated by using the following equations:

$$P_{DPH} = (I_{\parallel} - GI_{\perp})/(I_{\parallel} + GI_{\perp})$$

$$G = i_{\perp}/i_{\parallel}$$

where $G$ is the correction factor. The membrane fluidity was evaluated based on the reciprocal of polarization, $1/P_{\mathrm{DPH}}$.

### 2.7. Evaluation of membrane polarity

Fluorescent probe Laurdan is sensitive to the polarity around itself, which allows the local polarity in lipid membranes to be determined [Parasassi *et al*., 1990, Vincent *et al*., 2005]. Laurdan emission spectra exhibit a red shift caused by solvent attack and by solvent relaxation, thus its emission spectrum reflects the polarity (hydration state) of the self-assembly membrane. The Laurdan emission spectra were measured with an excitation wavelength of 340 nm, and the general polarization ($GP_{340}$), the membrane polarity, was calculated as follows:

$$GP_{340} = (I_{440} - I_{490})/(I_{440} + I_{490})$$

where $I_{440}$ and $I_{490}$ are the emission intensities of Laurdan excited at 340 nm. The obtained emission spectrum was furthermore analyzed by using Peakfit software (v.4.12, Systat Software Inc., San Jose, CA, USA) [Iwasaki *et al*., 2017]. After deconvolution, the area fraction of each component was compared.

## 3. Results and Discussion

### 3.1. Systematic characterization of DMPC/DHPC assemblies focusing on turbidity, size, membrane fluidity, and membrane polarity

For DMPC/DHPC suspensions at a total lipid concentration of 20 mM, the solution turbidity varied depending on the $X_{DHPC}$. The transparency of the suspension was dependent on the size of the assemblies; the vesicles were relatively large (diameter > 30 nm: Region (i)), whereas the micelles or bicelles were small (diameter < 30 nm: Region (ii)) (**Figure 2-1a**). By employing fluorescent probes (DPH and Laurdan), the membrane fluidity ($1/P_{DPH}$) and membrane polarity ($GP_{340}$) values were determined. The DHPC micelle was categorized as disordered membrane ($1/P_{DPH} > 6$, $GP_{340} < 0.3$). At 20 ºC (< $T_m$ of DMPC), some small assemblies (in Region (ii)) as well as the gel-phase DMPC vesicle showed rather ordered interfacial membrane properties (**Figure 2-1b**). The group of Region (ii) can be further divided into "ordered phase (ii-1)" and "disordered phase (ii-2)." The bicelle of DMPC/DHPC probably consisted of a micelle-like edge (rich in DHPC) and bilayer (rich in DMPC); therefore, the ordered phase found in Region (ii-1) could have been derived from the bilayer region of the bicelle. To classify each self-assembly, the threshold values of size, $OD_{500}$, $1/P_{DPH}$, and $GP_{340}$ are summarized in **Table 2-1**. Based on the systematic characterization, a diagram of self-assemblies in DMPC/DHPC system at 20 mM is described in **Figure 2-1c**. The assembled states of DMPC/DHPC were confirmed as vesicle (Region (i)), bicelle (Region (ii-1)), and micelle (Region (ii-2)).

### 3.2. Structural properties of DMPC/DHPC assemblies in dilute conditions

The turbidities of DMPC/DHPC suspensions are dependent on the morphology. Micelle solutions are transparent, whereas vesicle, cylindrical micelle, and holey lamellar suspensions are turbid [van Dam *et al*., 2004]. The DHPC micelle solution, wherein the average micelle size was 3-4 nm, was transparent. This suggests a rough correlation between turbidity and size of the self-assembly; therefore, the $OD_{500}$ (**Figure 2-2**) and size distribution (**Figure 2-3**) were investigated at different total lipid concentrations.

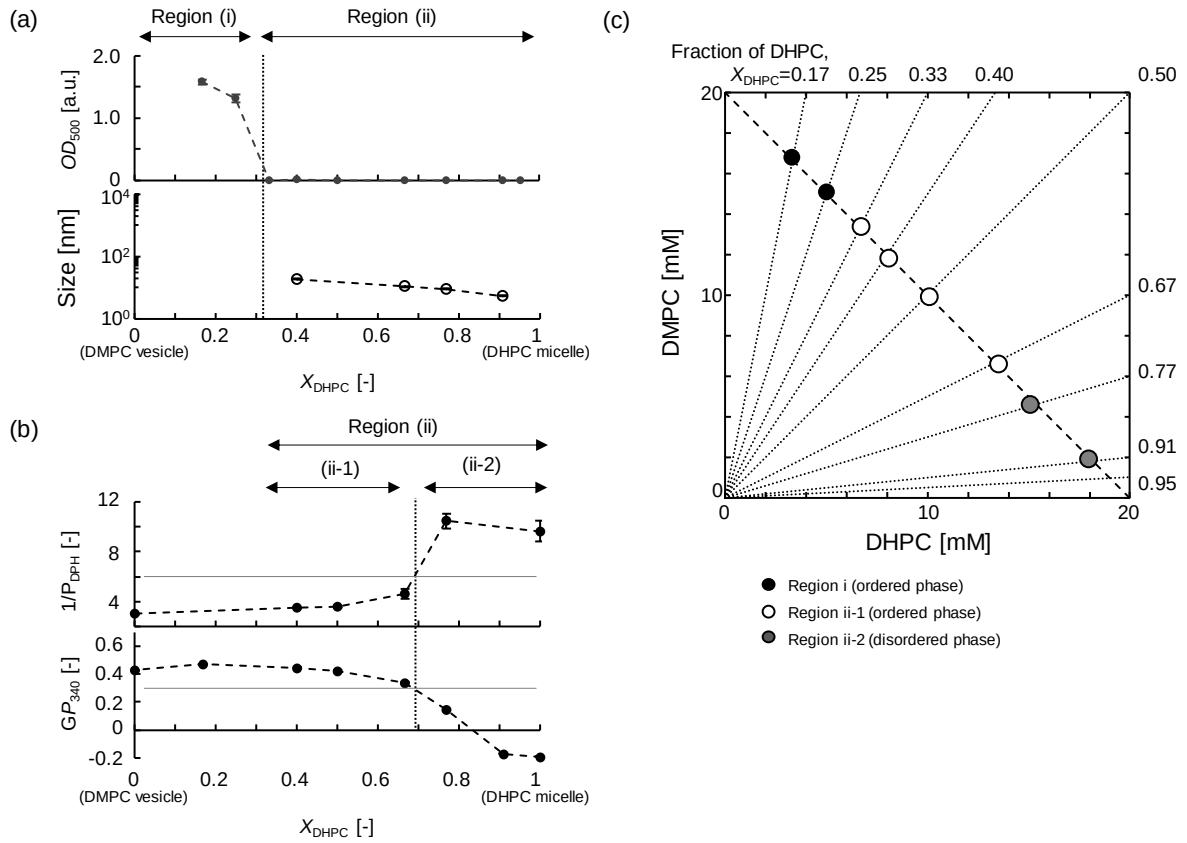


**Figure 2-1.** Systematic characterization of DMPC/DHPC assemblies at 20 ℃, total lipid concentration of 20 mM. As a function of DHPC fraction ($X_{DHPC}$), (a) turbidity ($OD_{500}$) and size distribution. Region (i), relatively large assemblies ($OD_{500}$ > 1.0, size > 30 nm); Region (ii), relatively small assemblies ($OD_{500}$ < 0.1, size < 30 nm). (b) Membrane fluidity ($1/P_{DPH}$) and membrane polarity ($GP_{340}$). Region (ii-1), ordered assemblies ($1/P_{DPH}$ < 6, $GP_{340}$ > 0.3); Region (ii-2), disordered assemblies ($1/P_{DPH}$ > 6, $GP_{340}$ < 0.3). (c) Phase diagram of DMPC/DHPC at total lipid concentration of 20 mM. Region (i), closed circle; Region (ii-1), open circle; Region (ii-2), half-tone circle.

**Table 2-1** Summary of the results for self-assemblies prepared at different regions.

| | Size (DLS) | Turbidity, $OD_{500}$ | Membrane fluidity, $1/P_{DPH}$ | Membrane polarity, $GP_{340}$ |
|---|---|---|---|---|
| Region (i) | > 30 nm | ≥ 0.1 | < 6 | > 0.3 |
| Region (ii-1) | ≤ 30 nm | < 0.1 | < 6 | > 0.3 |
| Region (ii-2) | ≤ 9 nm | < 0.1 | > 6 | < 0.3 |

### 3.2.1. Optical density ($OD_{500}$)

**Figure 2-2** shows the $OD_{500}$ values for DHPC/DMPC assemblies with different XDHPC ratios, and at various total lipid concentrations. As a trend, a higher $OD_{500}$ value was obtained with an $X_{DHPC}$ value lower than 0.4, in the total lipid concentration range of 8 to 20 mM. A similar tendency was observed at a total lipid concentration of 1 mM, although the $OD_{500}$ value was relatively low. At any total lipid concentration, a critical $X_{DHPC}$ value, with an increase in the $OD_{500}$ value, was observed. Herein, the $X_{DHPC}$ range for "turbid" suspensions is showed as Region (i), and that for "transparent" ones as Region (ii). For the samples with high total lipid concentrations (15 and 20 mM), the critical $X_{DHPC}$ was around 0.3. With a decrease in the total lipid concentration, the value shifted to a higher DHPC fraction; the critical $X_{DHPC}$ values for 10, 8, and 1 mM systems were around 0.4, 0.7, and 0.9, respectively. It was therefore considered that an increase in the ratio of long-chained DMPC molecules (decrease in $X_{DHPC}$) caused the formation of larger self-assemblies. Consequently, the morphology of DMPC/DHPC assemblies is roughly indicated by the turbidity; the formation of small-sized self-assemblies can be confirmed using the transparency of the suspension ($X_{DHPC}$ > 0.6). It was thus shown that there were two types of regions from the viewpoint of turbidity of the solution.

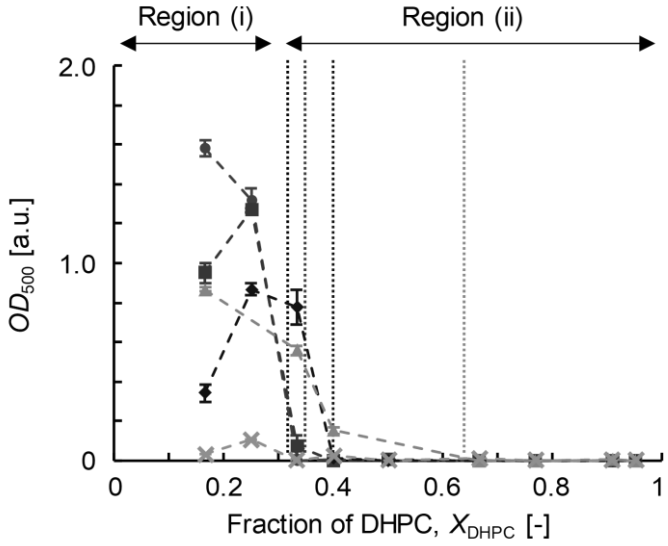


**Figure 2-2.** Turbidities ($OD_{500}$) of DHPC/DMPC solution at different DHPC fraction ($X_{DHPC}$) in various concentration of total lipid concentration at 20 mM (circle), 15 mM (square), 10 mM (diamond), 8 mM (triangle), 1 mM (cross) at 20 ºC.

### 3.2.2. Average Size estimated using DLS analysis

The size distribution of the self-assemblies formed in the DMPC/DHPC mixtures was analyzed by using DLS. As an example, the size distribution of the self-assembly at a total lipid concentration of 8 mM is shown in **Figure 2-3a**. In all the conditions tested here, a mono-dispersed distribution was obtained. The average size of the self-assembly was affected by the variation in the $X_{DHPC}$ value. As shown in **Figure 2-3b**, the average size of the DHPC/DMPC assembly was plotted against the DHPC fraction at various concentrations of total lipids. Self-assemblies with larger sizes (> 1 μm) were obtained for lower DHPC fractions ($X_{DHPC}$ < 0.3-0.4) at high total lipid concentrations (10-20 mM). In contrast, the average sizes were 10-20 nm when the $X_{DHPC}$ was higher than 0.4. A similar tendency was observed for a total lipid concentration of 8 mM, except for the self-assembly with $X_{DHPC}$ = 0.4. With a threshold value of 100 nm, self-assemblies were size-dependently classified: larger-sized assemblies (> 100 nm) as Region (i) and smaller-sized assemblies (10-20 nm) as Region (ii). The critical $X_{DHPC}$ values are denoted as dotted lines in **Figure 2-3b**, and a similar tendency was observed in $OD_{500}$ analysis (**Figure 2-2**). Particularly, in Region (ii), a self-assembly with a much smaller size (less than 10 nm) was observed at a high DHPC fraction ($X_{DHPC}$: ~0.95).

Although the $OD_{500}$ values cannot provide precise information about self-assembly size, an increase (or decrease) in the $OD_{500}$ value is suitable evidence to confirm the transformation of one state to another, especially in a continuous measurement (heating/cooling and dilution). Hence, the self-assembly that appeared in Region (i) was considered a vesicle, and that in Region (ii) as a micelle or micelle-like small assembly (i.e., bicelle). In the case of the DMPC/DHPC bicelle, a jump in the $OD_{500}$ value was observed upon heating [McKibbin *et al*., 2007], and can be applied to judge the existence of the bicelle. Among the self-assemblies categorized in Region (ii), two samples were picked-up to investigate dynamic changes in the $OD_{500}$ values upon heating (**Figure 2-4**). At a total lipid concentration of 20 mM, the DMPC/DHPC assembly with $X_{DHPC}$ = 0.4 showed a significant increase in the $OD_{500}$ value at 30 °C. At $X_{DHPC}$ = 0.95, the $OD_{500}$ value did not significantly vary upon heating and cooling, showing that the assembly state of the DMPC/DHPC assembly at $X_{DHPC}$ = 0.95 was stable, as micelle. It has been reported that a bicelle in an aqueous solution is not very stable; it transforms into a vesicle-like structure upon heating, and reversibly transforms into a bicelle upon cooling [Knight *et al*., 2016].

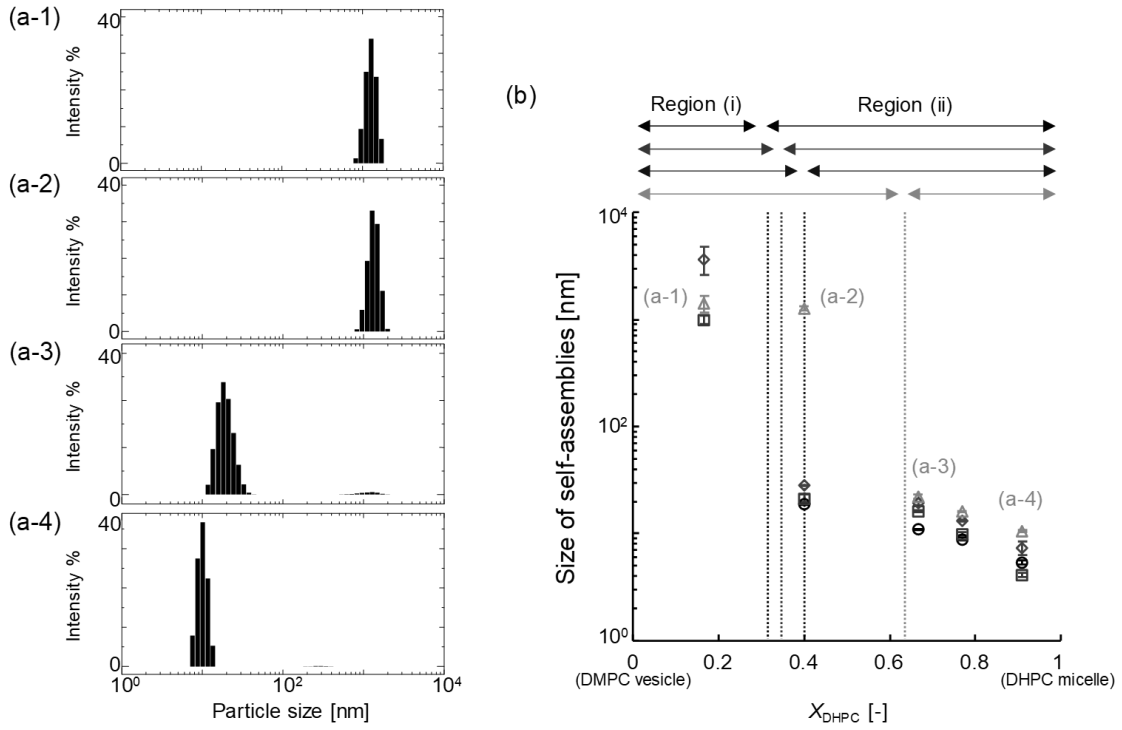


**Figure 2-3.** (a) Size distributions of DMPC/DHPC self-assemblies (8mM); 8 mM XDHPC = 0.17 (a-1), 0.4 (a-2), 0.67 (a-3), and 0.95 (a-4). (b) Average size of the self-assembly in the solution at different DHPC fraction; total lipid concentration 20 mM (circle), 15 mM (square), 10 mM (diamond), and 8 mM (triangle). A line between the arrows to show the region (i) and (ii), described in the top of figure, indicate the critical DHPC fraction that give a change in the turbidity of the solution, where the turbid solution was changed to the transparent one with increasing DHPC ratio, and the region (i) shifts rightward with the dilution.

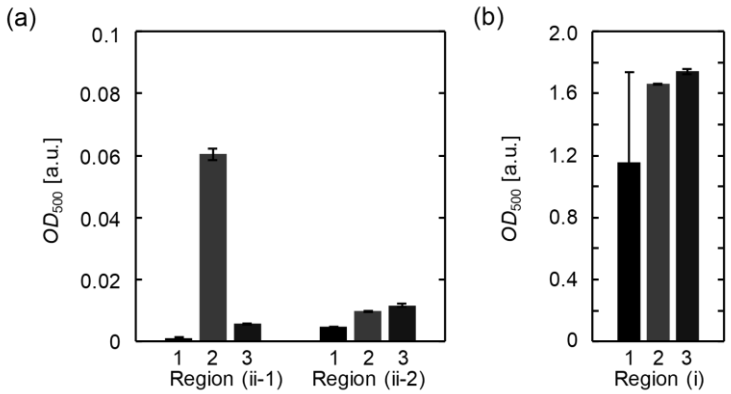


**Figure 2-4.** Temperature dependence on turbidity ($OD_{500}$) of 20 mM DMPC/DHPC self-assembly; $X_{DHPC}$ = 0.17 (Region (i)), 0.4 (Region (ii-1)), and 0.95 (Region (ii-2)). This experiment was conducted in turn heating (20 ºC (1) → 30 ºC (2)) to cooling (30 ºC (2) → 20 ºC (3)).

In summary, it was shown that a vesicle could form at Region (i), whereas a micelle or bicelle could form at Region (ii). Although it is difficult to distinguish a bicelle and micelle based on their sizes, a variation in the $OD_{500}$ can be a clue to identify bicelle formation. Considering these findings, the self-assemblies in Region (ii) were further categorized into Region (ii-1) (i.e., bicellar assembly) and Region (ii-2) (i.e., micellar assembly). To obtain more appropriate evidences, the interfacial properties can be helpful.

### 3.3. Interfacial membrane properties of DMPC/DHPC assemblies

DPH and Laurdan are widely used as membrane-bound fluorescent probes, and are known to indicate the membrane fluidity and membrane polarity, respectively. The combined use of DPH and Laurdan has been successful in investigating the membrane properties of various kinds of self-assemblies, except for those of bicelles [Mély-Goubert *et al*., 1980, Parasassi *et al*., 1990, Suga *et al*., 2013]. It is hence worthwhile to investigate the membrane fluidity and polarity of DMPC/DHPC assemblies of various compositions and concentrations.

#### 3.3.1. Membrane fluidity ($1/P_{DPH}$)

DPH is a non-polar molecule, which could be inserted into both the DHPC micelle and DMPC vesicle. By monitoring the fluorescence polarization of DPH as a parameter ($1/P_{DPH}$), the disordered state (liquid-crystalline phase, $1/P_{DPH} > 6$) and gel phase ($1/P_{DPH} < 6$) can be distinguished [Suga *et al*., 2013]. The membrane fluidities ($1/P_{DPH}$) of DMPC/DHPC assemblies were investigated as shown in **Figure 2-5**. At a total lipid concentration of 20 mM, an increase in $1/P_{DPH}$ values (> 6) was observed at high DHPC fractions ($X_{DHPC} > 0.77$). At a total lipid concentration less than 15 mM, an increase in the values was observed at DHPC fractions higher than 0.91. Region (ii) could be further divided into two regions: Region (ii-1) with $1/P_{DPH} < 6$ and Region (ii-2) with $1/P_{DPH} > 6$. The pure micelle of DHPC was categorized as Region (ii-2), revealing the disordered state of the micelle membrane. In Region (ii-1), the self-assemblies are small, and their membranes are in ordered states. Such ordered states could be due to the enrichment of DMPC, because only DMPC molecules can possibly form a gel-phase bilayer at this composition. Thus, in Region (ii-1), the DMPC/DHPC assemblies were shown to form ordered phases such as a gel phase, showing that the DMPC/DHPC bicelle was consistent with the ordered bilayer. The critical value of DHPC fraction to distinguish the two

regions gradually shifted from $X_{DHPC}$ = 0.7 (15-20 mM in total lipid concentration) to 0.9 (1 mM). DPH prefers to bind to the ordered phase [Suga *et al*., 2013]; therefore, the DMPC/DHPC assemblies with $1/P_{DPH}$ value higher than 6 were completely in a disordered state, similar to the liquid-crystalline phase.

### 3.3.2. Membrane polarity ($GP_{340}$)

In DMPC/DHPC assemblies with $X_{DHPC}$ > 0.77 (at 20 mM), the DMPC molecules did not form a gel phase (**Figure 2-1b**). In other words, the micellar structures were not perturbed by the presence of relatively longer acyl chain molecules (DMPC) at $X_{DHPC}$ values > 0.77, suggesting that DMPC molecules, having longer acyl chains as compared to DHPC, are able to diffuse in micelle membranes freely. Laurdan, having a C12 hydrocarbon chain, can also diffuse in the self-assembly membrane freely, and its emission spectrum can be used to monitor the polar environment of each DMPC/DHPC assembly.

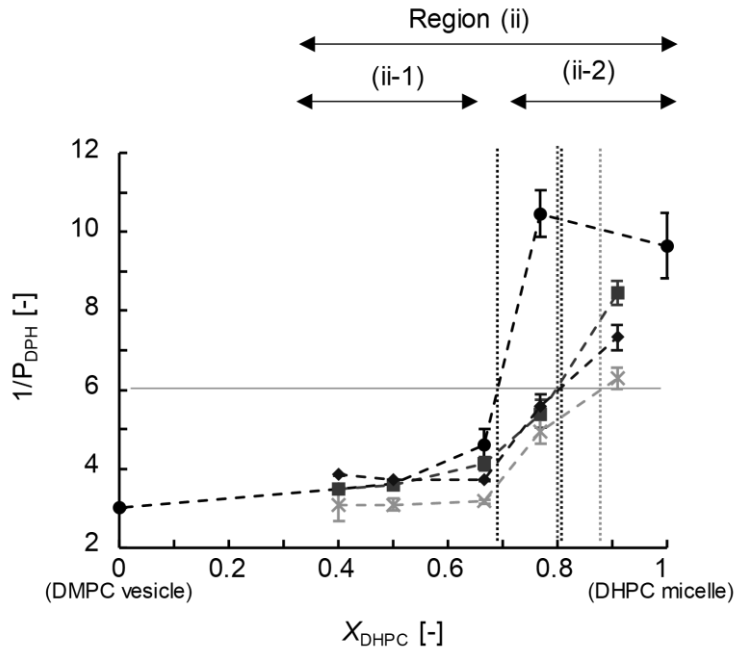


**Figure 2-5.** Membrane fluidities of DMPC/DHPC assemblies. Total lipid concentration 20 mM (circle), 15 mM (square), 10 mM (diamond), 8 mM (triangle), and 1 mM (cross). The drastic change of each value shows transition of lipid assembling state at $1/P_{DPH}$ = 6. The vertical dotted line in the figures displays the phase transition region (ii-1)/(ii-2) at each concentration: (ii-1) ordered phase, (ii-2) disordered phase.

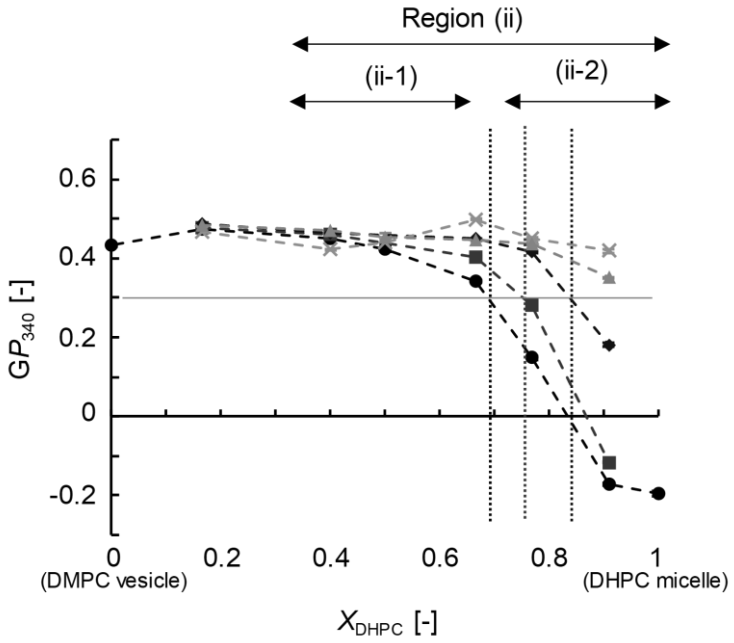


**Figure 2-6.** Membrane polarities of DMPC/DHPC assemblies; total lipid concentration 20 mM (circle), 15 mM (square), 10 mM (diamond), 8 mM (triangle), and 1 mM (cross). The drastic change of each value shows transition of lipid assembling state at $GP_{340}$ = 0.3. The vertical dotted line in the figures displays the phase transition region (ii-1)/(ii-2) at each concentration: (ii-1) ordered phase, (ii-2) disordered phase.

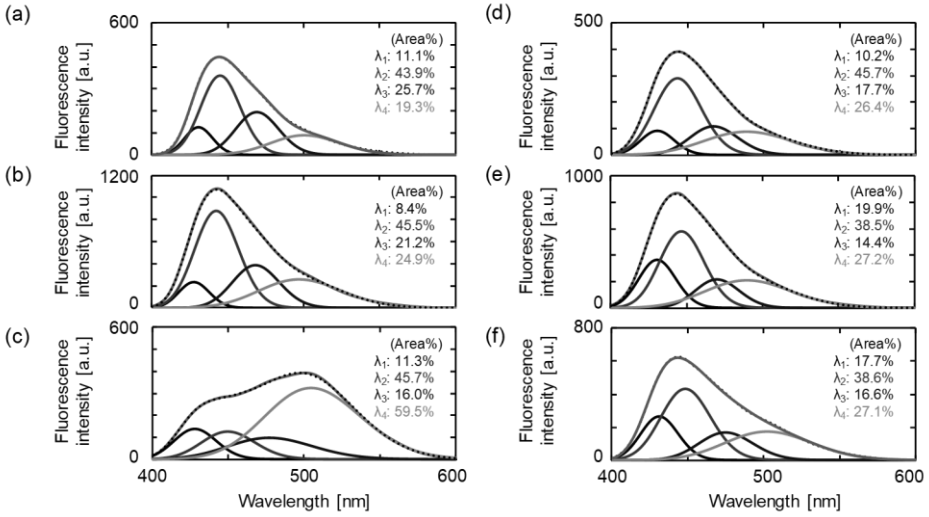


**Figure 2-7.** Spectra of Laurdan in each 20 mM DMPC/DHPC membrane at 20 ºC. (a) $X_{DHPC}$ = 0.17(Region (i)). (b) $X_{DHPC}$ = 0.4 (Region (ii-1)). (c) $X_{DHPC}$ = 0.95 (Region (ii-2)). The spectra were as follows:(d) $X_{DHPC}$ = 0.17, (e) $X_{DHPC}$ = 0.4 and (f) $X_{DHPC}$ = 0.95 at 8 mM total lipid concentration.

According to the packing of the lipid membrane, the emission properties of Laurdan can vary; thus, Laurdan is widely used to investigate the microscopic polarity at the lipid membrane interface [Parasassi *et al*., 1990]. At any concentration of total lipids, the $GP_{340}$ values did not change at low DHPC fractions ($X_{DHPC} < 0.4$) (**Figure 2-6**). However, the $GP_{340}$ values varied depending on the total lipid concentration. In this study, the $GP_{340}$ values of DMPC vesicle and DHPC micelle were used as the standard: DMPC vesicle, $GP_{340} = 0.40$ (gel phase); DHPC, $GP_{340} = -0.20$ (disordered phase). With high total lipid concentrations (15 and 20 mM), the $GP_{340}$ values slightly increased at the range of $0 < X_{DHPC} < 0.5$, suggesting a more ordered state (Region (ii-1), bicelle). The $GP_{340}$ values gradually decreased in proportion to the DHPC fraction at $X_{DHPC} > 0.6$. At the middle concentration levels (8-10 mM), the $GP_{340}$ values were constant at $0 < X_{DHPC} < 0.8$, and varied at $X_{DHPC} > 0.8$. The results of the $GP_{340}$ analysis were also helpful to identify the bicelle and micelle of DMPC/DHPC assemblies at total lipid concentrations less than 20 mM. The coexistence of DHPC could disturb the ordered properties of the DMPC vesicle [Takajo *et al*., 2010]. As compared to the pure DMPC vesicle, a slight increase in $GP_{340}$ values was observed for DMPC/DHPC assemblies at $X_{DHPC}$ of 0.33 or 0.4, suggesting more ordered (tightly packed) states of these membranes. The Laurdan emission spectrum was further analyzed by deconvolution (**Figure 2-7**). At $X_{DHPC}$ values of 0.33 and 0.4, the area fraction of $\lambda_2$ (440 nm) was slightly higher than that of pure DMPC, revealing a more stable gel phase in the bilayer region of the DMPC/DHPC assembly.

### 3.3.3. Comparison of interfacial membrane properties in Cartesian Diagram

By combining the information obtained from each fluorescent probe (DPH and Laurdan), the phase state and phase separation behavior of the membrane can be systematically discussed [Nakamura *et al*., 2015, Bui *et al*., 2016, Iwasaki *et al*., 2017]. The phase state (ordered phase or disordered phase) of the membrane can be investigated based on the positioning of the obtained data in the Cartesian diagram, where the quadrants are set using the transition of the membrane properties (polarity (*y*-axis) and membrane fluidity (*x*-axis)) [Suga *et al*., 2013]. By plotting the data obtained from each self-assembly system, the interfacial membrane properties of various kinds of self-assemblies can be directly compared [Nakamura *et al*., 2015, Iwasaki *et al*., 2017]. The details are summarized in the previous work (see the supporting materials of Bui *et al*.). In **Figure 2-8**, the DHPC membranes show a significantly

higher membrane fluidity and a low $GP_{340}$ value, which appeared in the boundary region of the first (partially disordered state) and fourth quadrants (fully disordered state). This clearly reveals that the DHPC micelle membrane is in a disordered state, showing higher fluidity.

For DMPC/DHPC assemblies with various $X_{DHPC}$ and total lipid concentrations, the obtained $GP_{340}$ and $1/P_{DPH}$ values were plotted in the Cartesian diagram, together with some standard data (obtained from liposomes, Nakamura *et al*. 2015). The data for the DMPC/DHPC

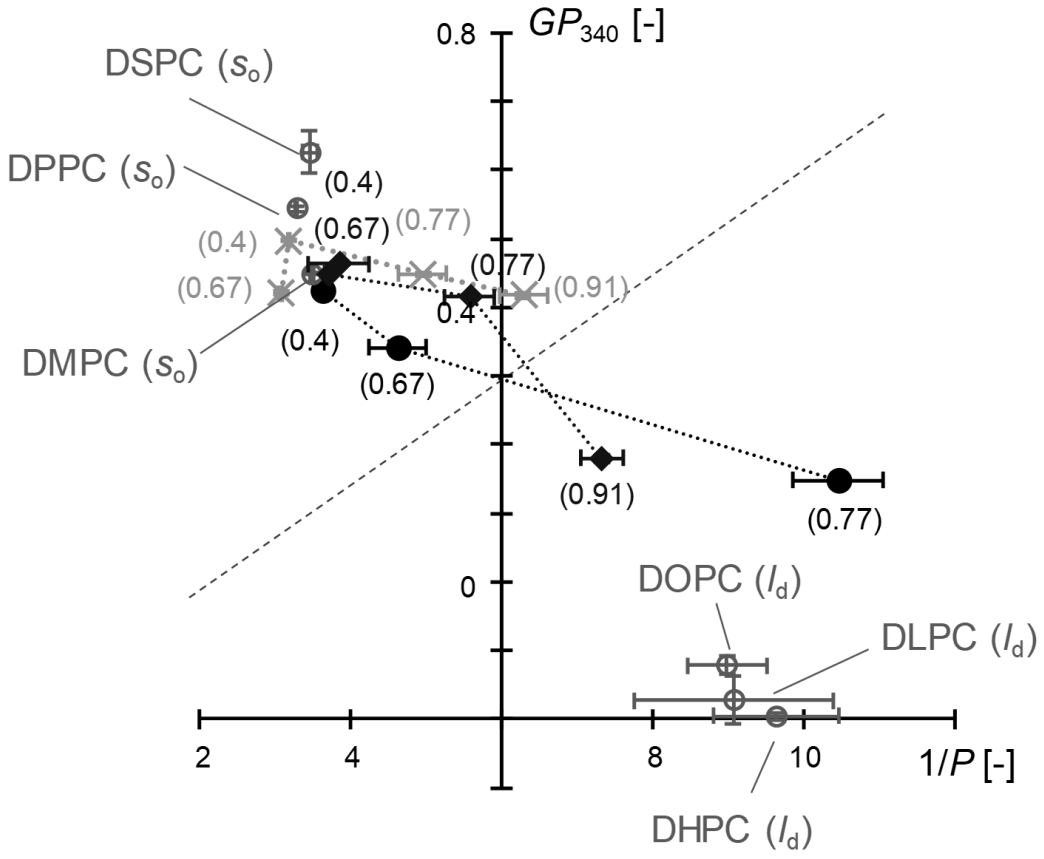


**Figure 2-8.** Comparison of interfacial membrane properties in Cartesian diagram. T = 20 ºC, DMPC/DHPC at 20 mM (filled circle), 10 mM (diamond), and 1 mM (cross). The value in the bracket neighboring to the data point show the DHPC fractions $X_{DHPC}$. The position plotted in the Cartesian diagram indicates the phase state of each membrane: the first and fourth quadrants for disordered phase, and the second quadrant for ordered (gel) phase. The reference values of various liposomes were plotted on the diagram (empty circle); $s_o$: solid ordered phase, $l_o$: liquid ordered phase, $l_d$: liquid disordered phase. The broken line crossing at $1/P_{DPH} = 6$ and $GP_{340} = 0.3$ is a boundary of ordered phase and partially-disordered phase.

mixtures (20 mM) at rather low DHPC fractions ($X_{DHPC}$ = 0.4 and 0.67) were plotted in the second quadrant, suggesting that these self-assemblies had an ordered bilayer as well as DMPC vesicles in the gel phase. In contrast, at $X_{DHPC}$ = 0.77, the data position was in the first quadrant. This indicates that the membrane fluidity was higher than that of the DHPC micelle, whereas the membrane was less hydrated as compared to the micelle. Since DHPC can behave as a detergent (surfactant), a mixed micelle [Fernández *et al*., 2002, Kučerka *et al*., 2011] might be formed in DMPC/DHPC mixture systems, but it is still difficult to compare the difference between a bicelle and mixed micelle. The variation in the membrane properties at $X_{DHPC}$ = 0.7 suggest that the assemblies were in disordered phases. It was difficult to distinguish the bicelle and micelle based on their sizes; in contrast, their interfacial membrane properties were clearly different. Hence, the DMPC/DHPC assemblies with $X_{DHPC} \geq 0.77$ were in a disordered phase, wherein DMPC molecules did not form (ordered) a bilayer. In addition to the unique structural characteristics of the bicelle, the interfacial properties also contribute to the investigation of the "ordered state" of the bicelle composed of DMPC/DHPC mixtures.

Limited to DMPC/DHPC systems, the bicelle assemblies required the interfacial membrane properties of the gel phase. By defining these assemblies as "gel-bicelles," a micelle (Region (ii-2)) and gel-bicelle (Region (ii-1)) can be clearly distinguished based on their interfacial properties. Similarly, a systematic characterization was carried out for the DMPC/DHPC assemblies at total lipid concentrations of 1-10 mM. While the $1/P_{DPH}$ and $GP_{340}$ values at $X_{DHPC}$ = 0.77 slightly changed, the interfacial membrane properties of the assemblies with $X_{DHPC}$ of 0.4 and 0.67 remained constant. In vesicle systems, the $GP_{340}$ values varied depending on the temperature: $GP_{340} > 0.3$ in gel phase ($T < T_m$), and $GP_{340} > -0.2$ in fluid phase ($T > T_m$) [Cyrus *et al*., 2012]. The $GP_{340}$ value gradually decreases at temperatures slightly higher than the $T_m$. When the $GP_{340}$ value is lower than 0.3, the membrane is heterogeneous (under phase transition, coexistence of two phases). These results imply that ordered membranes ($1/P_{DPH} < 6$, $GP_{340} > 0.3$) were maintained at $X_{DHPC}$ of both 0.4 and 0.67, at low total lipid concentrations. This is the first investigation of the interfacial membrane properties of DMPC/DHPC assemblies. I found that the bicelle membranes (Region (ii-1)) were in ordered states; the bilayer membranes are tightly packed as well as or better than the pure gel phase of DMPC vesicles.

### 3.4. Discussion on phase behavior of DMPC/DHPC assemblies

DMPC/DHPC self-assemblies were classified into three categories: Region (i), Region (ii-1), and (ii-2). The assemblies of Region (ii-1) were small micelles, which exhibited an ordered phase similar to that of the gel-phase vesicles. Hence, they can be considered as gel-phase bicelles. The phase behavior of the DMPC/DHPC assemblies at 20 ºC is showed as a diagram (**Figure 2-9**). The self-assemblies at Region (i) were observed, typically, with excess DMPC and less DHPC, due to which the DMPC/DHPC mixtures could form vesicles independent of the total lipid concentration. On the contrary, the transparent solutions including the self-assemblies of small size (less than 10 nm) were observed in the condition with excess DHPC and less DMPC (Region (ii-2)). These concentration levels well correspond with the well-known and usual conditions to prepare the DMPC liposome and DHPC micelle.

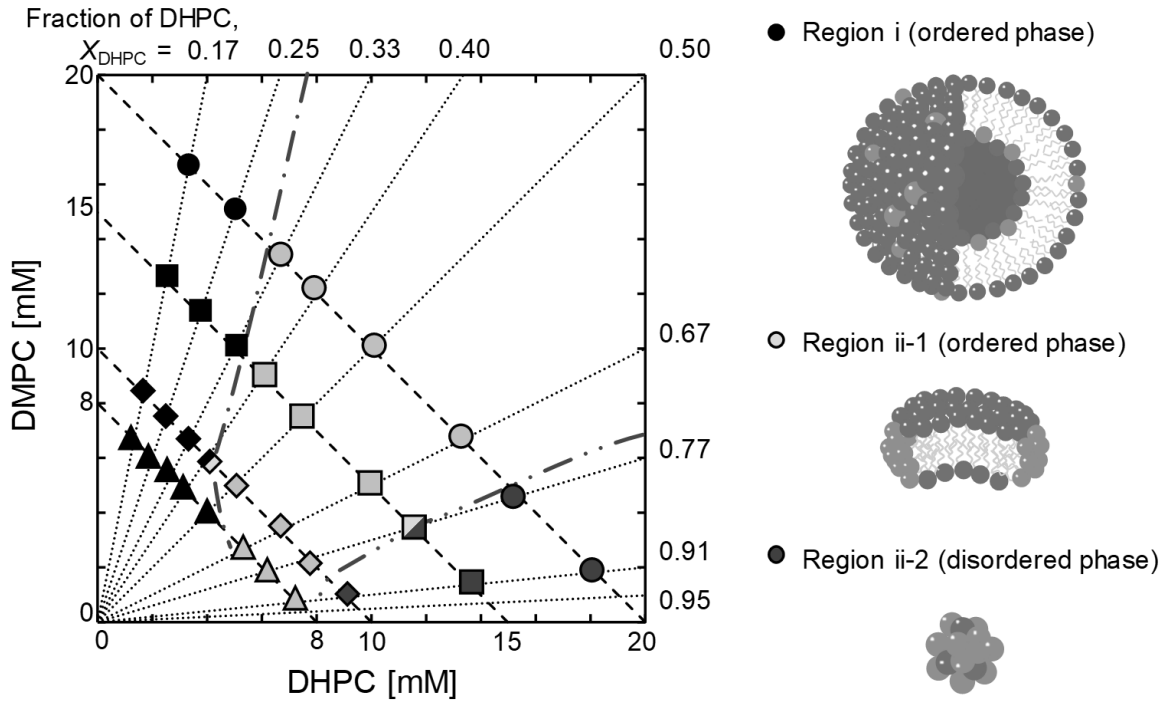


**Figure 2-9.** Phase diagram for DMPC/DHPC assemblies at 20 ºC, investigated by systematic characterization. The bold filled squares showed the increasing turbidities each DHPC fractions as the morphological change. The phase boundary concentrations of $X_{DHPC}$ = 0.77, 0.4, and 0.33, are 9 mM, 12 mM, and 16 mM, respectively (described in total lipid concentration). The light- and dark-gray circles are transparent assemblies due to form small assemblies. These had each membrane property; (light-gray) ordered phase, (dark-gray) disordered phase.

There is an extra region to obtain self-assembly with certain characteristics such as transparent solution, small size (10-20 nm), dependence of size on the DHPC fraction, rather ordered properties of surface (plotted at the second quadrant in the Cartesian diagram), and temperature-sensitive behavior of optical density. The gel phase is beneficial to form a planar bilayer; however, it is notable that the essential property of a bicelle should be magnetic orientation originating from its discoidal structure [Sanders *et al*., 1992]. In the case of the bicelle or discoidal assembly in the TEM image [van Dam *et al*., 2004], the self-assembly has two different patterns of shapes, such as face-on (sticky image) and edge-on (discoidal image). Together with the findings obtained in this study, a geometric consideration of the self-assembly, focusing on the molar ratio of DHPC and DMPC at Region (ii-1) (DMPC/DHPC = ~1:2-2:1), suggests that a bicelle-like structure could form. **Figure 2-10a** shows the TEM image of the DMPC/DHPC assembly with $X_{DHPC}$ = 0.5 (total lipid concentration of 20 mM), revealing a non-spherical shape, rather a discoidal shape. As schematically showed in **Figure 2-10b**, since both shapes (face-on and edge-on) could be revealed, the DMPC/DHPC assembly that satisfies a small size (< 30 nm) and "ordered" interfacial properties could be considered as a bicelle.

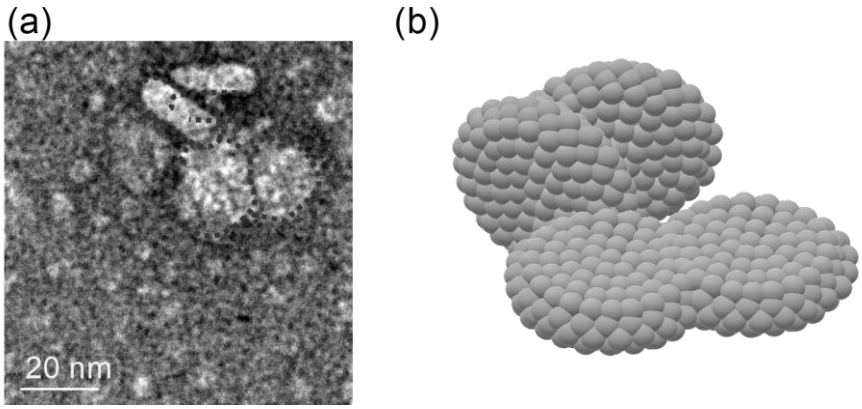


**Figure 2-10.** TEM images of DMPC/DHPC mixture; (a) $X_{DHPC}$ = 0.4, 20 mM, and (b) the image of the bicelle like structure.

## 4. Strategy to Prepare Membranous Functional Materials

As the summary of the classification of self-assemblies in DMPC/DHPC system, a general scheme to quality of the properties is shown in **Figure 2-11**. Together with "*bicelle*" diagram (**Figure 2-9**), the condition to prepare the self-assemblies can be optimized based on this "*qualitative*" scheme. The application of the diagram and scheme to utilization of bicelles in various membranous materials will be shown in the next chapters. The discoidal membrane was utilized for the nano-platform of functional molecules (chlorophyll *a*) in chapter 3. Furthermore, I focus on the morphological change of bicelle upon its dilution. The developments of large membrane materials, such as vesicles and planar membranes (supposed bilayer membranes) are shown in chapter 4 and 5, respectively. A sophisticated protocol of the preparation of membranous functional materials is then constructed after clarifying the control factors for the continuous preparation of membranous materials using bicelles.

The conventional membrane preparations are developed to apply the materials for functional materials. The thin film hydration can prepare a vesicle with high yield, regularly [Johnson *et al.*, 1971, Nakamura *et al.*, 2015]. Although organic solvents rarely remain in the membranes in this method, the preparation process is not suitable to continuous method because of its multi-steps and preparing morphology. Reverse phase evaporation (RPE) and similar semi-batch type methods are invented to solve the problem [Szoka *et al.*, 1978, Imure *et al.*, 2003]. Furthermore, continuous systems facilitate the industrial application of membrane materials [Wade *et al.*, 2017]. The preparation method based on RPE remined organic solvents in the hydrophilic inner membrane [Karamdad *et al.*, 2015], which is expected to weaken the packing of the bilayer membrane and to be different membrane properties. Therefore, a design of membrane preparation is required for various membranous materials.

In this chapter, I obtained the systematic information on the membrane properties, such as membrane fluidity and membrane polarity, of DMPC/DHPC self-assemblies with dilution at $C_{\mathrm{total}}$ = 1-20 mM. The assemblies showed variation of membrane properties at each condition (component and concentration) while transforming the morphology from bicelle to vesicle in dilution process. The morphological change occurred by removing DHPC molecules from the edge of a bicelle. I proposed that the controlling concentration of DHPC was a key factor for sophistication of preparation protocol of membranous functional materials. The following chapter, especially chapter 4 and 5, described the result of the preparation of the membranous materials based on this proposal and the result of chapter 2.

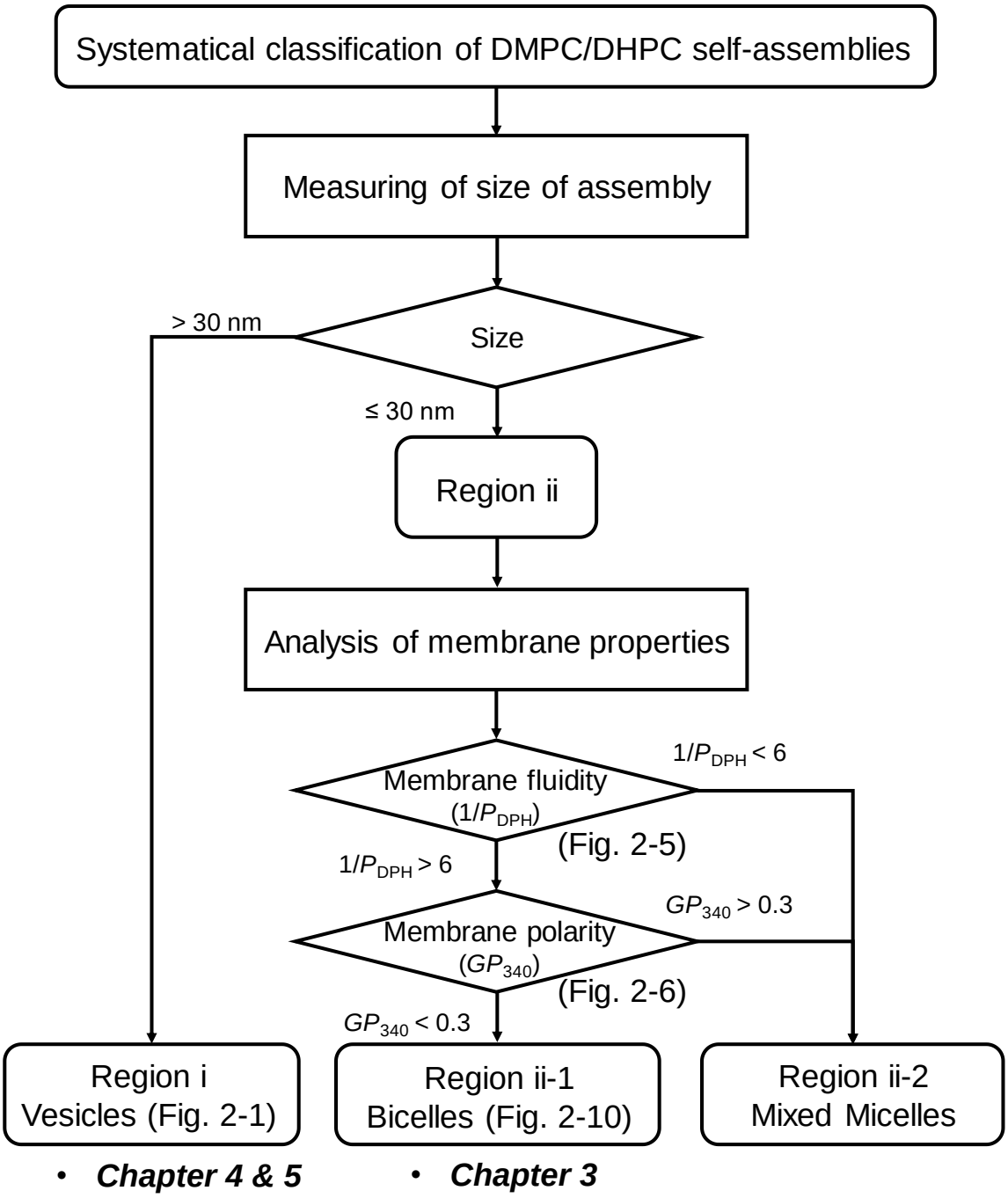


**Figure 2-11.** Scheme for classification of morphology of DMPC/DHPC self-assemblies. Region (i) and (ii-2) were applied to membrane materials in the following chapters.

## 5. Summary

I systematically characterized self-assemblies composed of DMPC/DHPC at total lipid concentrations less than 20 mM (< 1wt% lipid). The assemblies were categorized as Region (i), Region (ii-1), and Region (ii-2), in which the dominant state was large vesicle (> 30 nm), gel-bicelle (≤ 30 nm, "*ordered*" interfacial properties), and micelle (≤ 30 nm, "*disordered*" interfacial properties), respectively. In particular, the bicelles observed in the DMPC/DHPC mixture systems exhibited both low membrane fluidity ($1/P_{DPH} < 6$) and high membrane polarity ($GP_{340} > 0.3$). This reveals that the DMPC/DHPC bicelle structure could be observed only below 23 °C ($T < T_m$ of DMPC), because the mean head group area of DMPC increases and the bilayer packing decreases in the disordered phase. The transparency of the suspension is a good indicator to roughly judge the size of the self-assembly [Matsuzaki *et al*., 2000]. In the conditions of fixed total lipid concentration, the self-assembly structure could be controlled using the DHPC fraction ratio: bicelle for $0.33 \leq X_{DHPC} \leq 0.67$ and micelle for $X_{DHPC} \leq 0.77$. In the conditions of fixed $X_{DHPC}$ (especially at $0.33 < X_{DHPC} < 0.4$), dilution lead to transformation from bicelle to vesicle, with a jump-up in turbidity. The findings of this study are summarized in a diagram, which reveals the phase behavior of DMPC/DHPC assemblies at 20 ºC. Bicelle assemblies can be used as lipid sources in supported lipid bilayer preparation [Kolahdouzan *et al*., 2017]. Based on the phase equilibrium, DHPC molecules can be excluded from bicelle membranes by dilution. Utilizing this, bicelle assemblies can be applied for a continuous vesicle preparation process flow system.

# Chapter 3

## Preparation of Discoidal Functional Membrane;

## Aggregation of Chlorophyll *a* (Chl*a*) on DMPC/DHPC Bicelle

### 1. Introduction

Chlorophyll (Chl) molecules are natural photosynthetic pigments that form lateral aggregates in biological membranes of plant and photosynthetic bacteria [Niwa *et al*., 2014]. In a light-harvesting (LH) systems, the formation of Chl aggregates can expand the range of absorbance bands in the near-infrared region, which enables the capture of more photons over a wider range of wavelength in sunlight [Wang *et al*., 2009, Chen *et al*., 2011]. In the LH1 complex, chlorophyll *a* (Chl*a*) is usually present in an aggregated state due to the interaction with the histidine residue of the apoprotein. In this configuration, the Chl*a* molecules align in an orderly arrangement around the core protein in the lipid bilayers [Umena *et al*., 2011, LeBlanc *et al*., 2014, Yaghoubi *et al*., 2015, Bennett *et al*., 2016]. LH1 reconstructed on lipid membrane system can form an artificial photo antenna unit focusing on its light harvesting functions [Niroomand *et al*., 2017, 2018]. To maintain the function of LH1, the scaffold membrane must be optimized: Niroomand *et al*. reported about the importance of the phytyl structure of phospholipids in the reconstruction of LH1 in liposome membranes [Niroomand, Mukherjee *et al.,* 2017]. The absorbance wavelength range of LH1 units can be controlled by the aggregation state of antenna molecules. Aggregation of Chl*a* contributes to the absorption of red photons ($\lambda$ = 700–750 nm) [Porcar-Castell *et al*., 2014]. Chl*a* J-aggregate are crucial in expanding the absorbance wave range. In general, only a small fraction of Chl*a* (2–3%) remains in the living membranes [Santabarbara, *et al.,* 2001, 2001, 2006]. These collective findings have spurred investigations of the aggregation behavior of Chl*a* in biological and artificial photosynthesis systems.

Metal-porphyrin derivatives, including Chl*a*, have been used as LH antennae in solar energy systems [Toyoshima *et al*., 1977, Tsujisho *et al*., 2006, Patwardhan *et al*., 2012]. Chl can act as an electron donor/acceptor group for dye-sensitized solar cells. For example, zinc (Zn)-chlorophyll aggregates formed on a photo-electrode can enable efficient electron transfer

[Li *et al*. 2015]. Chl*a* has been utilized as photosensitizer to promote the photo-reduction of aqueous methyl viologen ($MV^{2+}$). Surfactants are required for this application because Chl*a* molecules are poorly soluble in aqueous media [Tomonou *et al.,* 2002, 2002, 2004]. The water-soluble porphyrins have also been studied to investigate their photo-reduction activities [Amao *et al*. 2002, Kondo *et al*. 2005]. Dimer formation of Zn-porphyrin decreases photo-reduction of $MV^{2+}$ [Kondo *et al*., 2015]. It is assumed that the J-aggregate of Chl*a* influences the photo-reduction of $MV^{2+}$, while this activity has not been verified due to the difficulty in forming J-aggregates.

Several reports have addressed the aggregation behaviors of Chl*a* in phospholipid membrane systems. Chl*a* molecules can embed into egg-yolk lecithin liposomes as a monomer (non-aggregation) [Bialek-Bylka *et al*., 1986]. It has been reported that 1.8 mol% of Chl*a* incorporated into 1-palmitoyl-2-oleoyl-*sn*-glycero-3-phosphocholine liposomes can form domains, suggesting the formation of lateral aggregates of Chl*a* [Yoshimoto *et al*., 2013]. Milenkovic *et al.* reported the influence of vesicle lamellarity on the Soret band and *Q* band spectra of Chl*a* because of the location (i.e., polar environment around chromophore) of Chl*a* [Milenkovic *et al*., 2013]. The presence of cholesterol in 1,2-dipalmitoyl-*sn*-glycero-3-phosphocholine vesicles alters the fluidity of the membrane and shifts the Soret band and *Q* band spectra of Chl*a* [Hiromitsu *et al*., 1987]. The Soret band spectra of Chl*a* can change depending on the phase state of liposome membranes [Taguchi *et al*., 2017]. These results clearly indicate that the local environment around Chl*a* is crucial in regulating the aggregation behaviors of Chl*a* molecules. However, the aggregated Chl*a* (J-aggregate) have rarely been observed at lower Chl*a* concentrations in membranes (molar fraction of Chl*a* [Chl*a*%] < 10 mol%) [Hoshina, 1981]. In seeking a possible platform for the formation of J-aggregates of Chl*a*, vesicles and other self-assembly systems, including micelles and bicelles [van Dam *et al*., 2004], should be studied.

The aim of this chapter is to demonstrate the advantage of a discoidal membrane for a core membrane material via the aggregation behaviors of Chl*a* molecules in the self-assembly of 1,2-dimyristoyl-*sn*-glycero-3-phosphocholine (DMPC), which is relatively longer, and 1,2-dihexanoyl-*sn*-glycero-3-phosphocholine (DHPC), which is relatively shorter, and to characterize the aggregated Chl*a* (**Scheme 3-1**). First, to understand the behavior of Chl*a* molecules with a phase state of bilayer membrane, the physicochemical properties of the

liposomes modified with Chl*a* were systematically characterized by using spectroscopic analyses. The fluidities of a bulk membrane of the lipid bilayer and the local membrane around a chromophore were characterized by using fluorescent spectra of 1,6-diphenyl-1,3,5-hexatriene (DPH) and Chl*a* itself, respectively. Next, using parameters such as the fraction of DHPC ($X_{DHPC}$) in DMPC/DHPC and total lipid concentration ($C_{lipid}$) calculated as [DMPC]+[DHPC]+[Chl*a*], the lipid membrane compositions capable of inducing J-aggregate formation of Chl*a* in aqueous solution were investigated. The local hydrophobicity around Chl*a* in DMPC/DHPC membranes was analyzed based on the deconvolution of the Soret band spectrum (400-440 nm). The photo-reduction activities of Chl*a* J-aggregates induced in DMPC/DHPC membranes were evaluated by monitoring the reduction kinetics from $MV^{2+}$ to $MV^{+\bullet}$.

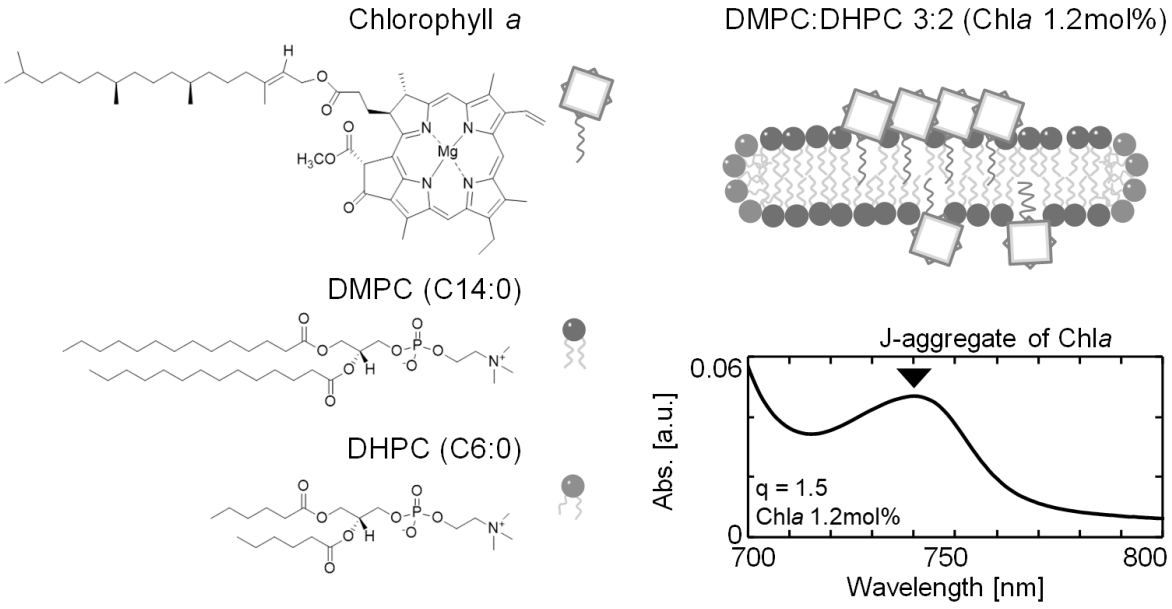


**Scheme 3-1** Chl*a* aggregation on bilayer of DMPC/DHPC bicelle.

## 2. Materials and Methods

### 2.1. Materials

Mg-chlorophyll a (Chl*a*) was purchased from Senshu Scientific Co., Ltd. (Tokyo, Japan). 1,2-Dipalmitoyl-*sn*-glycero-3-phosphocholine (DPPC, C16:0: $T_m$ = 41 ºC), 1,2-dihexanoyl-*sn*-glycero-3-phosphocholine (DHPC, C6:0) and 1,2-dimyristoyl-*sn*-glycero-3-phosphocholine (DMPC, C14:0: $T_m$ = 23 ºC) were purchased from Avanti Polar Lipids, Inc. (Alabaster, AL, USA). 1,6-Diphenyl-1.3.5-hexatriene (DPH) was purchased from Sigma-Aldrich (St. Louis, MO, USA). 1,1'-Dimethyl-4,4'-bipyridinium dichloride (Methyl viologen, MV) was obtained from Tokyo Chemical Industry Co., Ltd. (Tokyo, Japan). Ethylenediaminetetraacetic acid (EDTA) was purchased from DOJINDO Molecular Technologies, Inc. (Kumamoto, Japan). Ultrapure water was prepared with the Millipore Milli-Q system (EMD Millipore Co./Direct-Q® UV3).

### 2.2. Liposome and bicelle preparation by thin-film hydration method

A chloroform solution of phospholipids was dried in a round-bottom flask by rotary evaporation under vacuum [Komatsu *et al.,* 1995]. The resulting lipid films were dissolved in chloroform once more, and the solvent was evaporated. This operation was repeated at least twice. The obtained lipid thin film was kept under high vacuum for at least 3 h and then hydrated with distilled water at room temperature. The obtained DPPC liposome suspension was frozen at -80 °C and then thawed at 60 ºC to enhance the transformation of small liposomes into larger multilamellar vesicles (MLVs). This freeze-thaw cycle was repeated five times. MLVs were used to prepare large unilamellar liposomes by extruding the MLV suspension 11 times through 2 layers of a polycarbonate membrane with a mean pore diameter of 100 nm using an extruding device (Liposofast; Avestin Inc., Ottawa, Canada). Chl*a* (2mol%) included liposomes were also prepared by the same method. On the other hand, the obtained DMPC/DHPC suspension was frozen at -80 ºC and then thawed at 40 ºC ($T > T_m$ (DMPC)); this freeze-thaw cycle was repeated five times. Figuring the composition of DMPC/DHPC membranes, the fraction of DHPC is described as follows: $X_{DHPC}$ = [DHPC]/([DMPC]+[DHPC]). The Chl*a*–incorporated phospholipid membranes were prepared by the same method described in the above. Total lipid concentration is described as $C_{lipid}$ = [DMPC] + [DHPC] + [Chl*a*]. Each sample was incubated at 4 ℃ for 1 week from preparation, and then was used for following measurements. For the

diluted samples, they were incubated at 20 ºC at least for 1 h in dark, and then were applied for measurements.

### 2.3. Evaluation of the membrane fluidity of liposomes

The fluidity of the liposome membrane was evaluated based on the previous reports [Lentz *et al*., 1989, Hayashi *et al.*, 2011]. A fluorescent probe DPH was added to a liposome suspension with a molar ratio of lipid/DPH = 250/1; the final concentrations of lipid and DPH were 100 and 0.4 μM, respectively. The fluorescence polarization of DPH (Ex. = 360 nm, Em. = 430 nm) was measured using a fluorescence spectrophotometer (FP-8500; JASCO, Tokyo, Japan) after incubation at 30 ºC for 30 min. The sample was excited with vertically polarized light (360 nm), and emission intensities both perpendicular ($I_\perp$) and parallel ($I_\parallel$) to the excited light were recorded at 430 nm. The polarization ($P$) of DPH was then calculated by using the following equations:

$$P_{DPH} = (I_\parallel - GI_\perp)/(I_\parallel + GI_\perp)$$

$$G = i_\perp / i_\parallel$$

where $i_\perp$ and $i_\parallel$ are emission intensity perpendicular and parallel to the horizontally polarized light, respectively, and $G$ is the correction factor. The membrane fluidity was evaluated based on the reciprocal of polarization, $1/P_{\mathrm{DPH}}$.

### 2.4. Differential scanning calorimetry (DSC) analysis of liposomes

A differential scanning calorimeter (DSC-60; Shimadzu, Kyoto, Japan) was used for calorimetric measurements of liposomes. Chl*a*/liposome suspension (50 mM, 20 μL) samples were sealed in an alumina hermetic pan. Thermograms were obtained with a heating and cooling rate of 2 °C/min between 25 and 50 °C. There were no significant differences between the thermograms in heating and in cooling processes for one sample. At least, three cycles of heating/cooling were repeated in each experiment, and the accumulated data were used for the calculation of $T_{\mathrm{m}}$ values.

### 2.5. Fluorescence polarization of Chl*a* on liposomes

The fluorescence polarization of Chl*a* (Ex. = 584 nm, Em. = 670 nm) was measured using a fluorescence spectrophotometer (FP-8500; JASCO, Tokyo, Japan) after incubation at

different temperatures (30-50 ºC). The samples were excited with vertically polarized light, and emission intensities both perpendicular ($I_{VH}$) and parallel ($I_{VV}$) to the excited light were recorded at 670 nm. The steady-state polarization, $P$, of Chl*a* was calculated by using the following equations:

$$P = (I_{VV} - G\, I_{VH}) / (I_{VV} + G I_{VH})$$

$$G = I_{HV} / I_{HH}$$

where the different intensities are the steady-state vertical and horizontal components of the fluorescence emission, with excitation vertical ($I_{VV}$ and $I_{VH}$, respectively) and horizontal ($I_{HV}$ and $I_{HH}$, respectively) to the emission axis. The latter pair of components is used to calculate the $G$ factor.

### 2.6. UV-vis spectroscopy measurement

A UV-Vis spectrum of each self-assembly was measured by UV-1800 Spectrophotometer (Shimadzu, Kyoto, Japan), using a quartz cuvette with a light path length of 1 cm. Baseline was corrected by ultrapure water. To assess the morphology of assemblies, the turbidities of the sample solutions were recorded at 500 nm ($OD_{500}$). For each sample, the absorbance was recorded from 300 to 800 nm, at 20 ºC.

### 2.7. Deconvolution analysis of UV-vis spectra of Chl*a*

Chl*a* molecules have two overlapping absorption at Soret band (300-500 nm). The absorption band is split into four bands due to asymmetric structure. The overlapping band was deconvoluted by Peak Fit v.4.12 (Systat Software Inc., San Jose, CA, USA) [Taguchi *et al*. 2017]. The peak intensity ratio of $B_x$ (420 nm) and $B_y$ (440 nm) were investigated.

### 2.8. Photo-induced reaction of methyl viologen (MV)

The light energy can be efficiently transferred from Chl*a* to $MV^{2+}$, as the $MV^{2+}$ molecules act as electron acceptors in the presence of photosensitizer [Kondo *et al*., 2015]. The experiments were conducted according to a literature (**Scheme 3-2**) [Taguchi *et al*., 2017]. Briefly, a solution of ethylendiaminetetraacetic acid (EDTA: total concentration of 20 mM) containing 2 mM $MV^{2+}$ was prepared, and the solution pH was adjusted to neutral (6.9-7.2) by adding NaOH. In case of DPPC liposome, after 30 min incubation at several temperatures (20,

30, 40, 50 ºC), the solution was irradiated with 500 W Xenon lamp (Optical modulex, Ushio Inc.) at a distance of 30 cm. In contrast, Chl*a*-incorporated DMPC/DHPC suspensions were added to this solution; the final concentrations of lipid [DMPC+DHPC] and Chl*a* (0.3mol% vs. lipids) were 0.83 mM and 2.5 μM, and the final volume of sample was 3 mL. The accumulated $MV^{+\bullet}$ concentration was determined by the absorbance at 603 nm using the molar coefficient 13,000 $M^{-1}cm^{-1}$ [Watanabe *et al*., 1982]. The photo-reduction of MV was outlined as follows.

$$Chlorophylla\ (Chla) \xrightarrow{hv} Chla^*$$

$$Chla^* + MV^{2+} \xrightarrow{k_r} Chla^{+\cdot} + MV^{+\cdot}$$

$$Chla^{+\cdot} + EDTA \rightarrow Chla + EDTA_{ox}$$

The reaction rate constant ($k_r$) of the $MV^{+\bullet}$ accumulation was calculated by assuming the first-order kinetic model, $[MV^{+\bullet}] = A_m[1\text{-}\exp(-k_r t)]$, wherein $A_m$ represents saturated product concentration [Kondo *et al*., 2015]. The initial rate constant Vmax was calculated as the accumulation rate of $MV^{+\bullet}$ at 0-to-20 min span, and turnover number was calculated as $k_{cat} = V_{max}/[Chla]$.

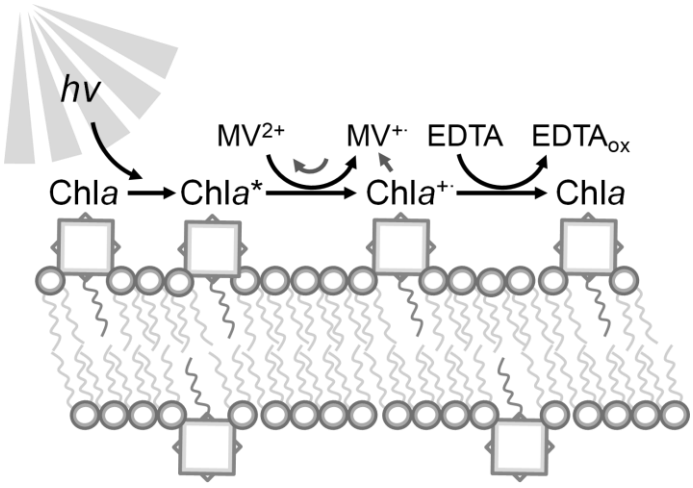


**Scheme 3-2** Photo-reduction of methyl viologen by excited Chl*a* on membrane.

## 3. Results and Discussion

### 3.1. Behaviors of Chl*a* Molecules on the bilayer of DPPC Membrane

In order to study the behaviors of Chl*a* molecules on a liposome membrane, UV-vis spectra of Chl*a* on the DPPC liposome membrane (DPPC/Chl*a*) were analyzed. As shown in **Figure 3-1**, the DPPC/Chl*a* was found to show Soret band (350 – 450 nm) and *Q* band (500 – 700 nm) similar to Chl*a*. In addition, the absorbance at the Soret band increased by raising temperature. This temperature dependence is considered to be caused by the activated interactions between Chl*a*-Chl*a* and Chl*a*-lipid molecules. It has been reported that the excitonic couplings among the Soret and $Q_y$ transitions were due to the pigment self-aggregates of Chl*a* molecules in a chlorosome, by assuming the directions of the transition-dipole vectors of the Chl*a* molecular planes [Shibata *et al*. 2010].

The membrane fluidity of the liposome modified with Chl*a* was analyzed by using DPH as a fluorescence probe. **Figure 3-2a** shows the temperature dependence of the membrane fluidity ($1/P_{DPH}$) of the DPPC liposomes with and without Chl*a*. While the $1/P_{DPH}$ value of the DPPC liposome was not changed below the $T_m$ (41.0 ºC), the $1/P_{DPH}$ value increased with the increase of the temperature at $T > T_m$, and reached a plateau (~13). A similar tendency was also observed in the case of the DPPC liposome modified with Chl*a*, except that the $T_m$ value was slightly shifted to the higher temperature ($T_m$ = 42.3 ºC) and that the $1/P_{DPH}$

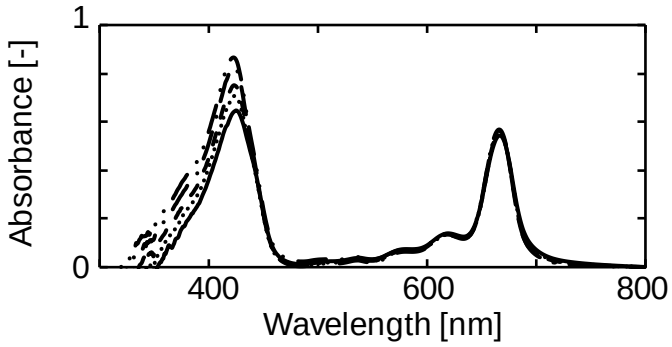


**Figure 3-1**. UV-vis spectra of the DPPC liposome with Chl*a* (DPPC/Chl*a*) liposome: (solid) 30 ºC, (dotted) 40 ºC, (broken) 41 ºC, (dot-dash) 42 ºC, and (two-dot chain) 50 ºC. These spectra were proofread by spectra for only the DPPC liposome. Soret: band 350-450 nm, *Q* band: 500-700 nm. These spectra were proofread by spectra for only DPPC vesicle.

value at the plateau (~9) was lower than that of the DPPC liposome. These results indicate the following: As Chl*a* possesses a hydrophobic chain and can be inserted into lipid bilayer, Chl*a* suppressed the fluidity of the DPPC membrane via interactions between DPPC and Chl*a* even after the fluidity increased over the phase transition temperature.

In order to estimate the ordered orientation of Chl*a* molecules in the DPPC membrane, the fluorescence polarization of Chl*a* was measured at various temperatures by a similar method used in membrane fluidity. **Figure 3-2b** indicated the temperature dependence of the reciprocal value of fluorescence polarization of Chl*a* ($1/P_{Chla}$). Below the $T_m$ (40.2 ºC), the $1/P_{Chla}$ value increased with the increase in temperature; the value was drastically increased at the $T_m$ and reached a constant value. It was previously reported that Mn-(5,10,15,20-tetrakis [1-hexadecylpyridium4-yl]-21H,23H-porphyrin) containing liposomes also showed similarity in the temperature dependence of membrane fluidities [Umakoshi *et al.,* 2008]. On the contrary

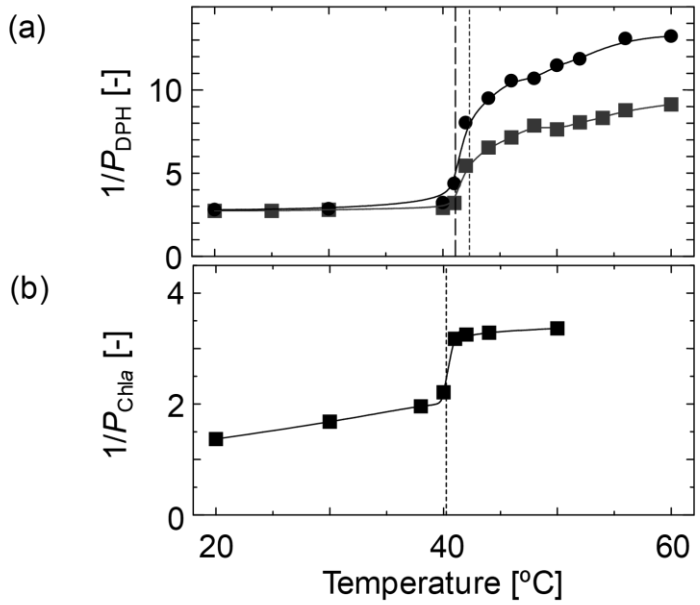


**Figure 3-2.** (a) Membrane fluidity (via DPH) of DPPC/Chl*a* liposome; (circle) DPPC liposome, (square) DPPC/Chl*a* liposome. At low temperature a membrane forms the ordered phase. The phase transition temperature ($T_{m,DPPC}$: 41.6 ºC) was shifted to disordered phase of membrane. It was found that the membrane fluidity of the inner DPPC/Chl*a* liposome was lower than that of the DPPC liposome. (b) The fluoresce polarization (*P*) of Chl*a* on the DPPC membrane. At over the phase transition temperature, the polarization of Chl*a* scarcely changed. An inverse number of the polarization decreased with lowering temperature.

to the previous finding, Chl*a* molecules are oriented at the interface of the DPPC membrane at gel phase and their ordered orientation was gradually broken with the temperature increase below the $T_m$.

The effect of Chl*a* on the phase transition temperature of the DPPC liposomes was furthermore examined by DSC measurements. **Figure 3-3** shows the heating curves of the DPPC and the DPPC/Chl*a* liposome, indicating that the phase transition temperature of DPPC was shifted to lower temperature by adding Chl*a*. The thermodynamic properties such as $T_m$ and enthalpy change ($\Delta H$) were summarized in **Table 3-1**. In the case of the DPPC/Chl*a* liposome, the $\Delta H$ value was increased by adding Chl*a*, which is attributed to the interactions between lipid molecules and Chl*a*.

From these results, I conclude that the influence of Chl*a* molecules on liposome membranes as well as the behavior of Chl*a*, which is depicted in **Figure 3-4**, can be analyzed by the UV-VIS spectra, fluorescence polarization, and DSC method.

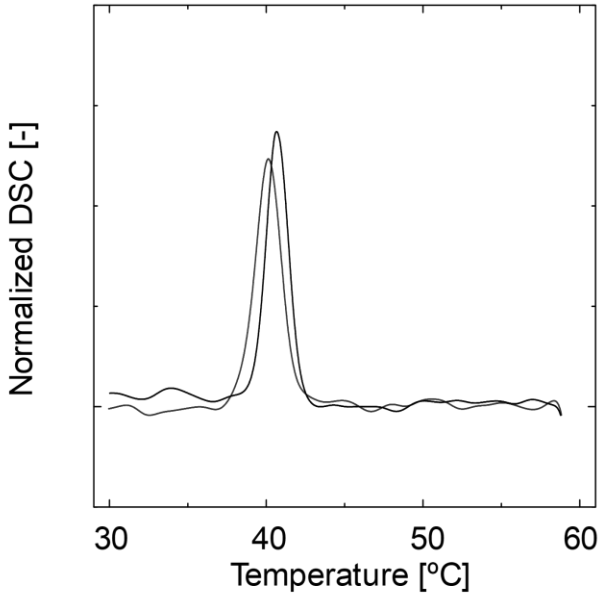


**Figure 3-3.** Differential scanning calorimetry (DSC) heating curves for the DPPC liposome (black) and the DPPC/Chl*a* liposome (gray) (50mM). The main transition temperatures of the DPPC, and the DPPC/Chl*a* were 40.7 ºC, and 40.1 ºC, respectively. The phase transition temperature of the DPPC/Chl*a* was slightly lower than that of the DPPC liposome.

**Table 3-1** The summary of thermodynamic properties for the phase transitions of the DPPC bilayer membranes.

| | $T_m$ [ºC] | Δ$H$ [kJ/mol] |
|---|---|---|
| DPPC | 40.7 | 29.91 |
| Chl*a*/DPPC | 40.1 | 31.54 |

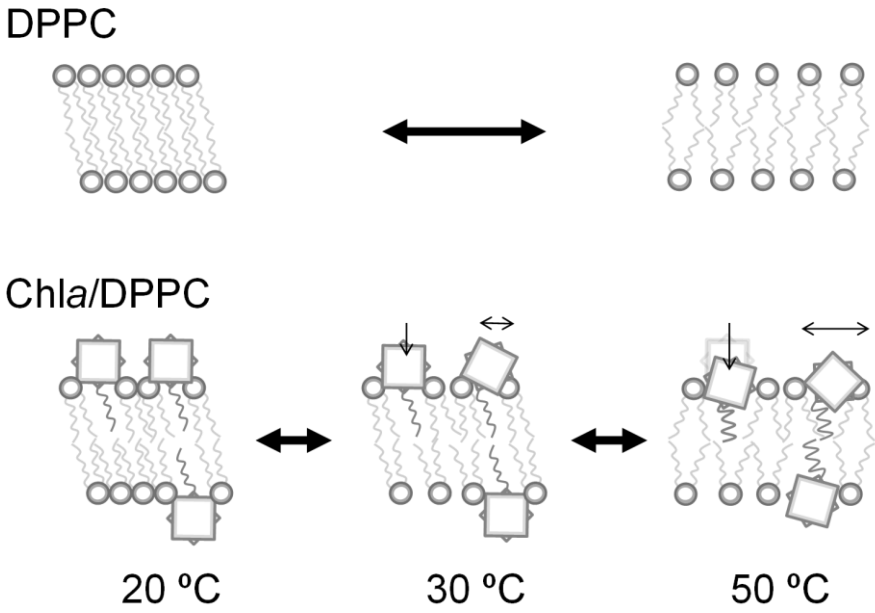


**Figure 3-4.** The illustration of DPPC membrane states with the increase in temperature.

### 3.2. Photosensitized function of liposome with Chl*a*

I have with selected MV as a redox material. The light energy can be efficient transferred from Chl*a* to $MV^{2+}$ because the reduction potential of $MV^{2+}$ is lower than one of photo-excited Chl*a* [di Matteo, 2007, Kobayashi *et al*., 2007]. Based on the plausible model of the Chl*a* molecules on a liposome membrane, the light-harvesting function of Chl*a* on the DPPC membrane was finally studied by selecting the reduction of MV under the irradiation of UV-visible light [Tsujisho *et al*., 2006]. **Figure 3-5a** shows the time course of the $MV^{+\bullet}$ concentration in the presence of the DPPC/Chla liposomes, where the initial rate of $MV^{+\bullet}$ formation varied depending on the temperature. From the obtained results at the various temperatures, the kinetic constant ($k_r$) of the $MV^{+\bullet}$ formation was calculated by assuming the first-order kinetic model, $[MV^{+\bullet}] = A_m[1-\exp(-k_r t)]$, wherein $A_m$ represents saturated product concentration, and the obtained $k_r$ values were plotted against the temperature as shown in

**Figure 3-5b**. As control experiment, I studied a photoreduction of $MV^{2+}$ with DPPC liposome without Chl*a*. The $MV^{+\bullet}$ formation used DPPC liposome was lower than one used DPPC with Chl*a* liposome at same period. So, the photoreduction of $MV^{2+}$ was accelerated by Chl*a* on membrane. Below the $T_m$, the $k_r$ value was gradually reduced with the increase of temperature and a relatively-large decrease was observed above $T_m$. The dissipation in light-irradiation energy is known to be gradually increased by temperature raising; however, a sudden decrease of the $k_r$ values cannot be explained by such a dissipation effect. The decrease in $k_r$ value was considered to be caused by the orientation of Chl*a* molecules on liposome membrane, which varied physicochemical properties with the increased temperature. Because the variation of the phase of phospholipid changed the membrane surface structure, the accessibility of Chl*a* to MV changed a photoreduction [Nacke *et al*., 2011]. Considering the behaviors of Chl*a* molecules on a liposome membrane (**Figure 3-4**), it is considered that the orientation of Chl*a* molecules themselves can relate to the light-harvesting function on the liposome membrane.

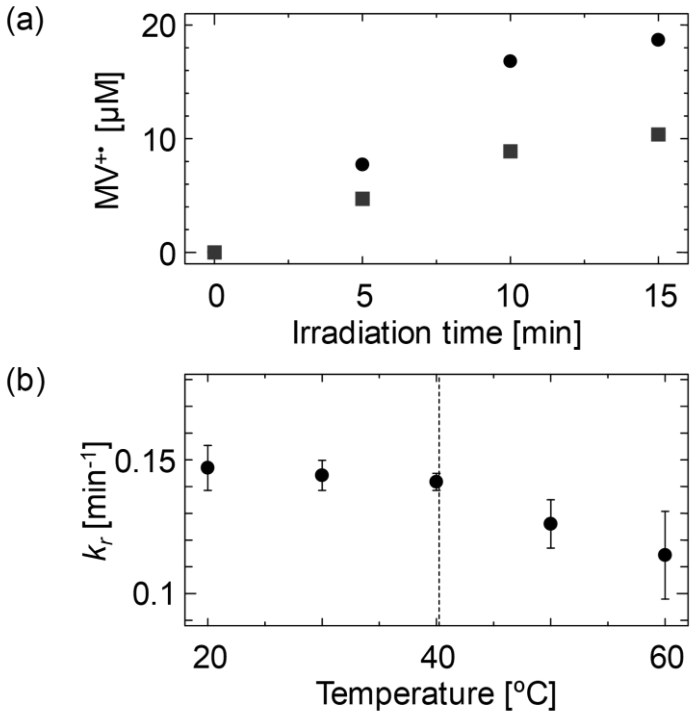


**Figure 3-5.** (a) The change in the concentration of $MV^{+\bullet}$ vs. irradiation time; (circle) 20 ºC, and (square) 50 ºC. (b) The reduction rate constant of methyl viologen at each temperature.

### 3.3. Ultraviolet-visible (UV-Vis) spectra of Chl*a*-incorporated on DMPC/DHPC assemblies

The UV-Vis absorption spectrum of Chl*a*-incorporated in DMPC/DHPC membranes at $X_{DHPC}$ = 0.4 is shown in **Figure 3-6**. A Chl*a* absorbed at approximately 420-440 nm (Soret band) and approximately 650-670 nm (*Q* band) [Agostiano *et al*., 1993]. Chl*a* J-aggregates were confirmed by the presence of a peak at 700-750 nm. At 20 ºC, the J-aggregates formed in DMPC/DHPC at $X_{DHPC}$ = 0.40, $C_{lipid}$ = 20 mM, Chl*a*% = 1.2 mol%, while J-aggregates did not form in the assemblies comprising solely of DMPC or DHPC (**Figure 3-7**). DMPC and DHPC formed vesicles and micelles ($C_{DHPC}$ >16 mM), respectively. DMPC/DHPC mixtures can form bicelles at a $C_{lipid}$ of approximately 200 mM [van Dam *et al*., 2004]. The differences in the turbidity could be related to the morphology of self-assemblies, in which a micelle solution is transparent, whereas a vesicle suspension is turbid. Thus, optical density (*OD*) provides an indication of the morphology of phospholipid assemblies. The states of self-assembly and Chl*a* aggregation were investigated by monitoring *OD* at 500 nm ($OD_{500}$), and the *Q* band.

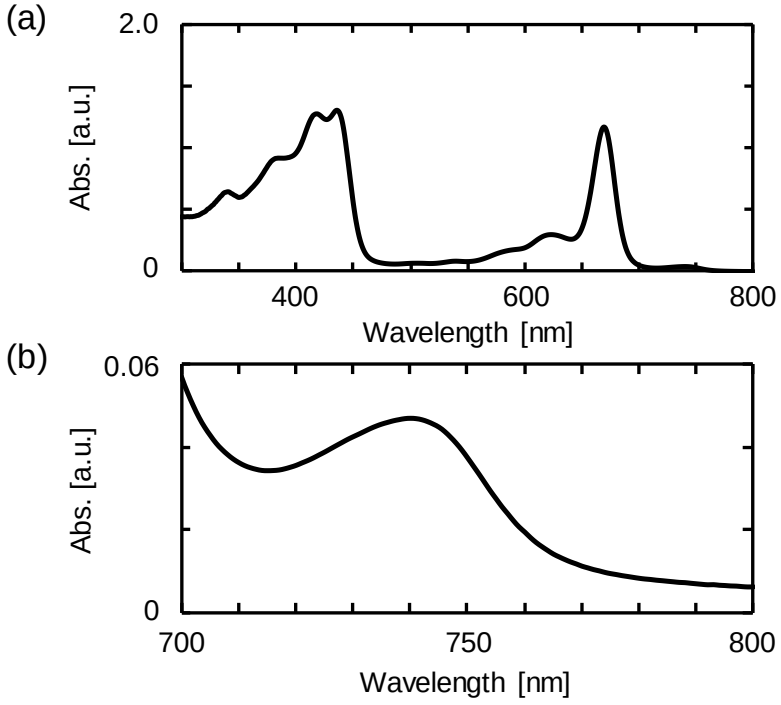


**Figure 3-6**. (a) UV-Vis spectra of Chl*a* molecules incorporated in DMPC/DHPC at $X_{DHPC}$ = 0.40. $C_{lipid}$ =20 mM, Chl*a*% =1.2 mol%. The measurements were conducted at 20 ºC. (b) Picked-up at 700-800 nm.

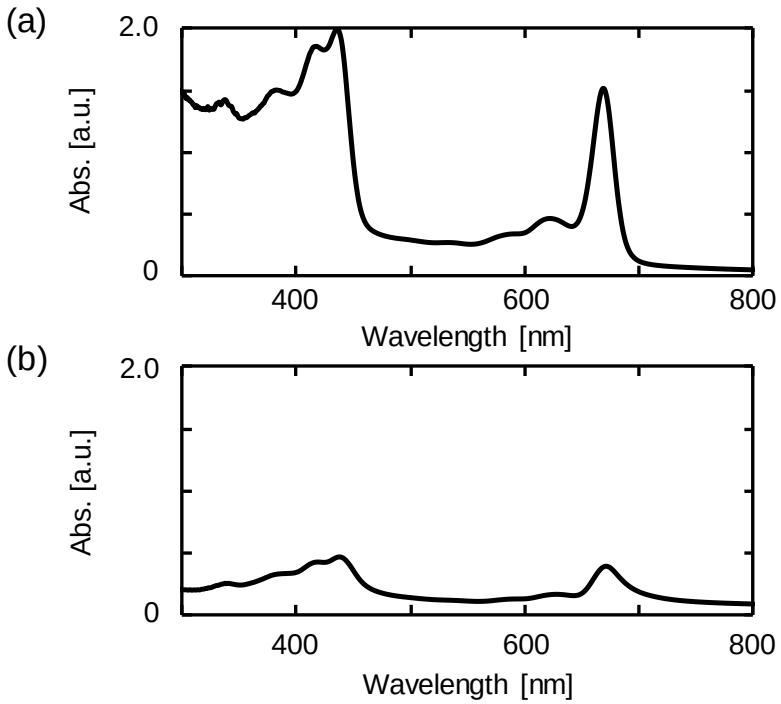


**Figure 3-7**. UV-Vis spectra of Chl*a* molecules incorporated in vesicles and micelles. (a) DMPC vesicle, $C_{lipid}$ =20 mM, Chl*a*% =1.2 mol%. (b) DHPC micelle, $C_{lipid}$ =20 mM, Chl*a*% =1.2 mol%. Measurements were conducted at 20 ºC.

### 3.3.1. Self-assembly states of Chl*a* incorporated in DMPC/DHPC mixtures

At $C_{lipid}$ 20 mM, the $OD_{500}$ values were dependent on DMPC/DHPC ratio ($q$) (**Figure 3-8a**). At $X_{DHPC}$ = 0.40, the $OD_{500}$ values also increased in proportion to the Chl*a* amount (Chl*a*%: 0 to 7.8mol%) (**Figure 3-8b**). The phase behaviors of DMPC/DHPC at such low $C_{lipid}$ values have not been investigated previously [van Dam *et al*., 2004, Ye *et al*., 2014]. The observation that the suspensions were almost transparent ($OD_{500} < 0.1$) at $X_{DHPC} > 0.33$ suggests that smaller self-assemblies could be formed by DMPC/DHPC at $X_{DHPC} > 0.33$ and 20 ºC. The suspension of DMPC/DHPC at $X_{DHPC} = 0.40$ was almost transparent, suggesting the formation of small assemblies. As shown in **Figure 3-8b**, the turbidity values increased with the amount of Chl*a*% ≥ 1.2 mol%. This might suggest further aggregation of self-assemblies (e.g., stacked bicelles), in which the anti-parallel arrangement of Chl*a* J-aggregates might be formed by face-to-face interaction between the interfaces of the self-assemblies. In our previous studies, the

turbidity of self-assembly suspensions can be varied depending on the composition [Hayashi *et al*., 2015, 2017]. By adding Chl*a*, the turbidity of the solution slightly increased. Agostiano *et al.* have reported that Chl*a* molecules tend to stabilize lamellar phases of sodium bis-2-ethylhexyl-sulfosuccinate (AOT) [Agostiano *et al.,* 2000]. When DMPC/DHPC suspensions at $X_{DHPC}$ = 0.40 were diluted, the turbidities increased in the absence or presence of Chl*a* (data not showed). This might be due to the morphological changes of the self-assemblies although the J-aggregates were maintained after dilution (see below).

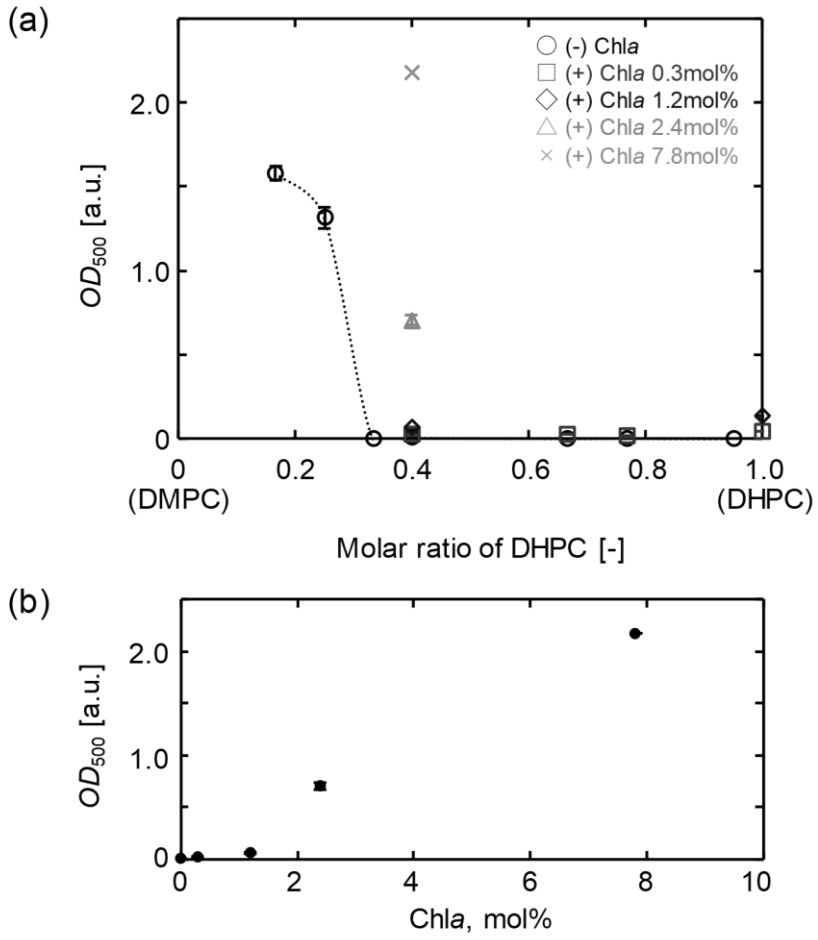


**Figure 3-8**. (a) $OD_{500}$ values of self-assembly suspensions, in the presence or absence of Chl*a*. Symbols indicate the different molar ratio of Chl*a*: 0 mol% (circle), 0.3 mol% (square), 1.2 mol% (diamond), 2.4 mol% (triangle), and 7.8 mol% (cross). For all samples, $C_{lipid}$ = 20 mM. (b) Relationship of Chl*a*% and $OD_{500}$ values, in DMPC/DHPC at $X_{DHPC}$ = 0.40. Measurements were conducted at 20 ºC.

### 3.3.2. Aggregation behaviors of Chl*a* molecules at membrane surfaces

Lateral aggregation of Chl*a* can be determined by the peak shift of *Q* band. In the solvent system, Chl*a* displayed the *Q* band peak at 660 nm in acetonitrile ($CH_3CN$). The peak shifted to 670 nm in $CH_3CN$/water at a ratio of 3:7, and a peak at 740 nm was generated, which can be evident for J-aggregates [Agostiano *et al*., 2002]. Peak shifts have been observed for the Chl*a* molecules incorporated in liposomes [Bialek-Bylka *et al.*, 1986, Milenkovic *et al.*, 2013]. The findings indicate that the polar environment around Chl*a* molecules could be a controlling factor in the induction of J-aggregate formation. In this study, the J-aggregates of Chl*a* were observed at $X_{DHPC}$ = 0.40, $C_{lipid}$ = 20 mM, Chl*a*% =1.2 mol% (**Figure 3-9**), but were not evident at Chl*a*% = 0.3 mol% with $X_{DHPC}$ = 0.40 and 0.67 (**Figures 3-9** and **3-10**). It seems that the fraction of DHPC is a dominant factor in the condensation of Chl*a* molecules in membranes. Correia et al. recently reported the aggregation behaviors of Chl*a* in detergent:lipid systems [Correia *et al*., 2014]. Using N-dodecyltrimethylammonium chloride and DMPC as the detergent and lipid, respectively, J-aggregate formation of Chl*a* was induced at a detergent:lipid ratio of 33.

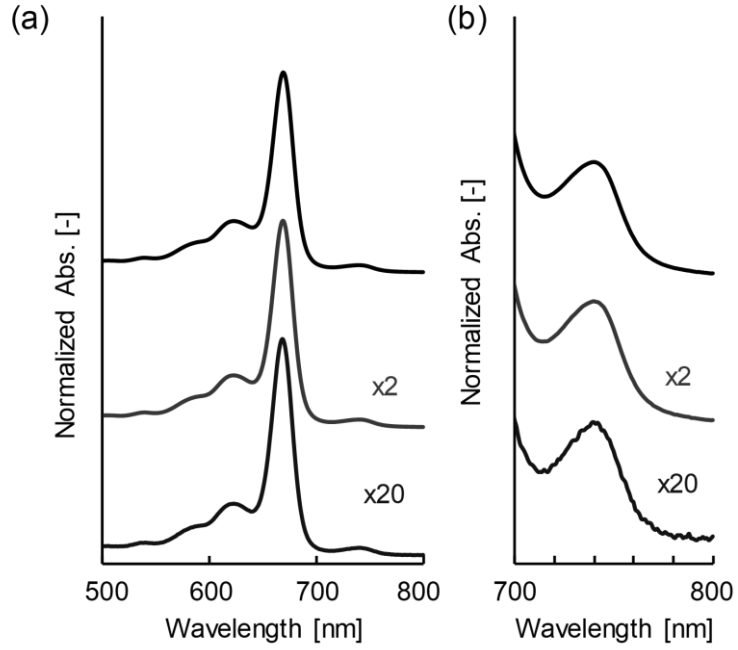


**Figure 3-9**. (a) *Q* band spectra of Chl*a* molecules in DMPC/DHPC at $X_{DHPC}$ = 0.40. Samples were prepared at $C_{lipid}$ =20 mM (*top*), and then diluted in 2 times (*mid*) or 20 times (*bottom*). Chl*a*% =1.2 mol%. *Q* band and J-aggregate peaks were appeared at 669, and 740 nm, respectively. (b) Picked-up at 700-800 nm. Measurements were conducted at 20 ºC.

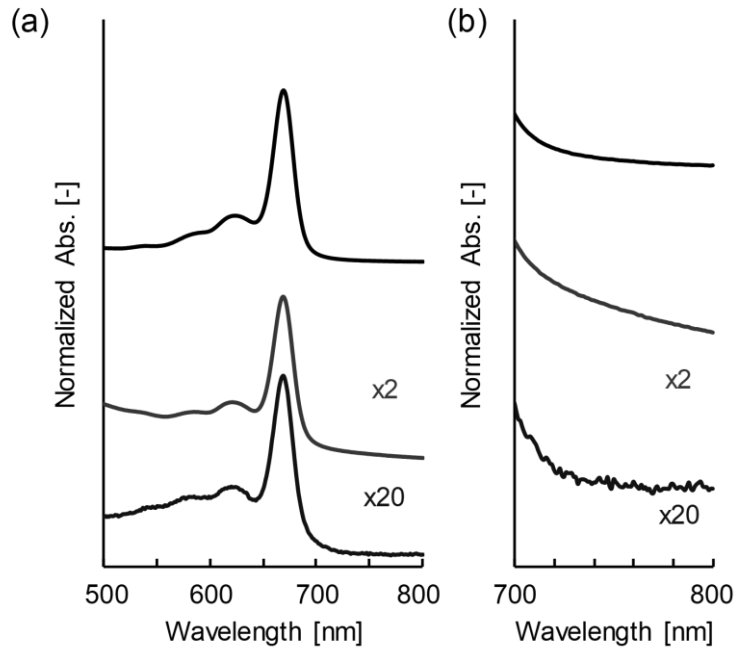


**Figure 3-10**. (a) *Q* band spectra of Chl*a* molecules in self-assemblies. Samples were prepared at $C_{\text{lipid}}$ = 20 mM (*top*), and then diluted in 2 times (*mid*) or in 20 times (*bottom*). DMPC/DHPC at $X_{\text{DHPC}}$ = 0.40, Chl*a*% = 0.3 mol%, *Q* band peak at 669 nm. (b) Picked-up at 700-800 nm. Measurements were conducted at 20 ºC.

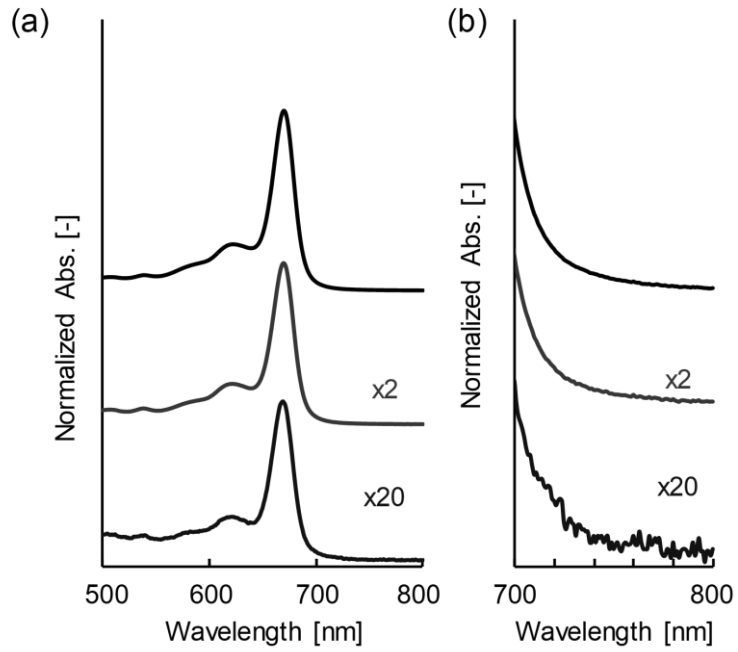


**Figure 3-11**. (a) *Q* band spectra of Chl*a* molecules in self-assemblies. Samples were prepared at $C_{\text{lipid}}$ = 20 mM (*top*), and then diluted in 2 times (*mid*) or in 20 times (*bottom*). DMPC/DHPC at $X_{\text{DHPC}}$ = 0.67, Chl*a*% = 0.3 mol%, *Q* band peak at 669 nm. (b) Picked-up at 700-800 nm. Measurements were conducted at 20 ºC.

In this ratio, bicelles and vesicles can coexist [Viseu *et al*., 2010]. It is thus assumed that the bicelle structure is a potential advantage for the induction of the J-aggregates of Chl*a*. Presently, the self-assembly structure of DMPC/DHPC at $X_{DHPC}$ = 0.40, with the potential to form bicelles [van Dam *et al*., 2004], could induce J-aggregate formation of Chl*a*, while DMPC vesicles or DHPC micelles could not. The models for chlorophyll J-aggregates can be considered as an anti-parallel arrangement that can be formed between "*two interfaces*", and a parallel arrangement that can be formed in "*an interphase*" [Huber *et al*., 2007]. The former arrangement might be formed between the planar bilayer regions between bicelles, whereas in the case of vesicles or micelles, the parallel arrangement might be difficult due to membrane curvature. The results demonstrated that the Chl*a* J-aggregates were generated in the DMPC/DHPC membranes at $X_{DHPC}$ = 0.40, $C_{lipid}$ = 20 mM, and the generated Chl*a* aggregates could be maintained after the dilution ($C_{lipid}$ = 1 mM). Furthermore, the thermal stability of the bicelle disk structure including the aggregates was improved (**Figure 3-12**). It is thought that Chl*a* molecule lowered the membrane fluidity of the DMPC bilayer membrane and worked to stabilize the disk structure. This correlated with the trend of Chl*a* on the liposome (section **3.1.** in this chapter).

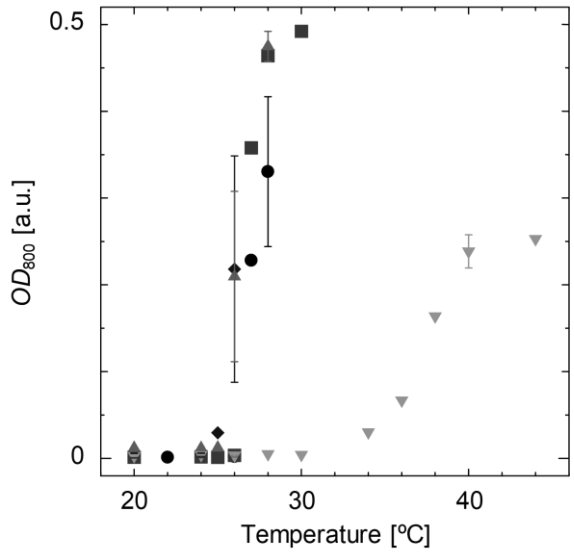


**Figure 3-12.** $OD_{800}$ values of DMPC/DHPC self-assembly suspensions ($X_{DHPC}$ = 0.40, $C_{lipid}$ = 20 mM), in the presence or absence of Chl*a*. Symbols indicate the different molar ratio of Chl*a*: 0 mol% (circle), 0.3 mol% (square), 0.6 mol% (diamond), 0.9 mol% (triangle), and 1.2 mol% (inverted triangle). Herein, the turbidity was observed at a wavelength 800 nm because that was not affected by the broadening of the spectrum width with aggregation of Chl*a*.

### 3.4. Local environment of Chl*a* molecules in DMPC/DHPC mixtures

The Soret band absorption spectrum of Chl*a* can be influenced by the dielectric environment of the solvent [Agostiano *et al*., 1993]. This phenomenon can be applied to estimate the location (surroundings) of Chl*a* in the self-assemblies. The peaks of the tetrapyrrole ring can be attributed to their transition dipoles, as calculated by the vectors from the central $Mg^{2+}$ to the nitrogen atom of the Chl*a* ring [Shibata *et al*., 2010]. Shifts of the Soret band can be induced by surrounding solvent molecules, such as water [Vladkova *et al*., 2000]. The Soret band spectra of Chl*a* in $CH_3CN$/water solutions were deconvoluted to each fraction. The intensity of the Soret band fraction at 440 nm ($B_y$) was lower than that at 420 nm ($B_x$) in water-

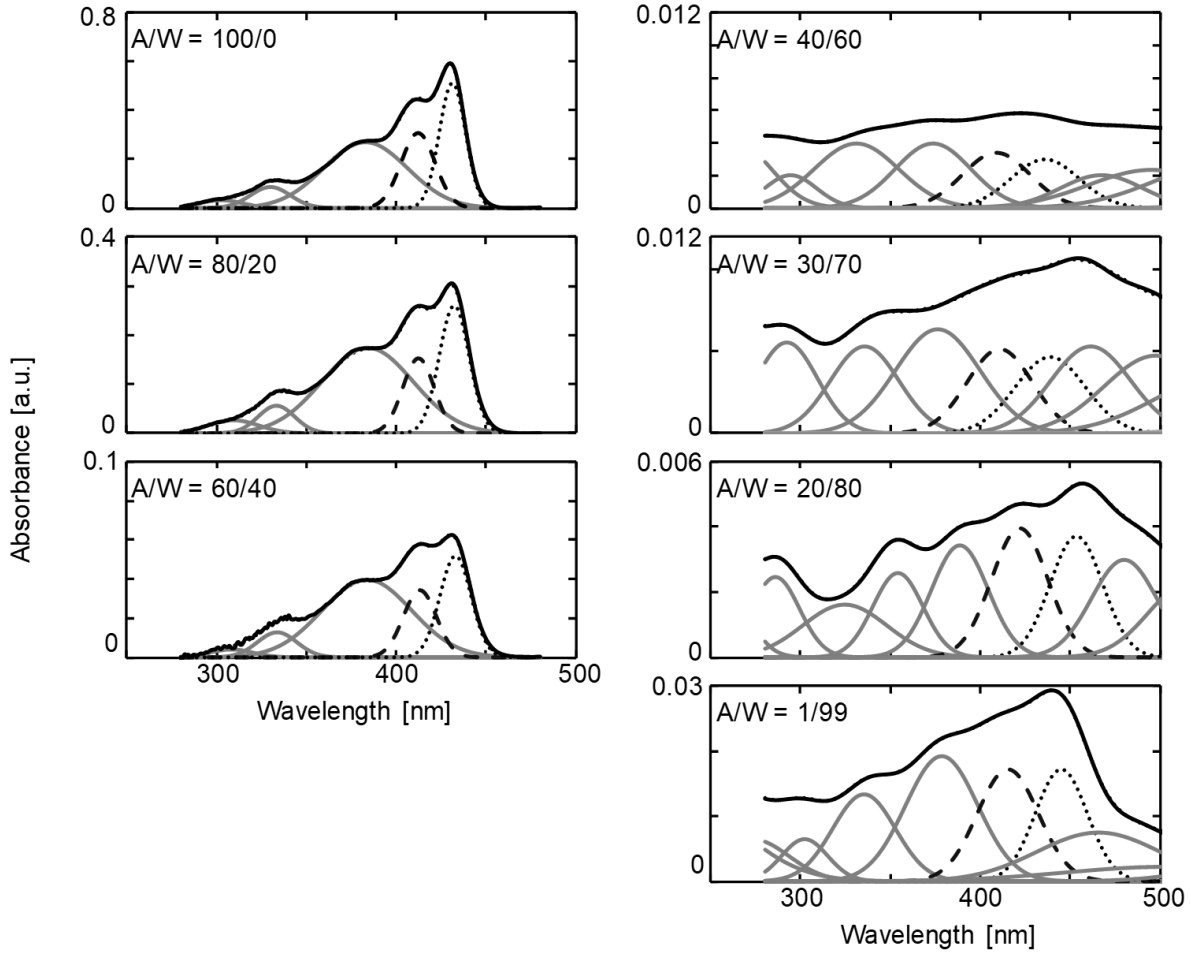


**Figure 3-13.** Deconvoluted Soret band spectra of Chl*a* in $CH_3CN$ (A)/water (W) solutions; (*dotted*) $B_y$ = 440 nm, (*broken*) $B_x$ = 420 nm. The concentration of Chl*a* was 0.1 mM. The stock solution of Chl*a* was prepared using $CH_3CN$, and then the stock solution was applied to $CH_3CN$/water mixtures. Measurements were conducted at 20 ºC.

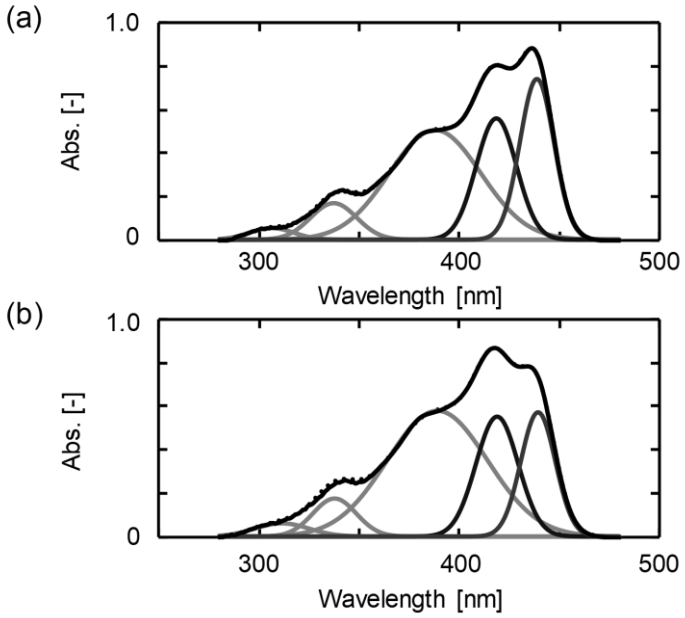


**Figure 3-14**. Deconvoluted Soret band spectra of Chl*a* molecules in self-assemblies. Samples were prepared at $C_{lipid}$ =20 mM, Chl*a*% =0.3 mol%. (a) DMPC/DHPC at $X_{DHPC}$ = 0.40. (b) DMPC/DHPC at $X_{DHPC}$ = 0.67.

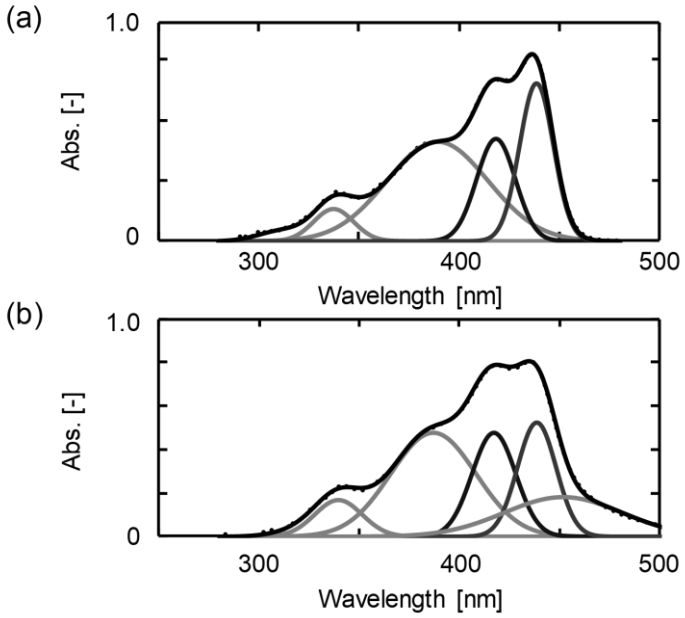


**Figure 3-15**. Deconvoluted Soret band spectra of Chl*a* molecules in (a) DMPC ($X_{DHPC}$ = 0) or in (b) DHPC ($X_{DHPC}$ = 1.0). Samples were prepared at $C_{lipid}$ = 20 mM, Chl*a*% = 0.3 mol%. Measurements were conducted at 20 ºC.

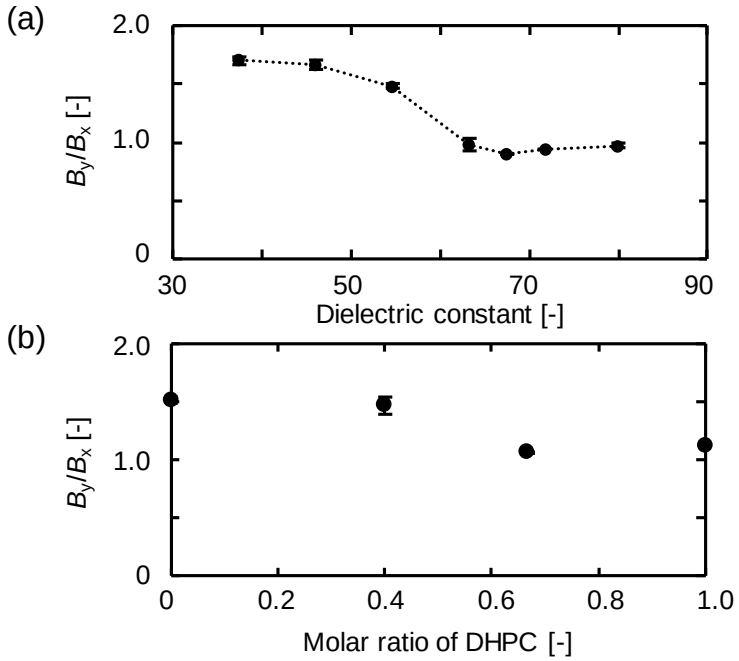


**Figure 3-16**. $B_y/B_x$ values of Chl*a* in (a) $CH_3CN$/water solution, and in (b) DMPC/DHPC self-assemblies: $C_{lipid}$ = 20 mM, Chl*a*% = 0.3 mol%.

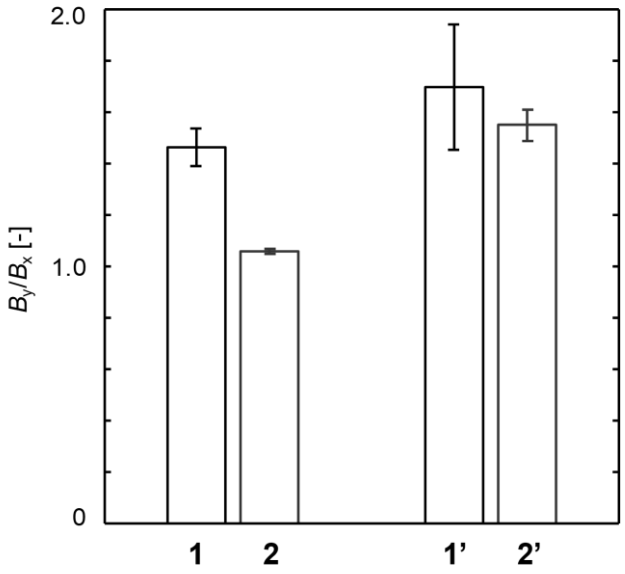


**Figure 3-17.** Effects of dilution on $B_y/B_x$ values. (1) DMPC/DHPC at $X_{DHPC}$ = 0.40, $C_{lipid}$ = 20 mM, Chl*a*% = 0.3 mol%, (1') DMPC/DHPC at $X_{DHPC}$ = 0.40, $C_{lipid}$ =1 mM (20 times dilution), Chl*a*% = 0.3 mol%. (2) DMPC/DHPC at $X_{DHPC}$ = 0.67, $C_{lipid}$ = 20 mM, Chl*a*% = 0.3 mol%, (2') DMPC/DHPC at $X_{DHPC}$ = 0.67, $C_{lipid}$ = 1 mM (20 times dilution), Chl*a*% = 0.3 mol%.

enriched solutions. The intensity ratio ($B_y/B_x$ value) decreased with increased water ratio (**Figure 3-13**). To investigate the surroundings of Chl*a* in the membrane, the $B_y/B_x$ values of Chl*a* in self-assemblies were estimated (**Figure 3-14**). For the $B_y/B_x$ values of Chl*a* in DMPC vesicles and in DHPC micelles were also estimated based on the Soret band spectra (**Figure 3-15**). The $B_y/B_x$ values of Chl*a* could be depended on the fraction of DHPC. In solution, the $B_y/B_x$ values were relevant to dielectric constants (**Figure 3-16a**). The $B_y/B_x$ values of DMPC vesicles and DMPC/DHPC at $X_{DHPC}$ = 0.40 were relatively higher, suggesting that the surrounding of Chl*a* in the DMPC/DHPC at $X_{DHPC}$ = 0.40 was hydrophobic, as well as that in DMPC vesicles (**Figure 3-16b**). On the other hand, the surrounding of Chl*a* in DMPC/DHPC at $X_{DHPC}$ = 0.67 was rather hydrophilic, as well as that in DHPC micelles. Membrane polarity depends on the phase state [Iwasaki *et al*., 2017]. A membrane in the gel (solid-ordered) phase is less hydrophilic than a membrane in the fluid (liquid-disordered) phase or in micelles. Since the experiments were conducted at 20 ºC (< $T_m$ of DMPC), DMPC/DHPC membranes at $X_{DHPC}$ = 0.40 could be in a gel phase-like ordered state, wherein Chl*a* molecules are condensed to form J-aggregates. In my study, the Chl*a* in 1,2-dipalmitoyl-*sn*-glycero-3-phosphocholine (DPPC) liposomes decreased membrane fluidity at temperatures above $T_m$ (section **3.1.** in this chapter), suggesting that Chl*a* molecules potentially lead the fluid membrane to adopt an ordered state. In contrast, the Chl*a* molecules in DMPC/DHPC at $X_{DHPC}$ = 0.67 could be located near the DHPC-enriched region (micelle-like environment). After dilution, the $B_y/B_x$ value of Chl*a* in DMPC/DHPC at $X_{DHPC}$ = 0.40 was slightly increased as compared to that before the dilution, indicating that Chl*a* molecules maintained on the bilayer region. On the other hand, the $B_y/B_x$ value of Chl*a* in DMPC/DHPC at $X_{DHPC}$ = 0.67 significantly increased after dilution (**Figure 3-17**). This suggests that the surroundings of Chl*a* molecules at $C_{lipid}$ 1 mM are more hydrophobic than the surroundings of Chl*a* at $C_{lipid}$ 20 mM, because the DHPC can be soluble in the diluted condition, and Chl*a* and DMPC can be reorganized due to self-assembly. Thus, the local environment of Chl*a* molecules differed depending on the membrane composition. After dilution, Chl*a* molecules accumulated in the bilayer (DMPC-enriched) region. In the case of $X_{DHPC}$ = 0.40, the Chl*a* J-aggregates could be maintained.

### 3.5. Photo-reduction function of Chl*a* aggregates in DMPC/DHPC assembly

The photochemical functions of Chl*a* in self-assembly systems is important. $MV^{2+}$ molecules act as electron acceptors in the photo-reduction of photosensitive pigments, and EDTA molecules act as a Chl*a* oxidant [Mizushima *et al*., 2006, Matteo *et al.*, 2007, Kobayashi *et al*., 2007, Watanabe *et al*., 2011]. The reduction of $MV^{2+}$ can proceed by a photosensitizer that has sufficient absorption at approximately 670 nm [Amao *et al.*, 2002, Sugiyama *et al.*, 2006]. Tomonou *et al*. reported that the optimized conditions for the Chl*a*-mediated photo-reduction of $MV^{2+}$ were [Chl*a*] = 9.0 μM, [$MV^{2+}$] = 2.0 mM and [NADPH] = 2.0 mM (electron donor), with the reaction carried out in Tris-HCl buffer (50 mM, pH 7.4) in the presence of 10 mM cetyltrimethylammoniumbromide (CTAB, micelle) [Tomonou *et al*., 2002]. In these conditions, the turnover number ($k_{cat} = V_{max}$/[Chl*a*]), was 0.70 $min^{-1}$. The type of surfactant could be a critical factor in photo-reduction activity. For instance, the nonionic surfactant Triton-X 100 drastically decreased the photo-reduction of $MV^{2+}$ as compared to CTAB [Tomonou *et al*., 2004]. In addition, the alkylchain length of surfactant affected the Chl*a*-mediated photo-reduction of $MV^{2+}$ [Sugiyama *et al*., 2006]. In vesicle systems, we reported a $k_{cat}$ value of 0.68 $min^{-1}$ in DPPC vesicles (**3.2.** in this chapter).

Herein, the formation of J-aggregates of Chl*a* was induced in DMPC/DHPC assemblies at $X_{DHPC}$ = 0.40, $C_{lipid}$ = 20 mM, Chl*a*% = 1.2 mol%, and the diluted suspension was used as the reaction medium for the photo-reduction reaction of $MV^{2+}$. After adjusting the Chl*a* concentration to 2.5 μM, the absorbance band at 750 nm was maintained. Thus, the photo-reduction activities of aggregated Chl*a* were investigated (**Figure 3-18**). The accumulation of $MV^{+\bullet}$ was saturated in 80 min, due to the reaction equilibrium ($MV^{+\bullet} \rightleftharpoons MV^{2+}$). Comparing the photo-reduction activities of Chl*a* (2.5 μM), the non-aggregated Chl*a* in DMPC vesicles (sample (i)) or in DMPC/DHPC at $X_{DHPC}$ = 0.40 (sample (ii), initially induced with $C_{lipid}$ = 20 mM, Chl*a*% = 0.3 mol%) showed higher activities. The differences of the conversions values might reveal the saturated concentration of $MV^{2+}$ for each self-assembly system (in **Table 3-2**). Kondo *et al*. reported that the zinc (Zn)-porphyrin dimer resulted in a decreased activity [Kondo *et al*. 2015]. In addition, the aggregated Zn-chlorophyll maintained the photo-induced charge separation [Li *et al*., 2015]. As shown in **Table 3-2**, Zn-porphyrin showed higher $k_{cat}$ values and the reaction soon reached to equilibrium state [Kondo *et al*., 2015]. This might be related to the

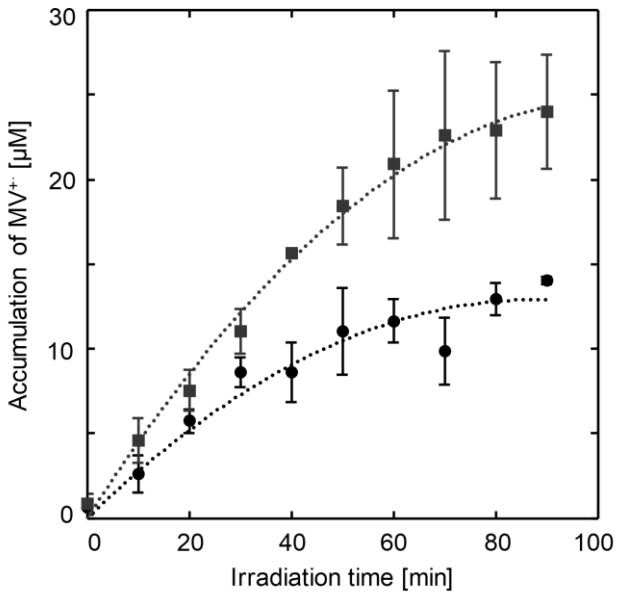


**Figure 3-18**. Photo-reduction of $MV^{2+}$, catalyzed by Chl*a* incorporated in DMPC/DHPC assemblies. Sample were prepared at DMPC/DHPC at $X_{DHPC}$ = 0.40, $C_{lipid}$ = 20 mM. (*Circle*) Chl*a*% = 1.2mol%, (*Square*) Chl*a*% = 0.3 mol%. The samples were diluted to adjust the total Chl*a* concentration of 2.5 μM. Experiments were conducted at 20 ºC.

**Table 3-2** Summary of photo-reduction activity of Chl*a* and Zn-porphyrin on self-assembly membranes.

| Sample | Chl*a* [μM] | $V_{max}$ [μM/min] | $k_r$ *$10^3$ [$min^{-1}$] | Conversion [%] | $k_{cat}$ [$min^{-1}$] |
|---|---|---|---|---|---|
| (i)[a] | 2.5 | 0.42±0.01 | 0.87±0.02 | 7.63±1.14 | 0.17±0.00 |
| (ii)[b] | 2.5 | 0.49±0.14 | 1.00±0.29 | 6.35±0.33 | 0.19±0.06 |
| (iii)[c] | 2.5 | 0.23±0.10 | 0.48±0.21 | 4.98±0.42 | 0.09±0.04 |
| Chl*a* in 10 mM CTAB micelle[d] | 9.0 | 6.25 | $2.1\times10^{-3}$ | ~9.5 | 0.70 |
| Zn-porphyrin monomer[e] | 10 | 21 | 4.37 | 9 | 2.1 |
| Zn-porphyrin dimer[e] | 10 | 10 | 2.73 | 6.5 | 1.0 |

[a] Prepared in DMPC vesicle at $C_{lipid}$ =20 mM, Chl*a*% = 1.2 mol%, then diluted to adjust the final concentration of [Chl*a*] = 2.5 μM. The kinetic parameters were obtained at 20 ºC.
[b] Prepared in DMPC/DHPC at $X_{DHPC}$ = 0.40, $C_{lipid}$ =20 mM, Chl*a*% = 0.3 mol% (non-aggregated), then diluted to adjust the final concentration of [Chl*a*] = 2.5 μM. The kinetic parameters were obtained at 20 ºC.
[c] Prepared in DMPC/DHPC at $X_{DHPC}$ = 0.40, $C_{lipid}$ =20 mM, Chl*a*% = 1.2 mol% (aggregated), then diluted to adjust the final concentration of [Chl*a*] = 2.5 μM. The kinetic parameters were obtained at 20 ºC.
[d] See Tomonou *et al.* for details [Tomonou *et al.*, 2002]
[e] See Kondo *et al.* for details [Kondo *et al.*, 2015]

stability of the photosensitizer. A trend was evident, in which a higher photo-reduction activity could be contributed by the photosensitizer that was stable during prolonged irradiation [Amao *et al.*, 2002, Tomonou *et al.*, 2002, Sugiyama *et al*., 2006]. For the use of Chl*a* as photosensitizer, the surfactants are necessary to disperse Chl*a* in an aqueous medium. Although this point seems to be a disadvantage in forming J-aggregates, the decreased reaction rate could be evidence that Chl*a* molecules retain the photo-induced electron longer. Furthermore, J-aggregate formation enables red photon absorption. Overall, a sustainable photo-reduction activity can be expected by utilizing Chl*a* with self-assembly systems.

## 4. Summary

I clarified the liposomal membrane properties based on the analyses of the membrane fluidity, the Chl*a* absorption bands, and the Chl*a* polarization. Moreover, the influence of the membrane properties on the photoreduction with methyl viologen was examined. Consequently, it was revealed that the kinetic constant value of the reduced species formation decreased with the increase in temperature over the phase transition temperature of the membrane, which means that the membrane properties largely influence the photochemical reaction. Based on these results, it is concluded that the behaviors and the orientations of Chl*a* molecules on the liposomal membrane are significantly important in the photochemical energy conversion system. Thus, this methodology and findings can be helpful for superior photochemical energy conversion by Chl*a* containing liposomes.

J-aggregates of Chl*a* molecules were induced in DMPC/DHPC phospholipid assemblies at $X_{DHPC}$ = 0.40 and $C_{lipid}$ =20 mM, and the J-aggregates were maintained after dilution to $C_{lipid}$ = 1 mM. The environment surround Chl*a* molecules could be polar in the DMPC/DHPC membranes, where the polarity at $X_{DHPC}$ = 0.40 was lower than $X_{DHPC}$ = 0.67, which could promote the formation of Chl*a* aggregates. The photo-reduction of $MV^{2+}$ was regulated by the aggregation states of Chl*a* molecules.

This is the first study to report that Chl*a* J-aggregates form in phospholipid assemblies at a lower Chl*a*-to-lipid ratio. The photo-reduction activity of aggregated Chl*a* is less than that of non-aggregated Chl*a*. Curiously, the bicelle-type assemblies more advantageously induce the formation of J-aggregates of Chl*a*, suggesting that the coexistence of micelle and bilayer regions could be a key to control the aggregation behaviors of Chl*a* molecules. By employing DMPC/DHPC self-assembly as a platform for Chl*a* aggregation, lateral interaction of Chl*a* within the membranes and vertical interaction of Chl*a* between membrane interfaces can occur. In the presence of appropriate additives, bicelles can be stacked to form a cylindrical structure [Yang *et al*., 2013]. Further investigation of the structural properties of Chl*a*-incorporated bicelles and their aggregated structures using a microscopy will be instructive. The current data provide insights concerning the use of J-aggregates of Chl*a* as a photosensitizer, which can lead to the development of powerful photosynthesis systems.

# Chapter 4

## Preparation of Vesicle Materials;

## Simple Method Using Continuous Flow Devices

### 1. Introduction

A phospholipid is one of the important molecules that are available for the preparation of a closed spherical vesicles (liposomes) with bilayer membrane structure in aqueous solution. The prepared vesicles can be utilized as functional biomaterials to encapsulate proteins, drugs, or other molecules because they have an inner aqueous phase similarly in the case of cell structure in nature [Mukhopadhyay *et al*., 1994, Zimmermann *et al.,* 2006, Peer *et al*., 2007]. Recent research shows the emergent properties of the membrane itself, such as the recognition of small molecules [Ishigami *et al*., 2015] and asymmetric reaction [Kumar *et al*., 2013, Iwasaki *et al*., 2015]. The phase states of the bilayer membrane (i.e., ordered gel phase and disordered liquid-crystalline phase) can be regulated via the change of the interaction between lipids, depending on the temperature and lipid composition [van Dam *et al*., 2004]. It is expected that the surface of the liposome membrane could be designable, through the control of the extensive and intensive parameters and its "design" could also be effective for the functionalization of the liposome surface.

Various methods to prepare the lipid membrane have been developed for many purposes (**Table 4-1**). The thin film hydration is one of the conventional methods of vesicle preparation [Johnson *et al*., 1971]. In this method, the thin film of lipids is formed on a round-bottom flask, and the vesicle suspension is obtained by hydration with an aqueous solution, where lipid molecules can be used to form bilayer in high yield. In most cases, the vesicles were obtained in a multilamellar form, and the size distribution of the vesicles is wide and is not mono-dispersed. In order to obtain mono-dispersed vesicles, an extrusion with polycarbonate filter is employed as an additional technique to adjust the size [Suga *et al*., 2013]. Small lamellar vesicles (SLVs) of uniform size can be obtained by treating the vesicle suspension by the fine pore filter. SLVs with about 100 nm in its diameter is often used research of a drug carrier. Alternatively, for observation of a biological membrane model, a giant vesicle preparation is

necessary [Szoka *et al*., 1978]. However, it is difficult to efficiently form large unilamellar vesicle (LUV) and giant unilamellar vesicle (GUV) by thin film hydration method. The ethanol injection [Kremer *et al*., 1977, Pons *et al.*, 1993] and the reverse phase evaporation [Szoka *et al.*, 1978] can therefore be used for the preparation of the giant vesicles that have large internal aqueous phase. Another approach for GUV preparation is the w/o/w emulsion method, which the aqueous solution core was dispersed in oil (water in oil emulsion) and the w/o emulsions were transformed to aqueous solution to obtain w/o/w emulsion. The volume of the aqueous solution core affects the final trapping efficiency of assembly, as water-in-oil-in-water emulsion, in an aqueous solution. These batch-wise preparation methods have evolved to meet the expectations of many purposes. However, a continuous preparation has been requiring for industrial use.

In the continuous preparation method using the flow system, bilayer membrane assemblies can be continuously obtained by injecting lipid molecules dispersed in a polar solvent (i.e. isopropanol) into an aqueous phase in a simple flow path [Cho *et al.*, 2015] (**Table 4-1**). Cho *et al.* achieved the continuous preparation of w/o/w emulsion by mixing phospholipids dispersing isopropanol and water with the flow. They optimized the size of the obtained emulsions (diameter: 100-250 nm) by setting a pore filter (pore size: 5 μm) in the flow path and manipulating the flow velocity. Continuous preparations of GUVs have also been studied, expensively. For example, Sugiura *et al.* developed the ice droplet technique [Sugiura *et al.*, 2008], where the ice droplet as vesicle core is mixed with the lipid dispersed solvent in flow path and leads to form an assembly with high volume inner water-phase. These preparation techniques can be effective for the improvement of batch-wise methods such as ethanol injection and reverse phase evaporation. Amphiphilic molecules at the interface between hydrophilic and hydrophobic solutions disperse in a continuous system.

Recently, some researchers reported the high-performance preparation method by microfluidic device, which has demonstrated potential for achieving higher control over the physical properties of the final product, particularly in terms of liposome size, shape and size distribution [Funakoshi *et al*., 2007, van Swaay *et al*., 2013]. Although the final products are the uniform vesicle membranes, there are only a few examples of constructing a heterogeneous vesicle membrane to mimic the biomembrane [Li *et al*., 2015]. In biological cells, a lipid raft on micro domain on the membrane, formed by both micro phase separation of lipid platform

**Table 4-1.** List of vesicle preparation methods

| | Organic solvent | System | Assembly | Residual solvent | Ref. |
|---|---|---|---|---|---|
| Thin film hydration | Use | Batch (non-continuous) | MLVs | No | LeBerre *et al.* 2008 |
| Ethanol injection | Use | Semi-batch (stepwise) | GUVs | Yes | Pons *et al*. 1993 |
| Reverse phase evaporation | Use | Semi-batch (stepwise) | LUVs | Yes | Szoka *et al.* 1978 |
| Flow / Microflow | Use | Continuous | SUVs~GUVs | Yes | Li *et al.* 2015 |
| $CO_2$/water interface | Non-use | Semi-batch (stepwise) | MLVs | No | Nakamura *et al.* 2015 |

and binding of specific lipids to inserted membrane protein, is utilized to maintain the functions of cells as signal transduction of membrane proteins and so on [Opella *et al*., 2004, Li *et al*., 2014, Wade *et al*., 2017]. Even though, microfluidic technique can generate monodisperse unilamellar phospholipid vesicle structures, there are still disadvantage such as remnant of organic solvents in a hydrophobic region of bilayer of production of vesicles, which is related to the properties (e.g. shape, phase state, and releasing rate) of the microencapsulated particles. Moreover, the conventional methods are suffered from preparation of heterogeneous membrane surface instead of homogeneous one. Therefore, I suggest the new type of the vesicle fabrication method that enables to design the "heterogeneous" membrane surface without any other process, which is necessary for the functionalization of the liposome surface.

I have been previously reported that discoidal self-assembled bilayer micelles, termed as "*bicelles*", comprise a mixture of long-chained phospholipids (e.g., 1,2-dimyristoyl-*sn*-glycero-3-phosphocholine, DMPC) and short-chained phospholipids (e.g., 1,2-dihexanoyl-*sn*-glycero-3-phosphocholine, DHPC) at high concentration in aqueous solution, wherein DHPC detergents cover the rim of DMPC bilayer (chapter 2). The bicelle suspension can support membrane-oriented hydrophobic molecules, such as peptides and apoproteins, and the geometrical structures of these proteins can be kept in dispersed aqueous solution [Beaugrand *et al*. 2014]. Small bilayers by DMPC molecules are stably dispersed in water due to the detergent effect of DHPC molecules [Takajo *et al*., 2010]. However, the disk structure is collapsed by hydration of DHPC molecules (critical micelle concentration, CMC: 16 mM) during dilution, in which the bicelles are transformed to the vesicles [Beaugrand *et al*., 2014].

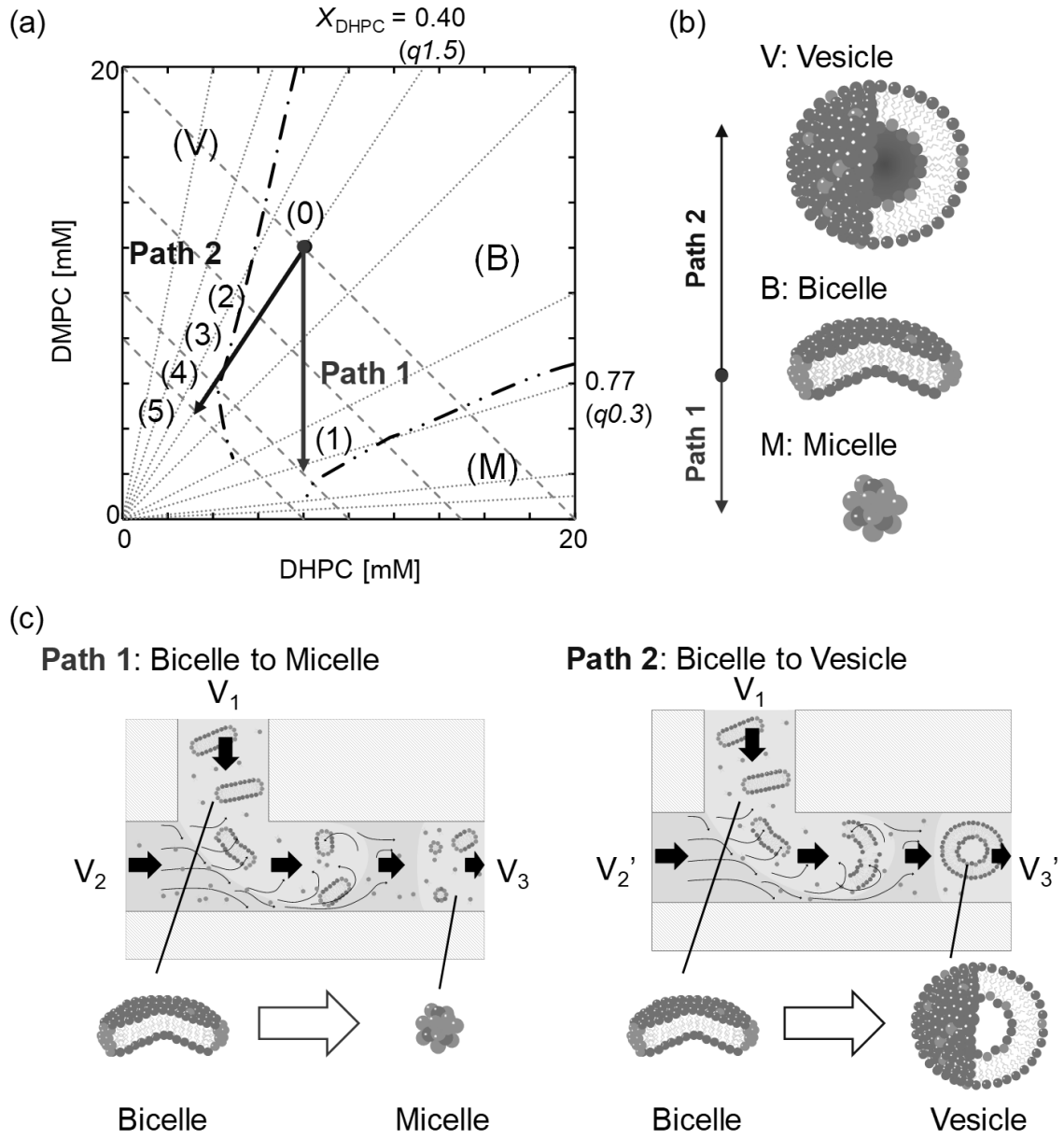


**Figure 4-1.** (a) Experimental conditions on the phase state diagram. Path 1: $V_1$ = bicelle solution, $V_2$ = DHPC solution (8 mM), Path 2: $V_1$ = bicelle solution, $V_{2'}$ = PBS solution (50 mM, pH7.0). The boundaries of self-assembled morphology on the phase state diagram were determined by using DLS and fluorescent probe method. (b) The morphologies of the assemblies on each region of the diagram was showed. (c) Illustration of DMPC/DHPC dilution and DMPC bilayer dispersion in flow path. Blue lipid is DMPC, Orange lipid is DHPC. The size of the bicelles varies depending on the operation within the bicelle region on phase state diagram. When the lipid composition reaches the vesicle region, the assembly form collapses, and a vesicle is obtained.

A new method to prepare the vesicles (liposomes) is expected to be achieved by utilizing the phase transition phenomena from bicelle to vesicle, simply, upon the dilution process.

The possibility to utilize the discoidal lipid membrane as a core material for membranous materials was discussed in this chapter. In order to find the control factors for the continuous preparation of vesicles using bicelles and to construct a sophisticated protocol of the preparation of membranous functional materials. A simple method to prepare the vesicle with heterogeneous membrane surface was newly investigated to apply the continuous flow by microfluidic device and employ the bicelle as a meso-scale to form the self-assembled vesicle. As illustrated in **Figure 4-1**, two dilution conditions with different lipid composition were selected on a "*bicelle*" scheme. In Path 1, the solution of the long-chained DMPC was diluted by DHPC solution, and in Path 2, the bicelle suspension was diluted by phosphate buffer. These conditions were set to study the mechanism of the structural and morphological change, such as disk-like assemblies to micelles or vesicles. The size distribution of the self-assemblies after dilution was studied by dynamic light scattering (DLS) analysis in order to determine the operational condition. The membrane properties of the obtained liposomes were characterized by using fluorescence probes.

## 2. Materials and Methods

### 2.1. Materials

1,2-Dihexanoyl-*sn*-glycero-3-phosphocholine (DHPC) and 1,2-dimyristoyl-*sn*-glycero-3-phosphocholine (DMPC) were purchased from Avanti Polar Lipids, Inc. (Alabaster, AL, USA). 1,6-Diphenyl-1,3,5-hexatriene (DPH) and 6-dodecanoyl-N,N-dimethyl-2-naphthylamine (Laurdan) were purchased from Sigma-Aldrich (St. Louis, MO, USA). Sodium dihydrogenphosphate (anhydrous) and disodium hydrogenphosphate were purchased from Wako Pure Chemical (Osaka Japan), and were used to prepare phosphate buffer (50 mM, pH 7.0). Ultrapure water was prepared with the Millipore Milli-Q system (EMD Millipore Co./Direct-Q® UV3). Other chemicals were used without further purification. The concentrations of the lipids were measured with an assay kit (Phospholipid C-Test; Wako Pure Chemical).

### 2.2. Bicelle preparation by thin-film hydration method

A chloroform solution of phospholipids was dried in a round-bottom flask by rotary evaporation under vacuum. The resulting lipid films were dissolved in chloroform once more, and the solvent was evaporated. This operation was repeated at least twice. The obtained lipid thin film was kept under high vacuum for at least 3 h, and then hydrated with phosphate buffer (PBS, 50 mM, pH 7.0) at room temperature. The phospholipid mixtures (20 mM) were prepared over the critical micelle concentration of DHPC (15 mM). The fraction of DHPC was as followings: $X_{DHPC}$ = [DHPC]/([DMPC]+[DHPC]) = 8 mM/(12+8 mM) = 0.40. Since the phase transition temperature ($T_m$) of DMPC bilayer is 23 ºC, the obtained DMPC/DHPC bicelle suspension was frozen at -80 ºC and then thawed at 40 ºC (over the $T_m$ of DMPC); this freeze-thaw cycle was repeated five times [Taguchi *et al*., 2017].

### 2.3. Liposome preparation by non-solvent $CO_2$ method

The liposome was prepared by using the stainless batch reactor, TSC-$CO_2$-08 (inside volume of 80 mL, Taiatsu Techno Co., Tokyo, Japan). The liposome was used to compare the membrane properties from each preparation method. A phospholipid powder (4.5 mg), distilled water (3 mL), and $CO_2$ (liquid, l) were incubated in the reactor with stirring at various temperatures (25, 50 ºC) and pressures (5, 10 MPa). After 20 min incubation for equilibration,

the sample solutions were decompressed by releasing $CO_2$. The lipid concentration was measured by using phospholipid C-test Wako® (Wako Pure Chemical Industries, Ltd.) [Takayama *et al.*, 1977].

### 2.4. Dilution of DMPC/DHPC Mixtures in Continuous Flow

The T-type flow injection chip (φ =1 mm) was employed to dilute DMPC/DHPC suspensions at several flow rates (**Figure 4-2**). The suspensions ($V_1$) had entered the flow of 8 mM DHPC in PBS solution ($V_2$) or PBS ($V_2$') by a syringe pump at 50-400 μL/min, which laminar flow with a low Reynolds number ($Re << 2300$). Then, the flow rate of the sample was constant (100 μL/min). At a low *Re* number in small flow path, the effect of *Re* can be neglected in the flow, whereas the injected droplets were depended on the value of capillary number (*Ca*), that is relating to the viscous forces onto the surface tension. [Ba *et al*. 2015]. Phospholipid suspension in aqueous solution has small viscous force compared with surface tension [Cogan *et al*. 1973, Sugiura *et al*., 2000, Uline *et al.,* 2012]. In addition, the droplet formation mechanism of the injected suspension is similar at low *Ca* ($Ca << 1$) for both symmetric and asymmetric T-junctions [Ba *et al*., 2015]. Thus, the flow rate was set in the range on same injection flow. After the dilution at several rates ($V_1/V_2$ or $V_2$') of injections, the samples were estimated membrane properties by each fluorescence probes. The total length of the flow path is about 30 cm from bicelle injection syringe to outlet.

### 2.5. Dynamic Light Scattering (DLS)

The apparent sizes of bicelles (total lipid concentration: 20 mM) were determined by dynamic light scattering (DLS). Measurements were performed with Particle Size Analyzer (LB-500, HORIBA). The average diameters were calculated based on a number-average diameter.

### 2.6. Evaluation of the membrane fluidity inner membrane

The fluidity of the vesicle membrane was evaluated based on the previous reports [Mary *et al*. 1976]. A fluorescent probe DPH was added to bicelle and vesicle suspension with a molar ratio of lipid/DPH = 250/1. The fluorescence polarization of DPH (Ex. = 360 nm, Em. = 430 nm) was measured using a fluorescence spectrophotometer (FP-8500; JASCO, Tokyo,

Japan) after incubation for 30 min. The sample was excited with vertically polarized light (360 nm), and emission intensities both perpendicular ($I_\perp$) and parallel ($I_\parallel$) to the excited light were recorded at 430 nm. The polarization ($P_{DPH}$) of DPH was then calculated by using the following equations:

$$P_{DPH} = (I_\parallel - GI_\perp)/(I_\parallel + GI_\perp)$$
$$G = i_\perp/i_\parallel$$

where $i_\perp$ and $i_\parallel$ are emission intensity perpendicular and parallel to the horizontally polarized light, respectively, and $G$ is the correction factor. The membrane fluidity was evaluated based on the reciprocal of polarization, $1/P_{DPH}$.

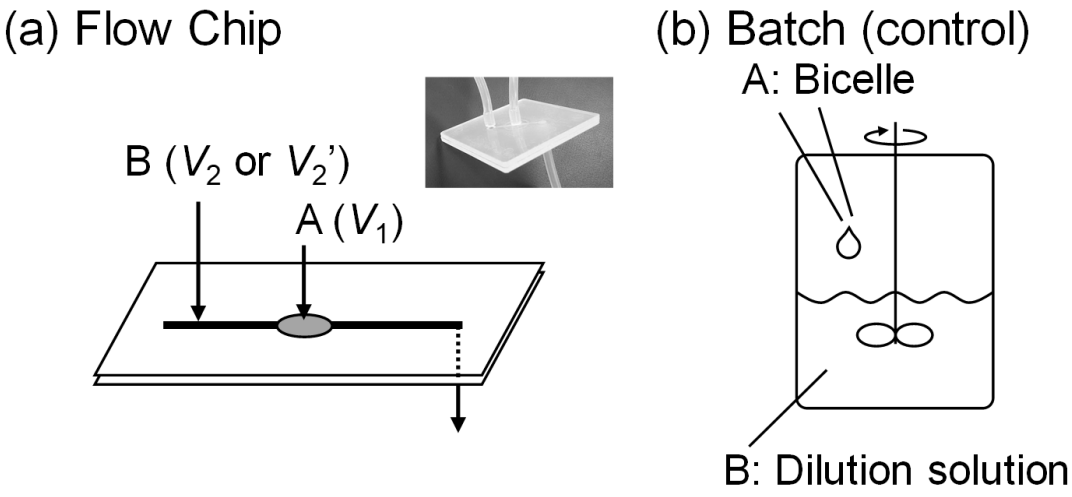


**Figure 4-2.** Schematic illustration of apparatus for vesicle preparation by diluting bicelles ($X_{DHPC}$ = 0.40) in (a) flow system and (b) batch system as control. In flow system, bicelle solution (A, $V_1$) was mixed with various dilution solution (B such as DHPC in PBS ($V_2$) or PBS ($V_2$')) in T-type flow injection chip (width 1 mm, depth 0.4 mm) at 20 ºC; $V_1$: DMPC (12 mM)/DHPC (8 mM) bicelle in PBS solution (50 mM, pH7.0), $V_2$: DHPC solution 8mM in PBS solution, $V_2$': PBS solution. In the batch system, the bicelle was directly diluted in bottles by dilution solution.

## 2.7. Evaluation of Membrane Polarity

Fluorescent probe Laurdan is sensitive to the polarity around itself, which allows the local polarity in lipid membranes to be determined [Parasassi *et al*., 1995, Nakamura *et al*., 2015]. Laurdan emission spectra exhibit a red shift caused by dielectric relaxation. Thus, emission spectra were calculated by measuring the general polarization ($GP_{340}$) for each emission wavelength as follows:

$$GP_{340} = (I_{440} - I_{490})/(I_{440} + I_{490})$$

where $I_{440}$ and $I_{490}$ are the emission intensities of Laurdan excited at 340 nm. The obtained emission spectrum was furthermore analyzed by using Peakfit software (v.4.12, Systat Software Inc., San Jose, CA, USA) [Iwasaki *et al*., 2017]. After deconvolution, the area fraction of each component was compared.

## 3. Results and Discussion

### 3.1. Comparison in preparation methods from membrane phase state

Three kinds of methods, such as (i) conventional thin film hydration, (ii) high pressure $CO_2$/water interface, and (iii) bicelle dilution, were compared to on the membrane properties of liposomes (**Figure 4-3**). The membrane properties were analyzed, and their features were summarized in **Figure 4-4** and **Table 4-2**.

The thin film hydration is one of the methods of the batch-wise vesicle preparation [LeBerre *et al*. 2008]. In this method, the thin film of lipids is formed on a round-bottom flask, and the liposome suspension can be obtained by hydration with some aqueous solution. The membrane properties of the vesicle prepared at different pressures and temperatures were mainly characterized in relation to the membrane fluidity ($1/P_{DPH}$) and membrane polarity ($GP_{340}$), by using the fluorescent probes DPH and Laurdan, respectively. In **Figure 4-4**, the position plotted in the Cartesian diagram indicates the phase state of each membrane: the first and fourth quadrants for disordered phase, and the second quadrant for ordered (gel) phase (refer to chapter 2). The DMPC liposome from thin film hydration was ordered phase at 16 ºC ($< T_{m,\,DMPC}$).

The $CO_2$ (*l*)/water (*l*) two-phase (heterogeneous) system, such as semi-batch system, resulted in the formation of DMPC and 1,2-dipalmitoyl-*sn*-glycero-3-phosphocholine (DPPC) liposomes with high yield (ca. 85-88% in **Figure 4-5**) [Nakamura *et al*., 2015]. High-pressure $CO_2$ liquid (*l*) could assist the dispersion of lipid molecules in the water phase. Because of the lower dielectric constant of high-pressure $CO_2$ (*l*), lipid molecules could be soluble in the $CO_2$ phases, and then the membrane could be formed at the interface of the $CO_2$ (*l*)/water (*l*). Then, the membrane properties of the DMPC liposome from high-pressure $CO_2$/water system showed a state of an ordered phase (**Figure 4-4**). In addition, the $CO_2$ gas was also dispersed from the suspension to the atmosphere. The liposome suspension obtained finally was found to be homogeneous.

It is suggested that high-pressure $CO_2$ can be used to form an appropriate hydrophobic-hydrophilic interface where phospholipid molecules as a self-assembled membrane. Although this method does not use organic solvents, it is difficult to control the behavior of the interface between $CO_2$ and water phases, and, furthermore, it is impossible to manipulate the heterogeneity and asymmetry of bilayer membranes.

■ Thin film hydration

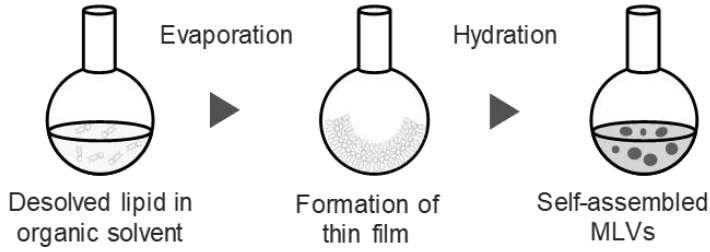


■ Reverse phase evaporation

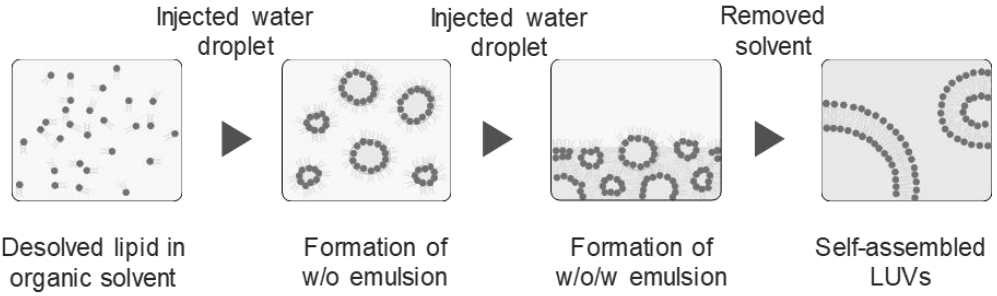


■ High-pressure $CO_2$/water inerface

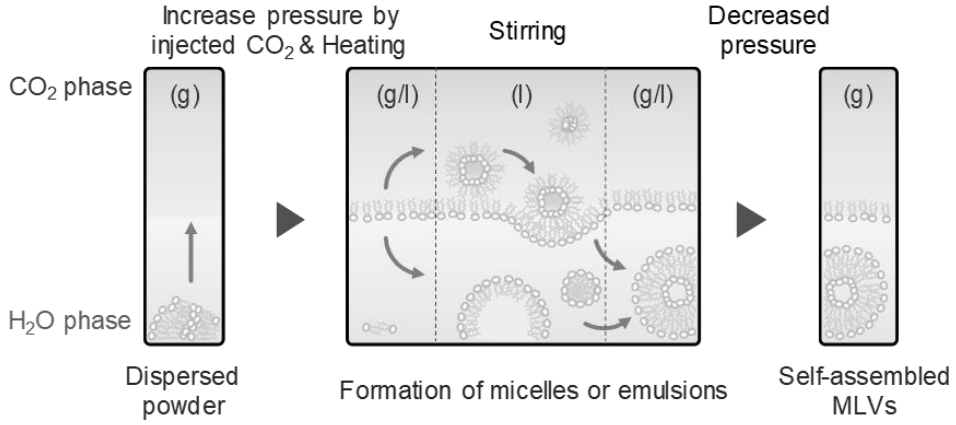


■ Bicelle dilution (in *Chapter 4*)

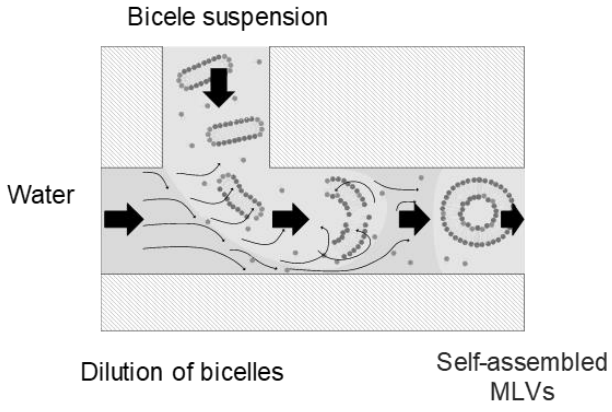


**Figure 4-3.** Outline of each vesicle preparation method.

On the other hand, a discoidal DMPC/DHPC bicelle changes to a spherical DMPC-rich vesicle by dilution (refer to chapter 2). The phenomenon is observed simply by the hydration of DHPC molecules with dilution. Then, an edge of a bicelle is destabilized and nearby DMPC bilayers fuse together. The membrane properties of the assembly were analyzed as noted above (**Figure 4-4**). The results showed that the assembly had similar membrane properties with conventional methods. In addition, it clarified that the membrane properties were stepwise shifted, depending on the dilution rate (section **3.2** in chapter 2). Therefore, bicelle can be utilized to vesicle preparation without organic solvents. Based on the knowledge of the morphological change of the assemblies to the lipid concentrations from "chapter 2", the bicelle dilution can be continuously prepared vesicles by flow system.

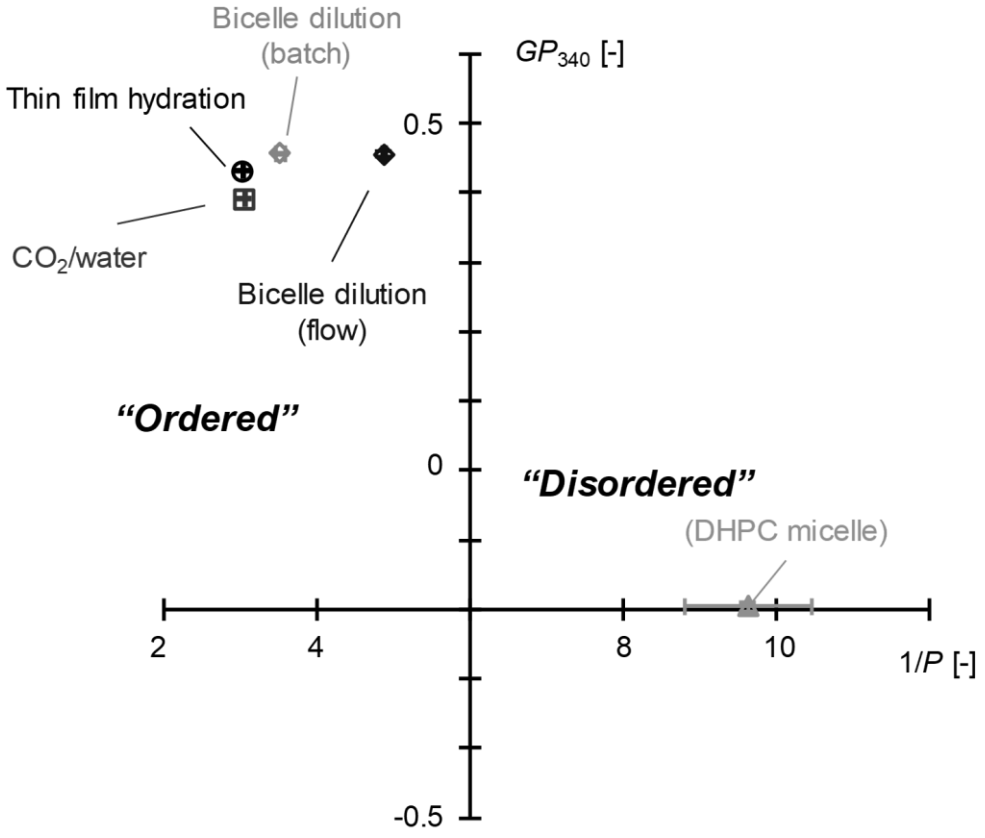


**Figure 4-4.** Comparison of the membrane properties of each DMPC vesicle (< $T_{m,DMPC}$); (circle) thin film hydration, (square) high-pressure $CO_2$/water interface, (diamond) bicelle dilution. 2nd quadrant means an ordered phase of a membrane in this diagram. The value of DHPC is plotted as reference of disordered micelle.

**Table 4-2.** List of features of each membrane preparation method.

| | Lipid | System | Assembly | Phase state (< $T_m$) |
|---|---|---|---|---|
| Thin film hydration | DMPC | Batch (non-continuous) | MLVs | Ordered |
| $CO_2$/water interface | DMPC | Semi-batch (stepwise) | MLVs | Ordered |
| Bicelle injection | DMPC | Continuous | MLVs | Ordered |

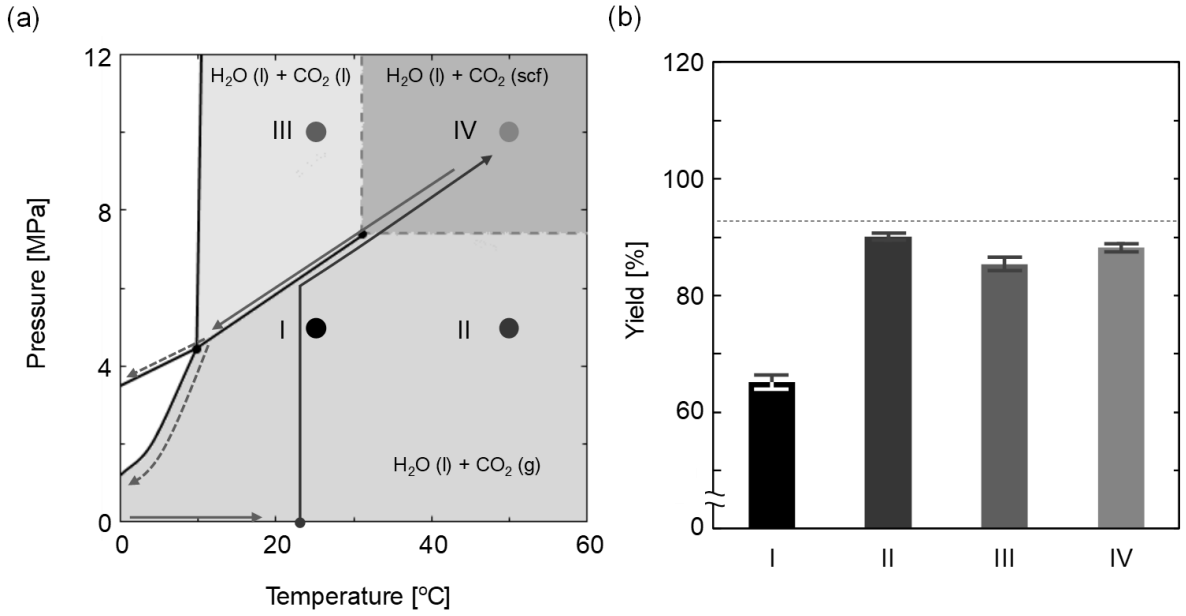


**Figure 4-5.** (a) Pressure-Temperature phase diagram of $CO_2$/$H_2O$ system. According to the literature [Dimond *et al.*, 2003], the state of $CO_2$ was represented as follows: (g), gas; (*l*), liquid; and (scf), supercritical fluid. Arrows indicate the vesicle preparation procedure in the $CO_2$/water/phospholipid system: solid and dashed arrows represent the compression and decompression steps, respectively. The total preparation time was in 20 minutes. The pressure and temperature for systems I, II, III, and IV are as follows: (I) 25 ºC and 5 MPa; (II) 50 ºC and 5 MPa; (III) 25 ºC and 5 MPa; and (IV) 50 ºC and 10 MPa. (b) Relationship between preparation condition of DPPC vesicle and yield. (I), (II), (III), and (IV) indicate the experimental conditions showed in (a), where the yield was calculated as follows: yield [%] = $C_{vesicle}/C_{ideal}\times100$. Dashed line indicates the yield of the DPPC liposome prepared by the conventional method (92.8±3.0 %).

### 3.2. Bicelle dilution method based on morphological change of DMPC/DHPC system

A possibility of vesicle preparation via dilution of bicelle solution was first investigated. As shown in **Figure 4-2**, its dilution was performed both in continuous dilution using flow chip system (**Figure 4-2a**) and in batch dilution system (**Figure 4-2b**).

**Figure 4-1** indicated the diagram to show the phase state of the lipid self-assembly (micelle: $l_d$, bicelle: $l_o$-bilayer with $l_d$-edge, vesicle: $l_o$-bilayer) as functions of both DMPC and DHPC concentration. Based on this phase diagram, it can be distinguished that the difference of the structure states of lipid solution under various condition. To study the phase transition phenomena of bicelles to micelles (Path 1) and vesicles (Path 2), the dilution was achieved by two dilution pathways and the boundaries of conditions for self-assembled morphology were investigated on the DMPC/DHPC diagram, which was determined by using DLS and fluorescent probe method. The operational conditions upon the dilution process using the flow chip system were summarized in **Table 4-3**. For the generation of vesicles or micelles by dilution methods, the initial solution was prepared with 12 mM DMPC and 8 mM DHPC ($X_{DHPC}$ = 0.40) solution, in which bicelle can be formed at initial condition. In case of Path 1, the initial solution of the bicelle was mixed with the pure DHPC solution (8 mM) by using the flow chip. **Figure 4-1** indicates that the final solution, after only the DMPC concentration can be diluted (15 mM to 2.4 mM) at the same DHPC concentration (8 mM), can be approached at the region to show the discoidal micelles (from (0) to (1)). In Path 2, the initial bicelle solution was diluted by PBS buffer solution without amphiphilic molecules at various ratios of $V_1/V_2$, (from (0) to (2)-(5)). In this operation, a phase transition from bicelle to vesicle can be carried out based on the diagram (**Figure 4-1**).

**Table 4-3** Summary of experimental conditions.

| | $V_1$ [μL/min] | $V_2$ or $V_2$' [μL/min] | $V_1/V_2$ or $V_2$' | Final DMPC conc. [mM] | [DMPC]/[DHPC] (q-value) | Re [-] |
|---|---|---|---|---|---|---|
| (1) | 100 | 400 | 0.25 | 2.4 | 0.3 | 10.6 |
| (2) | 100 | 50 | 2 | 8 | 1.5 | 3.2 |
| (3) | 100 | 67 | 1.5 | 7.2 | 1.5 | 3.5 |
| (4) | 100 | 100 | 1 | 6 | 1.5 | 4.2 |
| (5) | 100 | 200 | 0.5 | 4 | 1.5 | 6.4 |

$V_1$: DMPC (12 mM)/DHPC (8 mM) bicelle in PBS solution (50 mM, pH7.0)
$V_2$: DHPC solution 8mM in PBS solution (1), $V_2$': PBS solution (2-5)

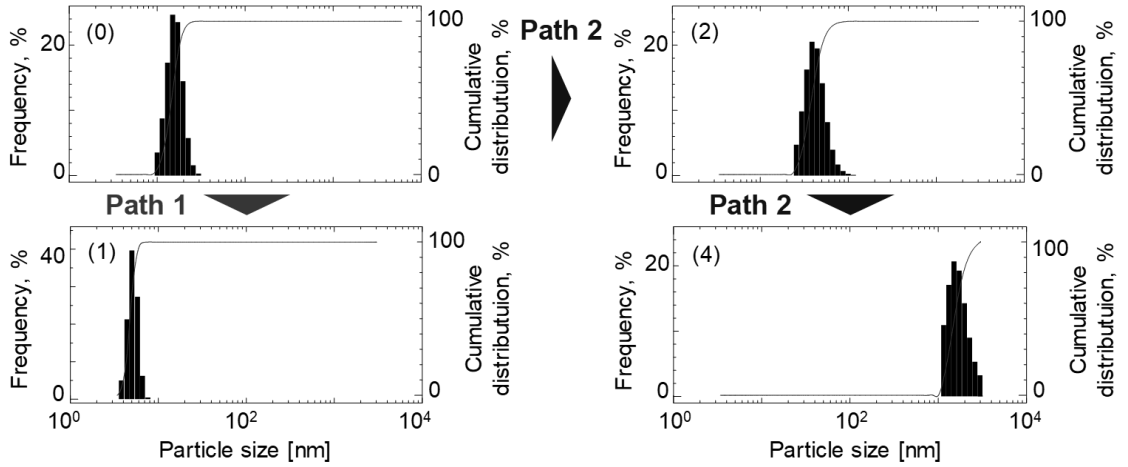


**Figure 4-6.** Representative size distribution of the suspension obtained by each flow path (Path 1 and 2) at 20 ºC. The conditions were aligned with those numbers (0, 1, 2, 4) of **Table 4-3**. The black bars are data of size distribution using DLS measurement for representative conditions and the red curves show cumulative distributions.

### 3.3. Morphological change of DMPC/DHPC self-assemblies relative to dilution path

The morphological change of the self-assembly in an aqueous solution was first studied by monitoring the optical density of the solution after the dilution. In order to obtain the physical character of the self-assembly more in details, the size distribution of the self-assemblies in the final solution after the dilution was measured by using the DLS analysis (**Figure 4-6**). That shows the size distribution of the original bicelle solution ((0) in **Figure 4-6**), showing that the average size of the bicelle is 10-20 nm. The size distribution of the self-assembly in solution (1) after dilution was shown in **Figure 4-6**, indicating that the average size was reduced and was equal to that of discoidal micelle (5-9 nm). It has been reported that the size of the DMPC/DHPC bicelle depends on the $X_{DHPC}$ through the batch dilution experiment, where the size decreases with the increase of DHPC concentration (the increase of $X_{DHPC}$) because of its fluidization effect. The obtained results were corresponding with the previous findings. The size distribution in the solution (2) and (4) in Path 2 was also shown in **Figure 4-6**, respectively. It was found that the average size was the greater than that of original bicelle and the size in the obtained solution increased with the increase of the dilution rate. It is known that the DHPC molecules can be accumulated at the edge of the bicelle structure and play an important role of the stabilization of the hydrophobic edge of the bilayer structure. By the

reduction of the total lipid concentration (i.e., via dilution), the DHPC molecules tend to be more hydrated in contrast to DMPC, resulting that the bicelle-edge was broken, and the vesicle was formed through the fusion of the bicelles. The results obtained in this study correspond with the previous finding examined in batch dilution experiments [Nakamura *et al*. 2015]. It was found that the size of obtained assembly in the dilution solution could be controlled by changing the fluidization rating in the flow chip.

### 3.4. Characterization of membrane properties according to continuous flow path

The membrane properties of the vesicles prepared by using the flow chip were furthermore studied by using the fluorescence probes. Then, the effect of type of (i) dilution path (Path 1 and 2) and (ii) ratio (Path 2) on the membrane properties were investigated in the continuous dilution method using a flow chip (**Figure 4-2a**), together with batch dilution method as a control. In all the experiments, relating to the DMPC/DHPC self-assemblies upon the dilution, both the membrane fluidity ($1/P_{DPH}$) and membrane polarity ($GP_{340}$) were analyzed by using DPH and Laurdan, as a molecular probe, respectively. Herein, the evaluation of inner membrane fluidity by probe DPH depends on rotation of probe molecules in the system [Mary *et al*., 1976] and Laurdan has the property that is easily inserted into the bilayer region due to the hydrophobic chain near the membrane surface [Parasassi *et al*., 1995]. Furthermore, a Cartesian diagram as functions of both $1/P_{DPH}$ and $GP_{340}$ values was plotted to estimate the state of the membrane of the self-assemblies according to the previous report [Nakamura *et al*., 2015].

First, the effect of (i) dilution path on the membrane properties was studied as shown in **Figure 4-7**. In batch dilution system on Path 1 as control method, the initial DMPC/DHPC bicelle ($X_{DHPC}$ = 0.40, 20 mM) had ordered gel phase, judging from the low membrane fluidity ($1/P_{DPH,\ Bicelle} < 6$, **Figure 4-7a**) and the high membrane polarity ($GP_{340,\ Bicelle} > -0.2$, **Figure 4-7b**) at the DMPC bilayer membrane of the bicelle which was obtained previous results [Nakamura *et al*., 2015]. On the other hand, the fluidity and polarity of membrane by flow chip system were furthermore investigated, indicating the ordered phase of the obtained liposomes. Generally, cartesian diagram analysis, where the ordered phase of the membrane appeared in the second quadrant. **Figure 4-7c** shows the obtained from micelle structure was plotted in first or fourth quadrants due to the higher membrane fluidity and the lower membrane polarity. After

the dilution of bicelle by DHPC solution on batch system, the self-assembled structure was plotted at the second quadrant as well as ordered phase. Thus, the molecular self-assembly according to dilution is considered to be a bicelle with bilayer structure. While the membrane properties of flow system were kept to be at the same regardless of whether before and after dilution of initial state based on the plot data. The assembled molecules have as like as a bilayer membrane structure, like bicelle because the size is close to micelle's one. In relation to vertically downward operation on the phase diagram on the region of bicelle (Path 1, **Figure 4-1**), bicelle did not collapse completely, and it became a smaller bicelle and dispersed in the solution.

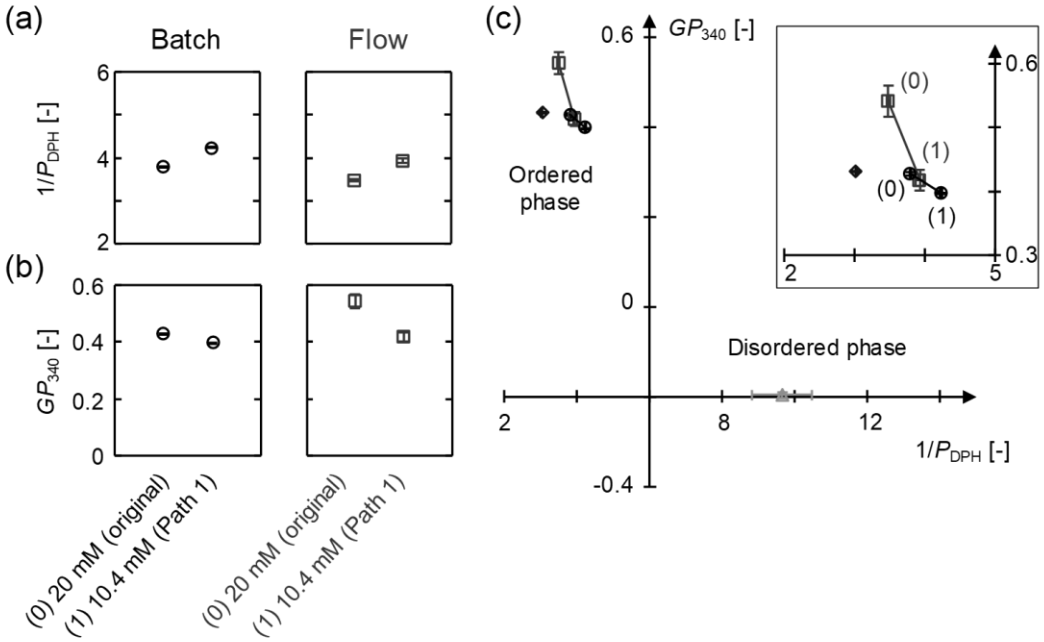


**Figure 4-7.** Comparison of membrane properties at Path 1 and at batch type dilution. For reference, the values of DHPC micelle and DMPC vesicle are listed in (a) and (b). (c) Cartesian diagram of each assemblies; (circle) batch system, (square) flow system, (diamond) DMPC vesicle, (triangle) DHPC micelle, at 20 ºC. Based on Cartesian diagram analysis, the vesicles exist in the first to fourth quadrants are in disordered phases, while those exist in the second quadrant are in ordered phases. As references, values of ordered DMPC vesicle ($1/P_{DPH}$ = 3.0±0.0, $GP_{340}$ = 0.43±0.0) and disordered DHPC micelle ($1/P_{DPH}$ = 9.6±0.8, $GP_{340}$ = -0.2±0.0) at 20 ºC were plotted the diagram.

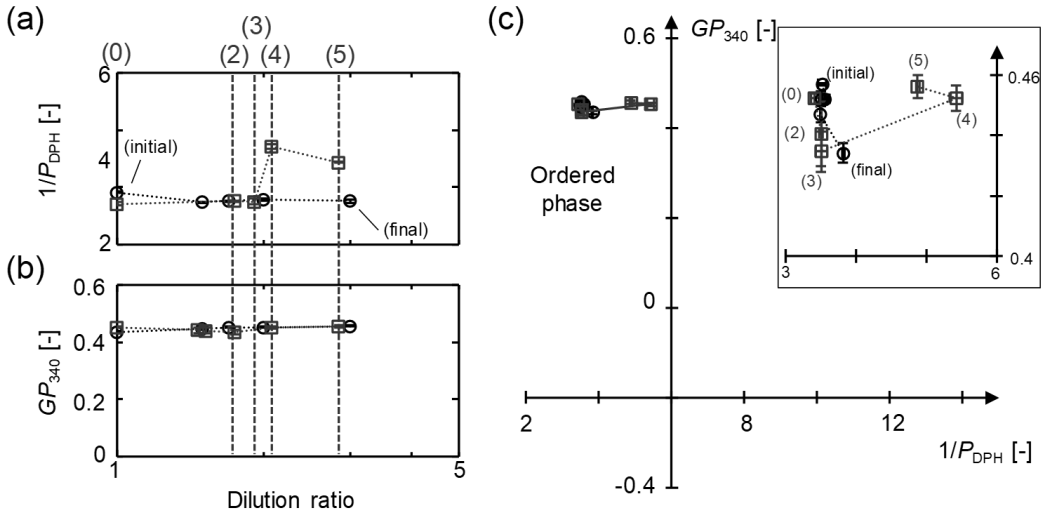


**Figure 4-8.** Each bicelles ($X_{DHPC}$ = 0.40, 20 mM) were diluted by injection of PBS solution which those membrane properties were analyzed at 20 ºC; (a) inner membrane fluidity, (b) membrane polarity; (circle) batch system, (square) flow system in Path 2.

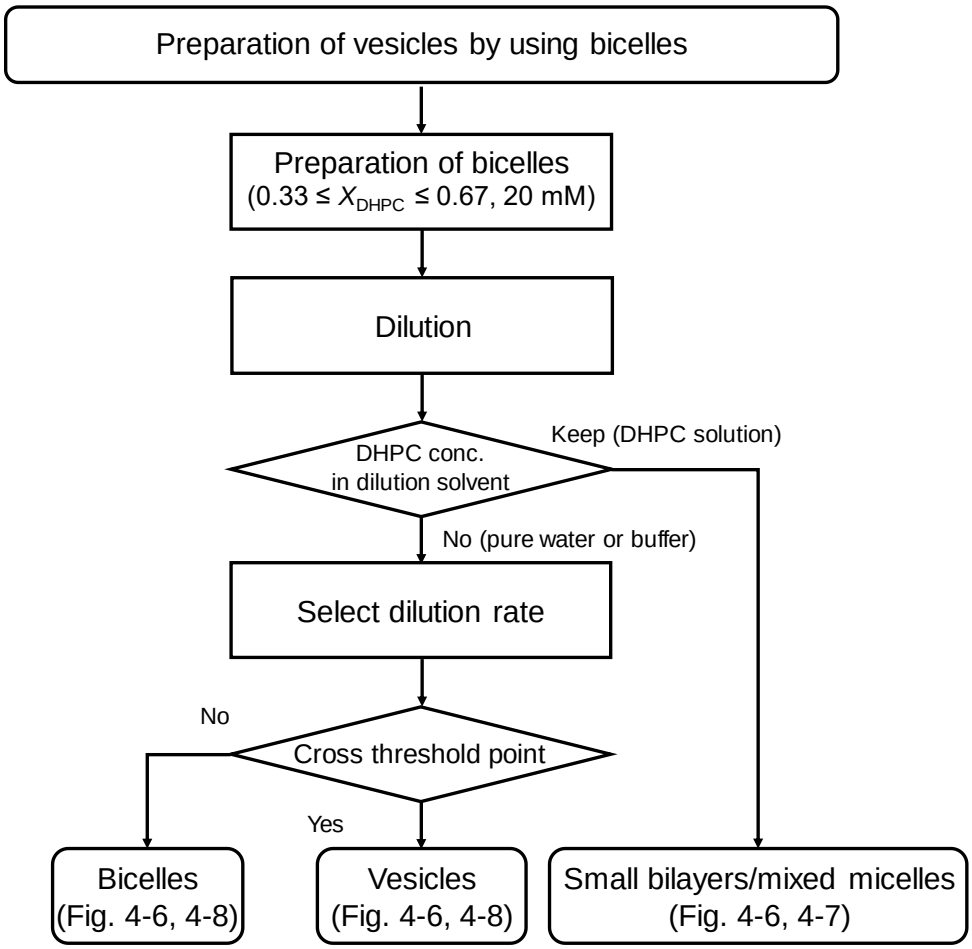


**Figure 4-9.** Protocol of planar membrane preparation as vesicles by using bicelles.

Secondly, the effect of (ii) dilution ratio on the membrane properties (Path 2) was investigated based on flow chip or batch dilution system as shown in **Figure 4-8**. In Path 2, the bicelles which is positioned at initial condition (0) in **Figure 4-1** were diluted by using the PBS solution, where the total lipid concentrations decreased proportionally along with a line of Path 2. **Figure 4-8a** and **4-8b** show the values of $1/P_{DPH}$ and $GP_{340}$ were plotted against the dilution ratio. In case of batch system, there was no significant change in the values [Suga *et al,*. 2013, Nakamura *et al*. 2015]. As shown in **Figure 4-8c**, the obtained data were plotted in the second quadrant, showing the characteristic of ordered phase properties. However, in the flow system, the $1/P_{DPH}$ value was slightly increased (**Figure 4-8a**), it should be indicated that DHPC molecules remains the inner bilayer membrane. While no significant change was observed in the $GP_{340}$ value (**Figure 4-8b**), it is suggested that the Laurdan molecules were localized at in DMPC bilayer region, wherein the membrane polarity did not depend on the morphological change upon the dilution operation. In the Cartesian coordinate plot (**Figure 4-8c**), since the micro-scale assemblies showed the ordered phase, it is considered that the obtained assembly could be regarded as DMPC-rich vesicle. The vesicle was assembled containing slightly heterogeneous (disordered) phases upon the dilution in the continuous flow path. Generally, the diffusivity of particles in a narrow flow path is the lower than in the vessel batch system. It is thought that the difference in diffusivity upon the dilution process affects on the membrane properties of the self-assembled structures formed. Therefore, it is expected that the self-assembly molecules can be controlled by operating the membrane component at the outlet of the flow channel (**Figure 4-9**).

## 4. Summary

A discoidal DMPC/DHPC bicelle was shown to be changed to a spherical DMPC-rich vesicle by dilution. The membrane properties, such as membrane fluidity and membrane polarity based on the analyses using fluorescence probes, were similar with those of liposomes based on the analysis using conventional membrane preparation methods (thin film hydration and high-pressure $CO_2$/water). The morphological change was found to be induced by hydrating and removing DHPC molecules on a DMPC bilayer with dilution. Whereas high-pressure $CO_2$/water system has advantage of non-used organic solvents, the hard condition such as pressure is difficult to control the property of $CO_2$/water interface preciously and to prepare the variation of phase separation on membrane surface as biomembranes.

Vesicle preparation was achieved by the continuous dilution of the DMPC/DHPC bicelle by a flow chip. The vesicle was found to be formed through the fusion of the bicelles in simple flow path device. The membrane properties of the obtained vesicle showed an ordered phase state close to DMPC bilayer membrane, while the obtained vesicle contained possess a weak character of heterogeneous phases. The benefits of the flow path dilution are to continuously change the lipid composition by simply change the flow rate in the flow path. It is expected that the technique could have the potentials to continuous-type preparation method to enable a heterogeneous membrane like a living cell membrane by designing a flow path.

# Chapter 5

## Preparation of Heterogeneous Supported Lipid Bilayers (SLBs)

### 1. Introduction

Supported lipid bilayers (SLBs) are artificial planar membranes made of amphipathic lipids on a solid substrate such as glass or metal [Green *et al.*, 2004, Boudard *et al.*, 2006]. SLB is often utilized for the platform of the sensing of biochemicals and/or biomacromolecules and that of the biomimetic technologies [Juhaniewicz *et al.*, 2015]. For example, a membrane film in which a bilayer membrane is immobilized on a glass or an electrode substrate has been studied as a material for observing the permeability of ions and molecules in a biological membrane [Watts, 1995, Juhaniewicz *et al.*, 2015]. Among the possible preparation methods, vesicular fusion method is well known as the SLB formation method [Abraham *et al*., 2018]. The vesicles added to the hydrophilized glass substrate adsorbs to the substrate through the electrostatic interaction ("vesicle adsorption"), and the vesicles collapse to obtain a planar film ("vesicle rupture"). For the adsorption of vesicles, a hydrophilic glass substrate containing silicon dioxide and mica are often used [Biswas *et al.,* 2018]. The interaction between vesicle and substrate depends on parameters, such as ionic strength, pH of the solution and divalent cation [Boudard *et al.,* 2006, Biswas *et al.,* 2018, Dacic *et al.,* 2016].

The SLB formation is known to depend on the membrane properties of the fed vesicles, where the lipid membranes with high fluidity can easily form SLB because it is prone to vesicle rupture. The ordered lipid membrane hardly causes the rupture, thus, the quality of SLB is lower for example involving cracks and unnecessary multi stacks of assemblies. Tabaei *et al.* reported the solvent-assisted lipid bilayer (SALB) as an SLB preparation method without using vesicles [Tabaei *et al.*, 2014]. This method is inspired by reverse-phase evaporation in batch-wise to make a unilamellar bilayer. The lipid molecules dissolved in the water/isopropanol solution assemble to the formation of a planar bilayer upon a gradual increase in the solvent water fraction. The 1,2-dioleoyl-*sn*-glycero-3-phosphocholine (DOPC, C18:1) bilayer film was formed on the substrate by continuously adding the DOPC solution. In this method, any materials besides silicon dioxide, such as alumina, gold, titanium, and silica, can be employed because of principle. It is noted that the water/oil flow ratio and the total lipid concentration

■ Vesicle fusion

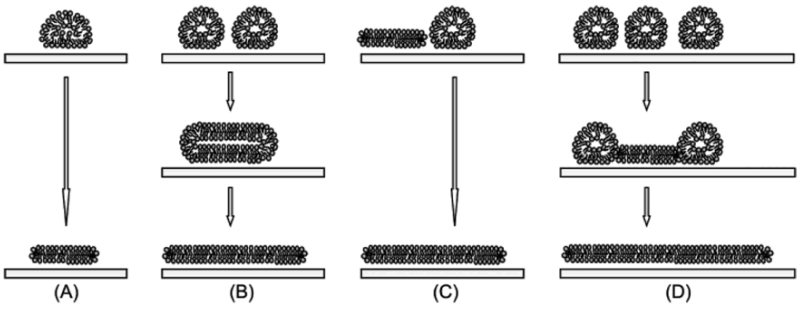


(Richter *et al.*, 2006)

■ SALB

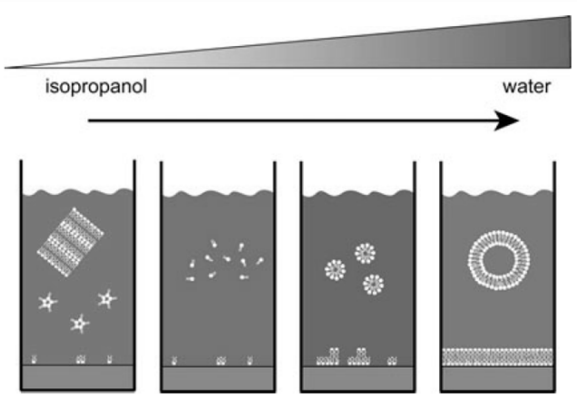


(Hohner *et al.*, 2010)

■ Continuous bicelle injection

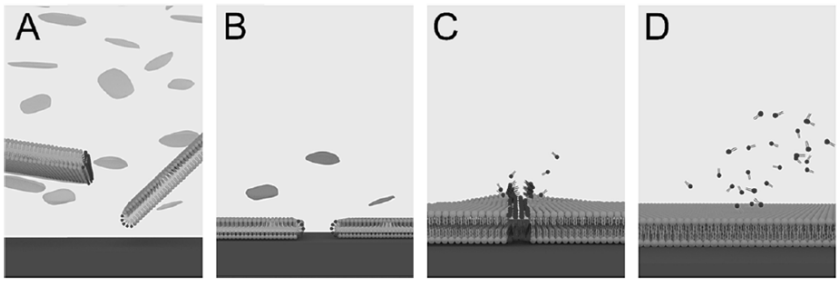


(Kolahdouzan *et al.*, 2017)

**Figure 5-1.** Outline of each representative SLB formation method.

**Table 5-1** List of operation factor of each SLB formation method.

| | Organic solvent | System | Operation factor | Residual solvent | References |
|---|---|---|---|---|---|
| Vesicle fusion | Non-use | Non-continuous | Salt, pH, Temperature | No | Abraham *et al*. 2018 |
| SALB | Use | Continuous | Solvent-to-water ratio | Unknown | Tabaei *et al*. 2014 |
| Bicelle injection | Non-use | Continuous | DHPC concentration | No | Kolahdouzan *et al*. 2017 |

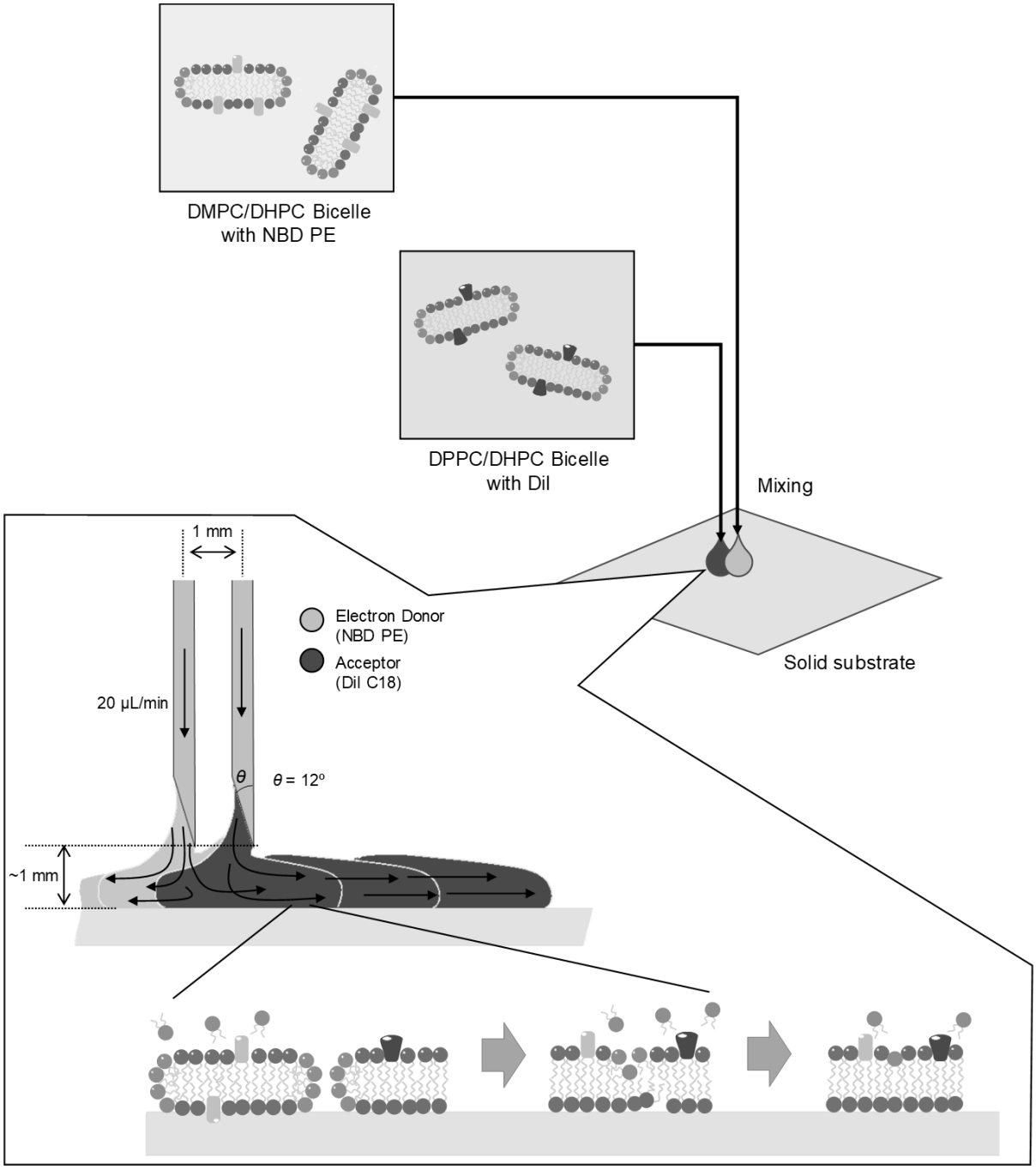


**Scheme 5-1.** SLB preparation by using bicelle suspension.

inside the flow channel must be operated to form a bilayer film. In their experimental system, it is necessary to maintain a lipid concentration, at least 0.1 mg/mL, in the organic solvent.

Recently, Kawasaki *et al.* reported planar membranes using 1-palmitoyl-2-oleoyl-glycero-3-phosphocholine (POPC, C16:0-18:1)/ 1,2-dihexanoyl-*sn*-glycero-3-phosphocholine (DHPC, C6:0) mixtures to solubilize and reconstitute membrane proteins on planar membranes at continuous system [Morigaki *et al.,* 2012]. Below the $CMC_{DHPC}$, the lipid membrane adsorbed on the substrate was not peeled off by rinsing. They evaluate the membrane properties of the SLB from the lateral diffusivity of lipid molecules by fluorescence recovery after photobleaching and the SLB has the same characteristics as SLB prepared by the vesicle fusion method. Preparation of SLB was achieved by using bicelles in the complete aqueous condition. Kolahdouzan *et al.* observed the process of SLB formation from DOPC/DHPC bicelle by fluorescence microscopy. According to their investigation, when the total lipid concentration is low ($< CMC_{DHPC}$), the lipid aggregate in the bulk and the lipid bilayer on the substrate are mainly DOPC. Then, DHPC molecules are present as monomers in the bulk. An unstable change in the mass on the substrate surface was observed after adsorption of the bicelle to the substrate at DHPC-rich condition. Because the DHPC molecule destabilizes in the membrane, it is claimed that control of DHPC concentration is important for the formation of SLB. The examples given above are summarized in **Table 5-1** and **Figure 5-1**. Kolahdouzan and colleagues claim that they formed a disc-like assembly with DOPC/DHPC system, while the evidence had not been showed. It is difficult to judge whether this SLB formation is due to the disk-like structure or the fluidity of the DOPC bilayer. In addition, experiments on multicomponent lipid membrane system for applying biomembrane mimetics have not been reported.

In this chapter, SLB was prepared by using a bicelle as a source material of the SLB. I studied the forming a heterogeneous SLB by adding bicelles with bilayer membranes of different compositions such as 1,2-dimyristoyl-*sn*-glycero-3-phosphocholine (DMPC, C14:0) and 1,2-dipalmitoyl-*sn*-glycero-3-phosphocholine (DPPC, C16:0) by non-continuous and also continuous system (**Scheme 5-1**). Discrimination of the disk-structure of a bicelle conformed to chapter 2. A fluorescence microscope monitored a formation of SLBs. Heterogeneous texture of the SLB surface was observed by using the Förster resonance energy transfer (FRET). These results presented were shown that the bicelle dilution method is effective technique to fabricate a planar lipid bilayer. The method is demonstrating that it has the potential to wide application.

## 2. Materials and Methods

### 2.1. Materials

DMPC, DPPC, DHPC, 1,2-dioleoyl-sn-glycero-3-phosphoethanolamine-N-(lissamine rhodamine B sulfonyl) (ammonium salt) (Rhod PE, C18:1), 1,2-dipalmitoyl-sn-glycero-3-phosphoethanolamine-N-(7-nitro-2-1,3-benzoxadiazol-4-yl) (ammonium salt) (NBD PE, C16:0), and were purchased from Avanti Polar Lipids, Inc. (Alabaster, AL, USA). 1,1'-Dioctadecyl-3,3,3',3'-Tetramethylindocarbocyanine Perchlorate (DiI, C18 (3)) was purchased from Thermo Fisher Scientific K.K. (Tokyo, Japan). Sodium dihydrogenphosphate (anhydrous) and disodium hydrogenphosphate were purchased from Wako Pure Chemical (Osaka, Japan), and were used to prepare phosphate buffer (50 mM, pH 7.0). Ultrapure water was prepared with the Millipore Milli-Q system (EMD Millipore Co., Darmstadt, Germany). Other chemicals were used without further purification.

### 2.2. Bicelle preparation

Lipid thin films of DMPC/DHPC or DPPC/DHPC mixtures were prepared by the mothed described on the above. Firstly, the self-assembly solution was prepared at the total lipid concentration of 20 mM, with various DHPC fractions, $X_{DHPC}$: 0.33, 0.40, and 0.67. Then, fluorescence lipids were involved 0.5-1.0mol% in lipids. The obtained lipid thin films were hydrated with phosphate buffer at 20 ºC. The stock solutions were adjusted to 20 mM total lipid concentration. No mechanical treatments (sonication, extrusion) were applied for DMPC/DHPC assemblies, to keep their spontaneous structures. The obtained self-assembly solutions were applied for monitoring dynamic light scattering.

### 2.3. Dynamic light scattering (DLS)

The apparent sizes of mixtures were determined by dynamic light scattering (DLS). Measurements were performed with the particle size analyzer (Zetasizer Nano ZS, Malvern Panalytical, Grovewood Rd, UK). The average diameters were calculated based on a number-average diameter.

### 2.4. SLB formation by continuous bicelle addition

SLB was formed on a glass substrate (18×18 mm), which surface was hydrophilized. Prior to each experiment, the substrate was rinsed within a mixture of sulfuric acids and hydrogen peroxide, that used to clean organic residues off substrates. The surface of the substrate is also hydroxylated most surfaces. The hydrophilized substrate was annealed at 400 ºC to smooth the surface. Bicelle suspensions were injected to the substrate under continuous flow conditions in a petri dish (φ90×15 mm), with the flow rate set at 20 μL/min (15 min) by a syringe pump (CX07100, Isis Co., Ltd., Osaka, Japan) at room temperature (**Scheme 5-1**). Then, the distance between injection needle (regular bevel: 12º, NN-2425, Terumo co., Tokyo, Japan) and a substrate was under 1 mm, and the edge of the needle sets perpendicular to the substrate. After the injection step, the bulk solution was sequentially washed out by PBS 1 mL at 20 times. The petri dish was filled with water because the poor stability of SLBs upon exposure to air [Fang, 2011].

### 2.5. SLB monitoring by fluorescence microscope

The SLB produced was observed with a fluorescence microscope. The excitation light range was changed by the fluorescent lipid. The observation of NBD PE was performed with 340-390 nm or 460-495 nm excitation light. Rhod PE and DiI were also excited at 530-550 nm and were and monitored. Emission light of the fluorescent lipid membrane on the substrate was monitored for various excitation lights for confirming formation of SLB. The ratio of phase separation on the SLB was confirmed from the captured image analysis.

### 2.6. Evaluation of phase separation based on Förster resonance energy transfer (FRET)

The non-uniformity of SLB in nano-scale was evaluated by using FRET technique [Loura, 2012]. The FRET occurs to energy transfer from an excited electron donor (NBD PE, Ex: 470 nm, Em: 540 nm) to an electron acceptor (Rhod PE or DiI). This energy transfer depends on some factors of donor-acceptor; distance, overlap of absorption spectra, and vector position of dipole moments [Loura, 2012]. Miscibility of lipid molecules after SLB formation on the substrate can be evaluated from the emission intensity of acceptor (Em: 560 nm)

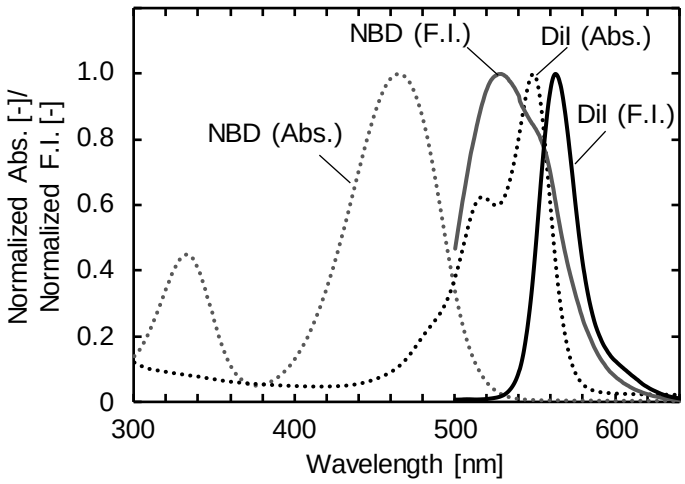


**Figure 5-2.** Spectroscopic properties of probes; (dotted curve) normalized absorption spectra, (solid curves), (gray) NBD PE in DMPC/DHPC ($X_{DHPC}$ = 0.40) bicelle, and (black) DiI in DMPC/DHPC ($X_{DHPC}$ = 0.40) bicelle.

enhanced by the energy transfer. DMPC/DHPC ($X_{DHPC}$ = 0.40) containing NBD PE (0.5mol% with lipids) and DMPC/DHPC ($X_{DHPC}$ = 0.67 and 0.33) including Rhod PE (0.5mol%) or DPPC/DHPC ($X_{DHPC}$ = 0.40) containing DiI (0.25mol%) [Gullapalli *et al.*, 2008] were mixed at several volume ratio. After the formation of SLBs, the planar membranes were analyzed fluorescent spectra, and the peaks of the spectra were compared to evaluate a miscibility;

$$\text{Energy transfer efficiency} = \frac{I_{560}}{(I_{530} + I_{560})}$$

where, $I_i$ is intensity of each peak, subscript "i" is wavelength of NBD PE donor (530 nm) and DiI acceptor (560 nm), respectively (**Figure 5-2**).

## 3. Results and discussion

### 3.1. Heterogeneity design and Characterization of Macro Domain on SLBs

The SLBs were prepared by using bicelles consisting of DMPC and DHPC at room temperature. In this section, DMPC, as the same long chain phospholipid, was employed to confirm the relationship between the size of a bicelle and the formation of SLB. The size of each assembly was measured by using DLS (**Table 5-2**). They were nano-scale assemblies, and it was predicted that disk-like assemblies would exist due to the compositions (refer in chapter 2). The bicelle suspension added on the substrate was repeatedly rinsed by PBS at 20 times after 1-2 hours of incubation at room temperature for removing DHPC molecules. The SLB was observed with a fluorescence microscope (**Figure 5-3**). From the observation from different excitation light (NBD PE: 460-490 nm and Rhod PE: 530-550 nm), it was confirmed that both NBD PE and Rhod PE were present on the substrate (data not shown). Thus, DMPC/DHPC assembly could transform to a planar SLB.

In the case of $X_{DHPC}$ = 0.40 (including Rhod PE) combined with $X_{DHPC}$ = 0.33 (including NBD PE), the SLB texture shows stripe pattern (**Figure 5-3a**). The actual area ratio of $X_{DHPC}$ = 0.33 and 0.40 was evaluated by using an image analysis from the fluorescence microscopic pictures (**Table 5-3**). The adsorption ratio of $X_{DHPC}$ = 0.40 was close to the ratio of the $X_{DHPC}$ = 0.33 (50.6±15.5%). The result was close to the theoretical adsorption rate (47.4%). In **Figure 5-3b**, $X_{DHPC}$ = 0.67 with NBD PE and $X_{DHPC}$ = 0.40 with Rhod PE were mixed and were added on a substrate at a volume ratio of 1:1v/v. The dark gray region was NBD PE in $X_{DHPC}$ = 0.67, and the light gray was Rhod PE in $X_{DHPC}$ = 0.40. It seems that the $X_{DHPC}$ = 0.40 bilayer including Rhod PE was dispersed in a whole of the substrate. The value of occupied region of $X_{DHPC}$ = 0.40 was smaller than that of $X_{DHPC}$ = 0.67 (10.8±3.7%). It is thought that the assembly of $X_{DHPC}$ = 0.67 formed a SLB faster than that of $X_{DHPC}$ = 0.40 on the substrate. The number of assemblies including in the suspension was calculated based on the average size of each assembly measured by DLS (refer to chapter 3). If these bicelles at same number adsorb to the substrate, it is calculated that the adsorption rate of $X_{DHPC}$ = 0.40 becomes about 64.3%. This calculation result implies that a small assembly ($X_{DHPC}$ = 0.67) forms a planar membrane faster than large assembly ($X_{DHPC}$ = 0.40). When SLB was made by reversing the ratio of the numbers of $X_{DHPC}$ = 0.40 and 0.67 (from 21.4 to 71.4%), the ratio of the occupied region of $X_{DHPC}$ = 0.40 was improved (38.3±23.9%). However, the amount of adsorption of $X_{DHPC}$ = 0.67

**Table 5-2** Size of each bicelle with fluorescence probe lipid.

| | Long-chain lipid | Fraction of DHPC, $X_{DHPC}$ | Probes | Diameter [nm] |
|---|---|---|---|---|
| (1) | DMPC | 0.67 | NBD PE | 8.8±0.2 |
| (2) | DMPC | 0.40 | Rhod PE or NBD PE | 22.5±0.3 |
| (3) | DMPC | 0.33 | NBD PE | 29.2±3.2 |
| (4) | DPPC | 0.40 | DiI | 17.1±2.1 |

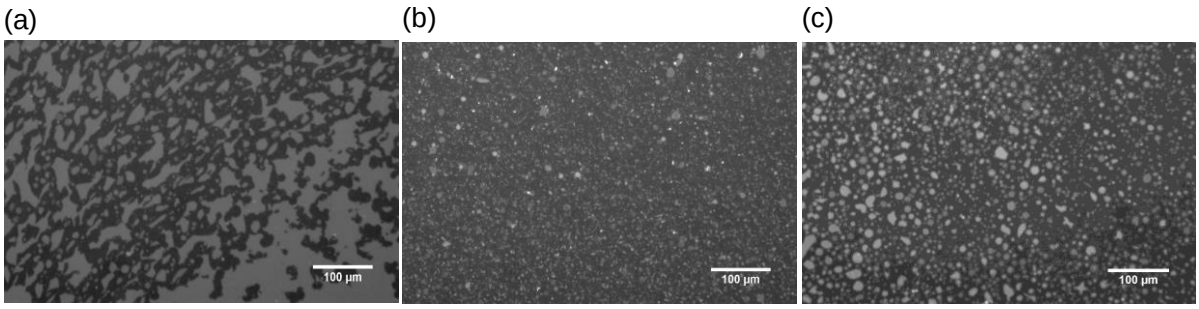


**Figure 5-3.** Fluorescence image of SLBs made from mixing DMPC/DHPC bicelles excited 530-560 nm light at room temperature. DMPC bicelle ($X_{DHPC}$ = 0.67 and 0.33) with NBD PE, DMPC bicelle with Rhod PE ($X_{DHPC}$ = 0.40); (a) ($X_{DHPC}$ =) 0.33:0.40 = 1:1v/v, (b) ($X_{DHPC}$ =) 0.40:0.67 = 1:1v/v, (c) ($X_{DHPC}$ =) 0.40:0.67 = 9:1v/v. These SLB were prepared based on; volume const. (a, b); number of bicelle const. (c).

**Table 5-3** The rate occupied by bicellar membrane at $X_{DHPC}$ = 0.40. The calculated number ratio of bicelles based on the measurement result of DLS in parentheses.

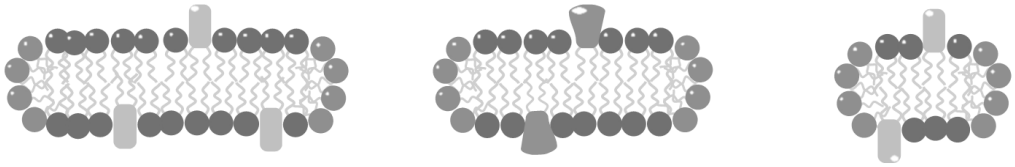

(1) $X_{DHPC}$ = 0.33 (NBD) (2) $X_{DHPC}$ = 0.40 (Rhod) (3) $X_{DHPC}$ = 0.67 (NBD)

| | | Charged volume ratio (Calculated number ratio) | Occupied rate of **(2)** on SLB |
|---|---|---|---|
| (a) | **(1) : (2)** | 1:1 (39.8:60.2) | 50.6 ± 15.5% |
| (b) | **(2) : (3)** | 1:1 (21.0:79.0) | 10.8 ± 3.7% |
| (c) | **(2) : (3)** | 9:1 (70.1:29.9) | 38.3 ± 23.9% |

was still larger (**Figure 5-3c** and **Table 5-2**). This result suggests that the size of the bicelles influences their adsorption on a substrate for SLB formation.

SLB formation by using bicelles is achieved by adsorption of bicelles to a substrate and diffusion of lipids between edges of adsorbed bicelles. The stability of the edge is affected by the size of the bilayer region of the bicelle and the presence of DHPC molecules around the edge because of the difference in line tension [Jiang *et al.*, 2004] and fluidization effect of DHPC to bilayer [Kolahdouzan *et al*., 2017], respectively. The hydrophobic edge of the bilayer fragment on the substrate works effectively for rapid SLB formation. Small assembly, like as $X_{DHPC}$ = 0.67, is expected to deform the edge more easily than large assembly, like as $X_{DHPC}$ = 0.40 or 0.33. In addition, the report by Kolahdouzan *et al*. is an evidence that the bilayer fluidization by DHPC molecules. Their DOPC/DHPC bicelle ($X_{DHPC}$ = 0.80, 9.4 min) covered the substrate by forming SLB faster than that of $X_{DHPC}$ = 0.29 (12.7 min). Therefore, a hydrophobic part of the edge of smaller bilayer membrane changes forms quickly than a larger one when it is exposed to a hydrophilic environment.

SLBs were thus found to be formed by using discoidal bicelles. The SLB formation by bicelle suspension can control uniformity/non-uniformity, depending on the size of the initial disk. It has been shown that "size" and "DHPC concentration" on a bicelle are important factors as design factors for designing membrane materials using bicelles.

### 3.2. Preparation of SLB by using bicelle at various conditions

The effect of some operational conditions (i.e., line bicelle size, its composition, temperature, mixing ratio of the bicelles) on the SLB texture was systematically studied in this section in order to find out key factors for the application to continuous SLB preparation (**Table 5-4**). Two kinds of bicelles were used for the SLB preparation; one bicelle was modified with NBD PE and another with Rhod PE, so heterogeneity can be observed under the fluorescence microscope. Prior to the main experiment, direct injection of both bicelles onto the substrate without pre-mixing was tested as a preliminary experiment, resulting in the formation of "*spotty*" textured SLB. The obtained "*spotty*" texture may imply the possibility of the random aggregation of different bicelles and same bicelles during the SLB formation process. By introducing "*pre-mixing*" of different bicelles in whole operation of SLB preparation, non-spotty surface was obtained. One important factor is to spread the bicelle solution during SLB

**Table 5-4.** List of images of SLBs at several conditions. The mixing ratio of bicelles (20 mM) was based on volume (v/v).

| Components | Initial injection ratio of long-chain lipid | Incubatioin temp. [°C] | Pre-mixing | Image |
|---|---|---|---|---|
| ($X_{DHPC}$=) 0.40 : 0.40 (bicelle) : (large assembly) | 1 : 1 | 25 | No | 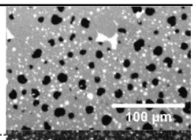 |
| 0.40 : 0.67 | 1 : 1 | 25 | No | 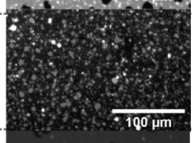 |
| 0.40 : 0.33 | 1 : 1 | 25 | No | 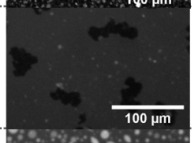 |
| 0.40 : 0.67 | 9 : 1 | 25 | No | 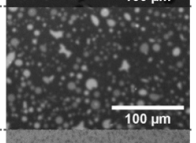 |
| 0.40 : 0.67 | 9 : 1 | 50 | Yes | 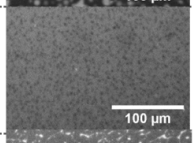 |
| 0.40 : 0.67 | 9 : 1 | 25 | Yes | 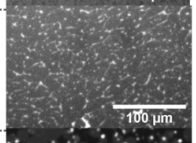 |
| 0.40 : 0.40 (DMPC/DHPC) : (DPPC/DHPC) | DMPC/DPPC 9 : 1 | 25 | Yes | 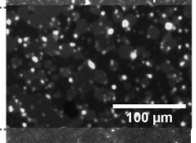 |
| 0.40 : 0.40 (DPPC/DHPC) : ((DOPC//Chol)/DHPC) | DPPC/DOPC/Chol 4 : 4 : 2 | 25 | Yes | 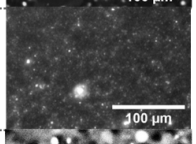 |
| 0.40 : 0.40 DMPC/DHPC : DPPC/DHPC | DMPC/DPPC 7 : 3 | 35 | Yes | 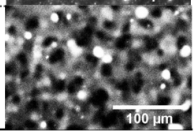 |

formation by employed "*pre-mixing*" to avoid their random aggregation.

The effect of size of bicelle was also found to affect the SLB texture, where the adsorbed amount of the larger bicelle (ca. 20 nm) was much greater than that of the smaller one (less than 10 nm). Especially in the case of the injection of different bicelles at same lipid component (DMPC), the larger domain of the larger bicelles was observed in the obtained texture. In addition, the size of the dispersed region in the heterogeneous texture was found to become the larger (≥ 20 μm) than that of original bicelle (ca. 10 nm). The above phenomena indicated the possibility of the fusion of bicelles at same composition before they reached to the substrate surface and they adsorbed there. So, in order to keep the "nano-scale" domain on the SLB, the bicelles should be dispersed in the solution without self-aggregation and the fusion, just before its injection onto the substrate.

The temperature is also important to obtain the better SLB, where the homogeneous texture was obtained by setting the temperature above phase transition temperature. It is considered that the mixing of lipids of different bicelles could be promoted on the substrate during the SLB formation, because of the fluidic nature. Furthermore, the SLB of DPPC that high temperature (> 41 ºC) was formed to be prepared at room temperature. It is well known that the SLB of DPPC cannot be formed via vesicle fusion method, unless the temperature is set above $T_m$. Generally, several liposomes (i.e., POPC, DOPC etc.) that show lower $T_m$ are utilized for the SLB preparation incorporating membrane proteins because of the temperature limitation against the proteins. That result clearly shows that this bicelle method conquest these conventional problems in the temperature and lipid limitation. The mixing ratio of different bicelles can also be another important factor; the mixing rate is considered to be proportional to the occupied area ratio of those feed ratio (DMPC to DPPC) of different bicelles because DHPC can be negligible after dilution. When the DMPC bicelle and DPPC bicelle were mixed at DMPC:DPPC = 9:1, the occupied area ratio was not same with the mixing ratio, resulting in the ratio governed by phase equilibrium.

In addition, the use of DOPC/DHPC bicelle was found to form the larger occupied area at micro meter scales. This is caused by the self-aggregation and fusion of DOPC/DHPC bicelles during the SLB formation because of its fluidic nature. The mixture of DPPC/DHPC and DOPC/Chol/DHPC bicelles also provide the planar SLB, while randomly-connected domains were observed on the substrate. It is noted that the injection method also determined

the quality of SLB texture. As a whole, key factors to obtain the SLB with good quality could be (i) dispersity of the bicelles and (ii) smooth spready on the substrate. It is therefore necessary to construct the continuous flow system to supply the above-mentioned key points.

### 3.3. Continuous Manufacturing of Micro-and-Nano Domain on SLB

To develop biomimetic membranes, nano-order domains were formed on the SLB by using bicelles. DMPC/DHPC bicelle and DPPC/DHPC bicelle were employed to prepare a multi-component SLB. DMPC membrane and DPPC membrane have different phase states at room temperature (25 ºC), such as unstable disordered phase and ordered phase, respectively. The DMPC/DPPC mixture has several phase states with component and temperature [Mabrey *et al.*, 1976]. The heterogeneity of SLB was evaluated from an appearance observation with a fluorescent microscope and, also, an emission spectrum measurement of energy transfer from NBD PE to DiI. DiI is reported to be oriented in an ordered phase [Gullapalli *et al.*, 2008]. Then, a DPPC/DHPC bicelle ($X_{DHPC}$ = 0.40) with DiI (0.25mol%) was similar size at 17.1±2.1

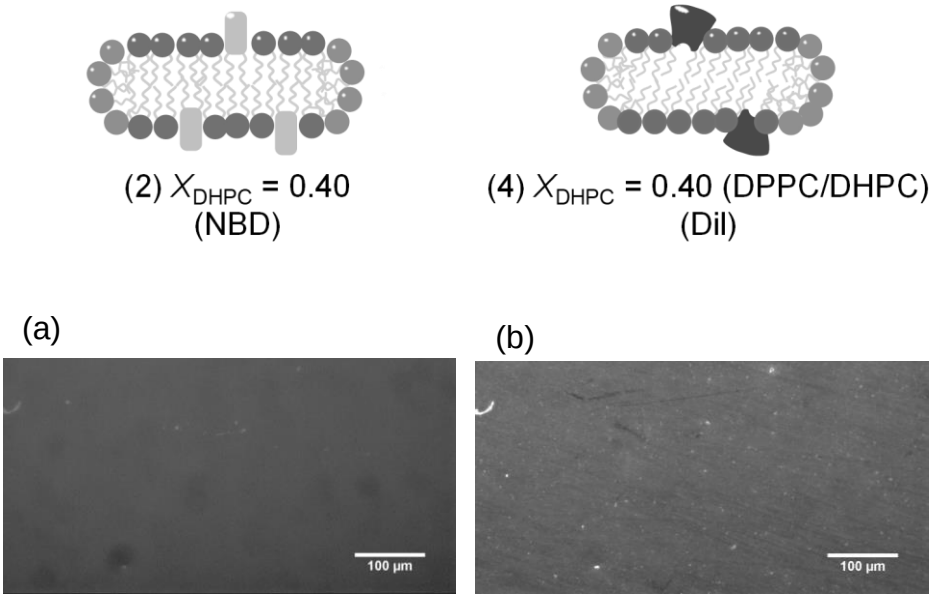


**Figure 5-4.** Fluorescence mage of **(2)**:**(4)** = 1:1 SLB obtained by fluorescence microscopy; excited (a) UV-light (340-390 nm), and (b) green-light (530-550 nm) at room temperature.

nm. DMPC/DHPC bicelle ($X_{DHPC}$ = 0.40) and DPPC/DHPC bicelle ($X_{DHPC}$ = 0.40) were close in size, both of which are expected to be discoidal shape. Those were injected on a substrate by continuous flow at 20 μL/min at 15 min. The injection needle was perpendicularly set to near a substrate. When the flow path became narrower about half of the tube, the flow was laminar because the increased *Re* number was small values. The next washing process was done in the same way as above section **3.1**. The SLB was monitored a fluorescent microscope (**Figure 5-4**) and these images showed presence of NBD PE and DiI and formation of SLB on the substrate due to the emission of each probes on the substrate. The result means that DPPC and DMPC mixture formed uniform appearance SLB.

The fluoresce spectra of the DMPC/DHPC and DPPC/DHPC mixed SLB were measured and compared to confirm the phase separation by energy transfer from NBD PE to DiI (**Figure 5-5a**). The fluorescence spectra of SLB of DMPC/DHPC including NBD (Em: 530 nm) and that of DPPC/DHPC including DiI (Em: 560 nm) are shown in **Figure 5-5a** by orange and pink broken lines, respectively. Coexisting system of these independent SLBs was employed to obtain an emission spectrum in a quartz cell (black curve). In addition, using a feature of bicelles as aggregation of fixing materials on a bilayer (see chapter 3), I prepared the dense coexistence of NBD PE and DiI on DMPC/DHPC bicelle. The spectrum of the SLB obtained by this is in a red curve (**Figure 5-5a**). The spectrum shows a drastic decrease of the peak of NBD PE peak and also increase of DiI peak. The obtained result shows the energy pass from NBD PE (electron donor) to DiI (acceptor). The SLB preparing continuous injection of DMPC/DHPC and DPPC/DHPC had both peaks of NBD PE and DiI. The spectrum clearly shows that the phases of DMPC with NBD PE and DPPC with DiI were separated at nano-scale. Moreover, when the case of changing the injection rate of each suspension, whereas there seemed uniform SLB membrane (image not shown), the spectral shapes varied according to the injection ratio (**Figure 5-6**).

These spectra also show the behavior of energy transfer, called FRET. The energy efficient transfer from NBD PE to DiI on the SLBs as shown in **Figure 5-5b**, focusing on the ratio of the peaks of NBD PE ($I_{530}$) and DiI ($I_{560}$). This parameter indicates the miscibility of lipid molecules on the substrate. The low values are hard to transport an energy (1 and 2 in **Figure 5-5b**), and high value investigate an energy transported (3 and 5 in **Figure 5-5b**). The value preparing continuous injection (4) is lower than (3) or (5). It is considered that energy

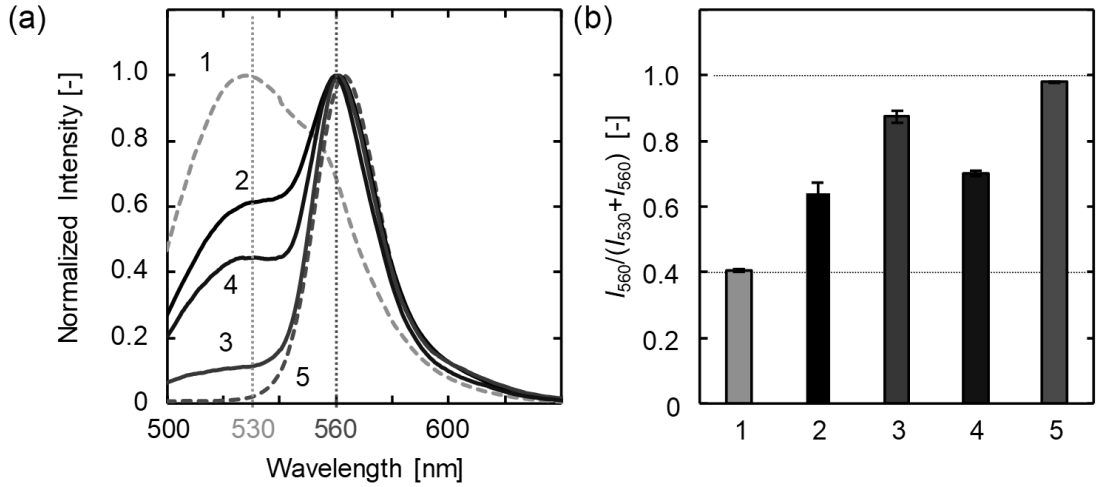


**Figure 5-5.** (a) Spectra showed NBD (530 nm, broken-curve, **1**) and DiI (560 nm, broken-curve, **5**) in SLB membranes of DMPC and DPPC, respectively at 25 ºC. The each SLB composition was described below; **2** independent SLB of DMPC/NBD and DPPC/DiI, **3** DMPC/NBD with DiI, and **4** DMPC/NBD and DPPC/DiI. (b) Enhanced Emission degree of DiI. The numbering of each bar corresponds to each spectrum in (a).

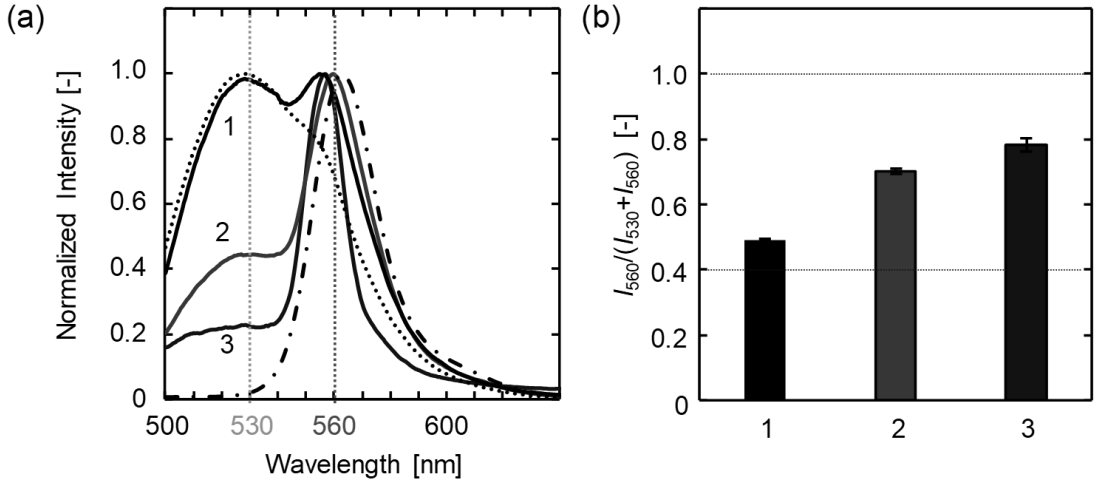


**Figure 5-6.** (a) Spectra of **(2)** with **(4)** SLB membranes on glass substrates (25 ºC) at each flow rate; **(2):(4)** [μL/min] = 30:10, **1**; 20:20, **2**; 10:30, **3**. NBD (dotted) and DiI (dot-chain) in SLB membranes of DMPC and DPPC, respectively, were plotted as references. (b) Enhanced Emission degree of DiI. The numbering of each bar corresponds to each spectrum in (a).

transport was not carried out significantly. Thus, mixing between DMPC and DPPC molecules was not done. FRET is used to estimate the distance between probe molecules on a membrane [Loura, 2012]. The calculation requires findings such as Förster radius which is kind of depending on the type of donor and acceptor. In this study, a miscibility between DMPC and DPPC bilayers was only discussed on the SLB membrane, the distance between probes will not declare. In my empirical opinion, when the Förster radius is 49 Å (e.g., NBD to Rhod [Watts, 1995]), the distance between donor and acceptors is calculated as around 34.9 Å. Then, the distance on SLB preparing continuous injection was 47.2 Å. In fact, these since the spectral overlap of NBD/DiI is larger than NBD/Rhod, the radius becomes larger than 49 Å.

Therefore, it was found that DMPC/DHPC bicelles and DPPC/DHPC bicelles added continuously in the flow channel could induce have a phase separation at nano-meter scale that cannot be observed with a microscope. Continuous preparation of SLB by using bicelle was able to create a phase separation system that is similar with biological membranes. The design scheme of the preparation of membranous materials is shown in **Figure 5-7**. The appropriate selection of the bicelle conditions and controlling DHPC concentration is required to prepare the target membrane materials. To expand the findings obtained in this work, following studies are recommended as future work.

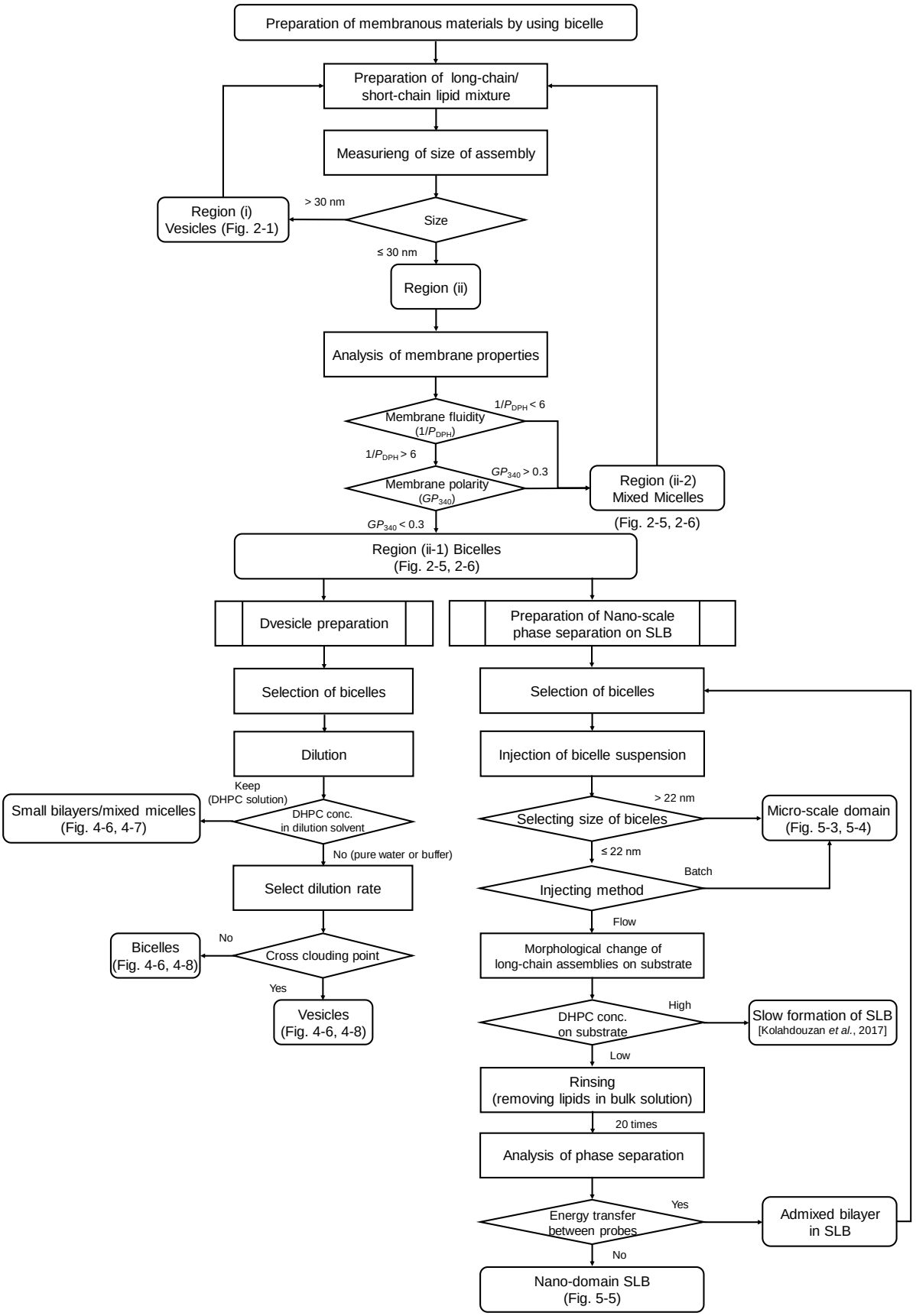


**Figure 5-7.** Design scheme for the functional membranous materials.

## 4. Summary

Multi-component SLB was formed by using discoidal bicelle. The formation of the discoidal assembly was determined from that size by measuring DLS. The adsorption rate of bicelles onto the glass substrate varied depending on the size of the assembly from monitoring fluorescence microscope. SLB formation by adsorbing bicelles on a substrate was affected by those size. Smaller bicelles adsorbed onto the substrate than larger bicelles. This is due to the stability of the edge of the discoidal membrane. It is expected that small bicelles rapidly form planar membrane on the substrate because of the small line tension of that edge and the fluidizing effect to the bilayer of DHPC molecules. The formation of formless domains from larger bicelles on the substrate was imposed by enough diffusion of the discoidal particles in the bulk solution. For SLB formation by using bicelle, it is necessary to devise the control method DHPC concentration and injection method of the bicelles.

When nano-sized bicelles with different compositions, DMPC/DHPC ($X_{DHPC}$ = 0.40) and DPPC/DHPC ($X_{DHPC}$ = 0.40), were added continuously to the substrate, the appearance of the SLB was a uniform bilayer. Nevertheless, the presence of nano-sized phase separation phases was inferred by analysis with fluorescent lipids (NBD PE and DiI). Discoidal bicelle can be utilized to form SLBs aimed at the preparation of biomimetic nano-ordered heterogeneous membrane on a substrate. A bicelle injection has no residual organic solvent in the SLB, that SLB can be formed continuously by simply controlling the concentration of DHPC on the substrate. This technology can be expected not only as a conventional biomaterial but also in the field of surface modification.

# Chapter 6

## General Conclusions

### General Conclusions

Design of membrane materials using discoidal bicelles can extend the applications of membrane materials. Membrane materials mimicking the function of biomembranes have the potential to be applied to new manufacturing system. Especially, discoidal bicelle is expected to create functional membranous materials. The feature of bicelles is suitable to reproduce the environment of biomembranes. In this chapter, it will be summarized previous studies in this thesis and will be described the growth of that technology (future work). In this chapter, I describe the general features of the membranous materials, such as vesicles (liposomes), supported bilayer membrane (SLB), and bicelles, from both viewpoints of fundamental and applied aspect. A possible advantage of a discoidal membrane (bicelle) for its utilization for functional materials is discussed, followed by the review of some researches relating to this research.

In chapter 2, from the classification of formed self-assemblies, the conditions, such as the component rate and the concentration, were found to form discoidal bicelles. DMPC and DHPC were employed as compositions of the assembly. The findings of this study are summarized in a diagram. From combining evaluations, such as based on the appearance of an assembly by DLS and turbidity and based on membranous phase state by fluorescence probes, the assemblies were categorized as the dominant state; large vesicle (> 30 nm), gel-bicelle (≤ 30 nm, "*ordered*" interfacial properties), and micelle (≤ 30 nm, "*disordered*" interfacial properties). In particular, the behavior of the formation was observed in the vicinity of the critical micelle concentration of DHPC. In the conditions of fixed total lipid concentration, the self-assembly structure could be controlled using the DHPC fraction ratio: bicelle for $0.33 \leq X_{DHPC} \leq 0.67$ and micelle for $X_{DHPC} \leq 0.77$. In the conditions of fixed $X_{DHPC}$ (especially at $0.33 < X_{DHPC} < 0.4$), dilution lead to transformation from bicelle to vesicle, with a cloudy point in turbidity. The morphological stability of discoidal assembly is affected by concentration of DHPC. It is showed the possibility of application of bicelles to membrane materials that "stepwise" morphological change of bicelles by dilution. Utilizing this, bicelle assemblies can

be applied for a continuous planar membrane, such as vesicles, process flow system.

In chapter 3, the function of discoidal bicelle was shown by monitoring behavior of photo-functional molecule, chlorophyll *a* (Chl*a*), in the bicelle membrane. It was clarified that the liposomal membrane properties could be characterized based on the analyses of the membrane fluidity, the Chl*a* absorption bands, and the Chl*a* polarization. These results show that the positioning of Chl*a* in the membrane differs depending on phase states of the bilayer. In addition, the influence of the membrane properties on the photoreduction with methyl viologen was examined. It is concluded that the behaviors and the orientations of Chl*a* molecules on the liposomal membrane are significantly important in the photochemical energy conversion system. Thus, the finding can be helpful for superior photochemical energy conversion by Chl*a* containing bilayer membranes. The environment surround Chl*a* molecules could be polar in the DMPC/DHPC membranes, where the polarity at $X_{DHPC}$ = 0.4 was lower than at $X_{DHPC}$ = 0.67, which could promote the formation of Chl*a* aggregates. The photo-reduction of $MV^{2+}$ was regulated by the aggregation states of Chl*a* molecules. Furthermore, J-aggregates of Chl*a* molecules were induced in DMPC/DHPC bicelles at $X_{DHPC}$ = 0.4 and $C_{lipid}$ = 20 mM, and the J-aggregates were maintained after rupture of bicelle structure with dilution. The bicelle-type assemblies more advantageously induce the formation of J-aggregates of Chl*a*. The use of Chl*a*-incorporated bicelles as a photosensitizer can lead to the development of powerful photosynthesis systems.

In chapter 4, the vesicle was prepared by dilution of bicelles using the flow devices based on the bicelle diagram. The membrane properties of the vesicles prepared by bicelle dilution were compared to those made by conventional preparation methods (thin film hydration and high-pressure $CO_2$/water) which were similar liposomes. Whereas high-pressure $CO_2$/water system has advantage of non-used organic solvents, the hard condition such as pressure is difficult to control the property of $CO_2$/water interface preciously and to prepare the variation of phase separation on membrane surface as biomembranes. The dilution removes DHPC molecules in the bilayer because of hydration of those and leads to change morphology of the assemblies. Vesicle formation was achieved by the continuous dilution of the DMPC/DHPC bicelle in flow path. The vesicle preparation was found to be formed stepwise through the fusion of the bicelles in simple flow path device. It is expected that the technique could have the potentials to continuous-type preparation method to enable a heterogeneous

membrane like a living cell membrane by designing a flow path.

In chapter 5, the formation of supported lipid bilayer (SLB) was confirmed by using discoidal bicelles. In order to prepare nano-domain on a membrane like a biomembrane, SLB fabrication was performed by using multicomponent bicelles. The adsorption of bicelles to the glass substrate was monitored fluorescence lipids in each bicelle by fluorescence microscope. SLB formation by adsorbing bicelles on a substrate was affected by those size. Smaller bicelles adsorbed to the substrate than larger bicelles. Then, the larger bicelles formed larger formless domains on the substrate. These results suggested morphological changes and fusion of bicelles at bulk solution. The unfavorable bicelle fusion was found to be eliminated by the selecting the suitable pre-mixing and injection method in adding bicelle suspension to the substrate. A flow system was employed for dispersion of bicelle particles in the suspension and for continuous injection to the substrate. When nano-sized bicelles with different compositions, DMPC/DHPC and DPPC/DHPC, were added continuously to the substrate, the appearance of the SLB was a uniform bilayer. The presence of nano-sized phase separation phases was inferred by analysis of energy transfer between fluorescent lipids (NBE PE and DiI). It has been clarified that the discoidal bicelle can be utilized to prepare the target SLBs aiming at biomimetic nano-ordered heterogeneous membrane on a substrate by simply controlling the concentration of DHPC on the substrate. This technology can be expected to be applied to not only the preparation of conventional biomaterial but also the surface coating or modification of any materials.

A strategy on the designs of various membranous materials by using discoidal bicelles was finally established based on the analysis of membrane properties of the discoidal membrane (bicelle) and its relating membrane. These findings are expected to be expanded to the utilization of membrane materials to the development of various functional materials. To expand the findings obtained in this work, following studies are recommended as future work.

**Suggestions of Future Work**

**(1) Bicelle based Preparation of Heterogeneous Supported Lipid Bilayers (SLB): Continuous Manufacturing of SLB using Flow-Device**

In this study, the bicelle characters were applied to the preparation of planar membrane. From these findings, it is expected that a new method of SLB preparation could be developed continuous flow device. SLBs are often utilized to immobilized membrane protein complexes, such as channels and transporters in the biological membrane [Lee, 2004]. The preparation from bicelles requires only the control of the operational condition of DHPC concentration and the pre-mixing to obtain a uniform dispersion of the bicelle particles on the substrate. A continuous system is suitable to regulate those factors appropriately. The microchannel in the flow device can control the dispersion and mixing of the bicelle suspension, by designing the flow path to meet the above requirements. Moreover, by providing a chamber in the channel, it is possible to form an SLB in the device (**Figure 6-1**). The micro flow path made from dimethylpolysiloxane is transparent, and observation of internal pathway is possible. The artificial biomembrane constructed in the chamber can be used for observing the reaction field and biological function of membrane proteins.

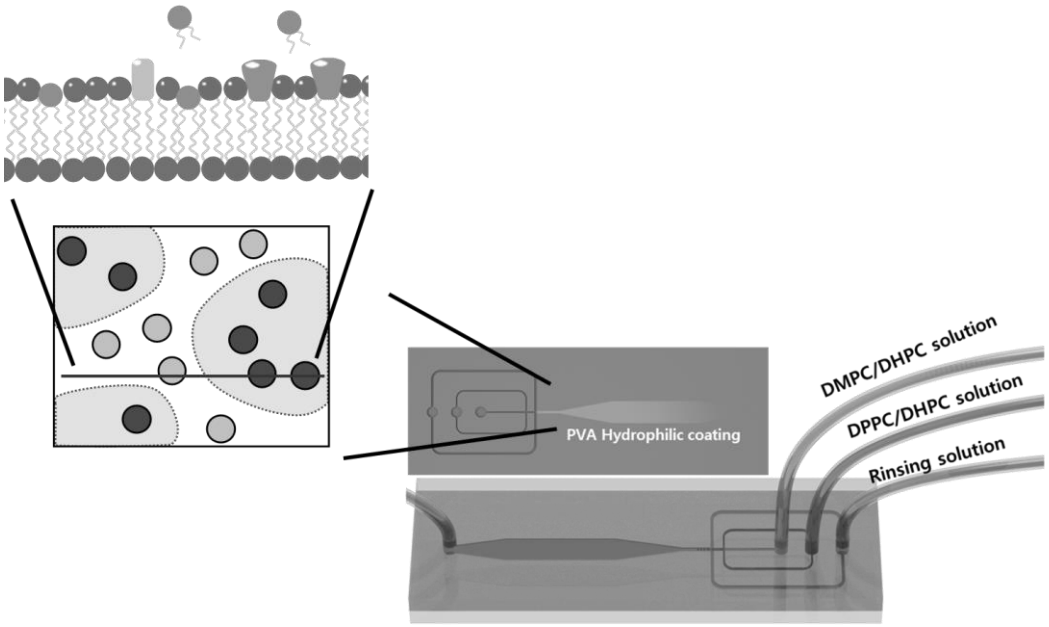


**Figure 6-1.** Hydrophilic chamber in micro-flow chip for preparing nano-domain in SLB (made it by Kang, B.-S., Kyungpook National University, South Korea).

**(2) Introduction of bicelle constructing molecules instead of phospholipids**

A bicelle consisting phospholipids can be expected to be applied to prepare various functional membranous materials. However, because preparation of bicelles requires much lipid molecules, there are problems with cost. Thus, amphiphilic (synthetic) surfactants and fatty acids should be employed as "*building-block*" for the formation of the discoidal assembly (bicelle). From these findings obtained in this thesis, a key factor for forming a bicelle is phase separation between ordered and disordered phases of assemblies. For example, Iwasaki *et al*. and Charoenthai *et al.* have reported the self-assembled molecules, such as DDAB (cationic double-chained surfactant) or span/tween (nonionic surfactant), respectively [Iwasaki *et al*., 2018, Charoenthai *et al*., 2011]. As exampled in these previous studies, the investigation on other kinds of amphiphiles and their self-assembly would contribute to the reduction of these molecules have been reported to exist as an ordered orientation at the surface of these assembly in aqueous solution. Production cost and the promoted development to industrial utilization of membrane materials.

# Abbreviation

| | | |
|---|---|---|
| $B_i$ | = | Soret band at transition dipoles "*i*" |
| Chl*a* | = | chlorophyll *a* |
| CMC | = | critical micelle concentration |
| CVC | = | critical vesicle concentration |
| DHPC | = | 1,2-dihexanoyl-*sn*-glycero-3-phosphocholine |
| DiI C18 (3) | = | 1,1'-Dioctadecyl-3,3,3',3'-tetramethylindocarbocyanine perchlorate |
| DLS | = | dynamic light scattering |
| DMPC | = | 1,2-dimyristoyl-*sn*-glycero-3-phosphocholine |
| DOPC | = | 1,2-dioleoyl-*sn*-glycero-3-phosphocholine |
| DPH | = | 1,6-diphenyl-1,3,5-hexatriene |
| DPPC | = | 1,2- dipalmitoyl-*sn*-glycero-3-phosphocholine |
| EDTA | = | ethylenediamine-*N,N,N',N*'-tetraacetic acid, disodium salt, dihydrate |
| Laurdan | = | 6-dodecanoyl-*N,N*-dimethyl-2-naphthylamine |
| MV | = | Methyl viologen |
| NBD PE | = | 1,2-dipalmitoyl-*sn*-glycero-3-phosphoethanolamine-N-(7-nitro-2-1,3-benzoxadiazol-4-yl) (ammonium salt) |
| $Q_i$ | = | *Q* band at transition dipoles "*i*" |
| Rhod PE | = | 1,2-dioleoyl-*sn*-glycero-3-phosphoethanolamine-N-(lissamine rhodamine B sulfonyl) (ammonium salt) |
| SLB | = | supported lipid bilayer |

# Nomenclature

| | | | |
|---|---|---|---|
| $Ca$ | = | capillary number | [-] |
| $C_{lipid}$ | = | lipid concentration | [µ- or mM] |
| $GP_{340}$ | = | general polarization calculated at exciting light at 340 nm | [-] |
| $k_{cat}$ | = | turnover number | [$min^{-1}$] |
| $k_r$ | = | constant of reaction | [$min^{-1}$] |
| $P$ | = | polarization | [-] |
| $1/P$ | = | membrane fluidity | [-] |
| $Re$ | = | Reynolds number | [-] |
| $T_m$ | = | phase transition temperature | [ºC] |
| $V_i$ | = | flow rate | [µL/min] |
| $V_{max}$ | = | initial rate constant | [µM/min] |
| $X_{DHPC}$ | = | fraction of DHPC with DMPC | [-] |

# References


Abraham, S.; Heckenthaler, T.; Bandyopadhyay, D.; Morgenstern, Y.; Kaufman, Y. Quantitative Description of the Vesicle Fusion Mechanism on Solid Surfaces and the Role of Cholesterol. *J. Phys. Chem. C.* **2018**, *122*, 22985-22995.

Agostiano, A.; Monica, M. D.; Palazzo, G.; Trotta, M. Chlorophyll *a* Auto-Aggregation in Water Rich Region. *Biophys. Chem.* **1993**, *47*, 193-202.

Agostiano, A.; Catucci, L.; Colafemmina, G.; Della Monica, M.; Scheer, H. Relevance of the Chlorophyll Phytyl Chain on Lamellar Phase Formation and Organization. *Biophys. Chem.* **2000**, *84*, 189-194.

Agostiano, A.; Cosma, P.; Trotta, M.; Monsù-Scolaro, L.; Micali, N. Chlorophyll *a* Behavior in Aqueous Solvents: Formation of Nanoscale Self-Assembled Complexes. *J. Phys. Chem. B*. **2002**, *106*, 12820-12829.

Amao, Y.; Tomonou, Y.; Ishikawa, Y.; Okura, I. Photoinduced Hydrogen Production with Water-Soluble Zinc Porphyrin and Hydrogenase in Nonionic Surfactant Micellar System. *Int. J. Hydrogen Energy* **2002**, *27*, 621-625.

Amao, Y.; Shuto, N.; Iwakuni, H. Ethanol Synthesis based on the Photoredox System Consisting of Photosensitizer and Dehydrogenases. *Applied Catal., B.* **2016**, *180*, 403-407.

Asgari M.; Biria, A. Free Energy of the Edge of an Open Lipid Bilayer Based on the Interactions of Its Constituent Molecules. *Int. J. Non-Linear Mechanics* **2015**, *76*, 135-143.

Ariga, K.; Li, J.; Fei, J.; Ji, Q.; Hill, J. P. Nanoarchitectonics for Dynamic Functional Materials from Atomic-/Molecular-Level Manipulation to Macroscopic Action. *Adv. Mater.* **2016**, *28*, 1251-1286.

Ba, Y.; Liu, H.; Sun, J.; Zheng, R. Three dimensional simulations of droplet formation in symmetric and asymmetric T-junctions using the color-gradient lattice Boltzmann model. *Int. J. Heat and Mass Transfer* **2015**, *90*, 931-947.

Baillie, A. J.; Florence, A. T.; Hume, L. R.; Muirhead, G. T.; Rogerson, A. The Preparation and Properties of Niosomes-Non-Ionic Surfactant Vesicles. *J. Pharmacy Pharmacology* **1985**, *37* (12), 863-868.

Barros, T.; Kuhlbrandt, W. Crystallization, Structure and Function of Plant Light-Harvesting Complex II. *Biochim. Biophys. Acta - Bioenergetics* **2009**, *1787*, 753-772.

Bayburt, T. H.; Carlson, J. W.; Sligar, S. G. Reconstitution and Imaging of a Membrane Protein in a Nanometer-Size Phospholipid Bilayer. *J. Structural Biol*. **1998**, *123*, 37-44.

Beaugrand, M.; Arnold, A. A.; Hénin, J.; Warshawski, D. E.; Williamson, P. T. F.; Marcotte, I. Lipid Concentration and Molar Ratio Boundaries for the Use of Isotropic Bicelles. *Langmuir* **2014**, *30*, 6162-6170.

Bell, F. P. Lipid Exchange and Transfer Between Biological Lipid-protein Structures. *Progress in Lipid Research* **1978**, *17* (2), 207-243.

Bennett, T.; Niroomand, H.; Pamu, R.; Ivanov, I.; Mukherjee, D.; Khomami, B. Elucidating the Role of Methyl Viologen as a Scavenger of Photoactivated Electrons from Photosystem I under Aerobic and Anaerobic Conditions, *Phys. Chem. Chem. Phys.* **2016**, *18*, 8512-8521.

Ben-Shem, A.; Frolow, F.; Nelson, N. Crystal Structure of Plant Photosystem I. *Nature* **2003**, *426*, 630-635.

Bialek-Bylka, G. E., Wróbel, D. Temperature-Induced Spectral Properties of Chlorophyll *a* Incorporated into Egg-Yolk Lecithin Liposomes and Lipo-Protein Complexes. *Acta Biochim. Biophys. Hungarica* **1986**, *21*, 369-379.

Biswas, K. H. Jackman, J. A.; Park, J. H. Groves, J.T. Cho, N.-J. Interfacial Forces Dictate the Pathway of Phospholipid Vesicle Adsorption onto Silicon Dioxide Surfaces. *Langmuir* **2018**, *34*, 1775-1782.

Boudard, S.; Seantier, B.; Breffa, C.; Decher, G.; Félix, O. Controlling the pathway of formation of supported lipid bilayers of DMPC by varying the sodium chloride concentration. *Thin Solid Films* **2006**, *495*, 246-251.

Bui, T. T.; Suga, K.; Umakoshi, H. Roles of Sterol Derivatives in Regulating the Properties of Phospholipid Bilayer Systems. *Langmuir* **2016**, *32* (24), 6176-6184.

Buoninsegni, F. T.; Becucci, L.; Moncelli, M. R.; Guidelli, R.; Agostiano, A.; Cosma, P. Electrochemical and Photoelectrochemical Behavior of Chlorophyll *a* Films Adsorbed on Mercury *J. Electroanal. Chem.* **2003**, *550-551*, 229-240.

Burns Jr., R. A.; Roberts, M. F.; Dluhy, R.; Mendelsohn, R. Monomer-to-Micelle Transition of Dihexanoylphosphatidylcholine: 13C and Raman Studies. *J. Am. Chem. Soc.* **1982**, *104*, 430-438.

Chen, M.; Blankenship, R. E. Expanding the Solar Spectrum Used by Photosynthesis. *Trends in Plant Sci.* **2011**, *16*, 427-431.

Cho, H.; Kim, J.; Suga, K.; Ishigami, T.; Park, H.; Bang, J. W.; Seo, S.; Choi, M.; Chang, P.-S.; Umakoshi, H.; Jung, H.-S.; Suh, K.-Y. Microfluidic platforms with monolithically integrated hierarchical apertures for the facile and rapid formation of cargo-carrying vesicles. *Lab Chip* **2015**, *15*, 373-377.

Cogan, U.; Shinitzky, M.; Weber, G.; Nishida, T. Microviscosity and Order in the Hydrocarbon Region of Phospholipid and Phospholipid-Cholesterol Dispersions Determined with Fluorescent Probes. *Biochem*. **1973**, *12*, 521-528.

Correia, R. F.; Viseu, M. I.; Andrade, S. M. Aggregation/Disaggregation of Chlorophyll *a* in Model Phospholipid-Detergent Vesicles and Micelles. *Photochem. Photobiol. Sci.* **2014**, *13*, 907-916.

Craig, A. F.; Clark, E. E.; Sahu, I. D.; Zhang, R.; Frantz, N. D.; Al-Abdul-Wahid, M. S.; Dabney-Smith, C.; Konkolewicz, D.; Lorigan, G. A. Tuning the Size of Styrene-maleic Acid Copolymer-lipid Nanoparticles (SMALPs) using RAFT Polymerization for Biophysical Studies. *Biochim. Biophys. Acta* **2016**, *1858*, 2931-2939.

Cyrus, S. R.; Kai, E. L. Materials Chemistry: Liposomes Derived from Molecular Vases. *Nature* **2012**, *489* (20), 372-374.

Dacic, M.; Jackman, J. A.; Yorulmaz, S.; Zhdanov, V. P. Kasemo, B. Cho, N.-J. Influence of Divalent Cations on Deformation and Rupture of Adsorbed Lipid Vesicles. *Langmuir* **2016**, *32*, 6486-6495.

de Angelis, A. A.; Opella S. J. Bicelle Samples for Solid-State NMR of Membrane Proteins. *Nat. Protocols* **2007**, *2* (10), 2332-2338.

di Matteo, A. Structural, Electronic and Magnetic Properties of Methylviologen in Its Reduced Forms. *Chem. Phys. Lett.* **2007**, *439*, 190-198.

Diamond, L. W.; Akinfiev, N. N. Solubility of $CO_2$ in Water from -1.5 to 100 ºC and from 0.1 to 100 MPa: Evaluation of Literature Data and Thermodynamic Modelling. *Fluid Phase Equilibria* **2003**, *208*, 267-290.

Discher, D. E. Eisenberg, A. Polymer Vesicles. *Sci.* **2002**, *297*, 967-974.

Dowhan, W. Molecular Basis for Membrane Phospholipid Diversity: Why Are There So Many Lipids? *Annu. Rev. Biochem*. **1997**, *66*. 199-232.

Eytan, G. D. Use of Liposome for Reconstitution of Biological Functions. *Biochim. Biophys. Acta -Rev. Biomembranes* **1982**, *692* (2), 185-202.

Fang, Y. Air Stability of Supported Lipid Membrane Spots. *Chem. Phys. Lett.* **2011**, *512*, 258-262.

Farese, Jr., R. V.; Walther, T. C. Lipid Droplets Finally Get a Little R-E-S-P-E-C-T. *Cell* **2009**, *139* (5), 855-860.

Feigenson, G. W. Phase Diagrams and Lipid Domains in Multicomponent Lipid Bilayer Mixtures. *Biochim. Biophys. Acta* **2009**, *1788*, 47-52.

Fernández, C.; Hilty, C.; Wider, G.; Wüthrich, K. Lipid-Protein Interactions in DHPC Micelles Containing the Integral Membrane Protein OmpX Investigated by NMR Spectroscopy. *Proc. Nat. Acad. Sci.* **2002**, *99* (21), 13533-13537.

Ferreira, K. N.; Iverson, T. M.; Maghlaoui, K. Barber, J.; Iwata, S. Architecture of the Photosynthetic Oxygen-Evolving Center. *Sci.* **2004**, *19*, 4336-4344.

Funakoshi, K.; Suzuki, H. Takeuchi, S. Formation of Giant Lipid Vesicle Like Compartments from a Planar Lipid Membrane by a Pulsed Jet Flow. *J. Am. Chem. Soc.* **2007**, *129*, 12608-12609.

García-Sáez, A. J.; Chiantia S.; Schwille, P. Effect of Line Tension on the Lateral Organization of Lipid Membranes. *J. Biol. Chem.* **2007**, *282*, M706162200.

Gerebtzoff, G.; Li-Blatter, X.; Fischer, H.; Frentzel, A.; Seelig, A. Halogenation of Drugs Enhances Membrane Binding and Permeation. *Chem. Biochem.* **2004**, *5* (5), 676-684.

Green, J. D.; Kreplak, L.; Goldsbury, C.; Li Blatter, X.; Stolz1, M.; Cooper, G. S.; Seelig, A.; Kistler, J.; Aebi, U. Atomic Force Microscopy Reveals Defects Within Mica Supported Lipid Bilayers Induced by the Amyloidogenic Human Amylin Peptide. *J. Mol. Biol.* **2004**, *342*, 877-887.

Gullapalli, R. R.; Demirel M. C.; Butler, P. J. Molecular dynamics simulations of DiI-C18(3) in a DPPC lipid bilayer. *Phys. Chem. Chem. Phys.* **2008**, *10*, 3548–3560.

Guo, Z.; Hauser, N.; Moreno, A.; Ishikawa, T.; Walde, P. AOT Vesicles as Templates for the Horseradish Peroxidase-triggered Polymerization of Aniline. *Soft Matter* **2011**, *7*, 180-193.

Haagsman H. P.; van Golde, L. M. G. Regulation of Hepatic Triacylglycerol Synthesis and Secretion. *Veterinary Research Comm.* **1984**, *8*, 157-171.

Hayashi, K.; Shimanouchi, T.; Kato, K.; Miyazaki, T.; Nakamura, A.; Umakoshi, H. Span80 Vesicles have a More Fluid, Flexible and "Wet" Surface Than Phospholipid Liposomes. *Colloid Surf. B* **2011**, *87*, 28-35.

Hiromitsu, I.; Kevan, L. Effect of Cholesterol on the Solubilization Site and the Photoionization Efficiency of Chlorophyll *a* in Dipalmitoylphosphatidylcholine Vesicle Solutions As Studied by Electron Spin Resonance and Optical Absorption Spectroscopies. *J. Am. Chem. Soc.* **1987**, *109*, 4501-4507.

Hayashi, K.; Iwai, H.; Shimanouchi, T.; Umakoshi, H.; Iwasaki, T.; Kato, A.; Nakamura, H. Formation of Lens-Like Vesicles Induced via Microphase Separations on a Sorbitan Monoester Membrane with Different Headgroups. *Colloids Surfaces B* **2015**, *135*, 235-242.

Hayashi, K.; Iwai, H.; Kamei, K.; Iwamoto, K. Shimanouchi, T.; Fujita, S. Nakamura, H.; Umakoshi, H. Tailor-Made Drug Carrier: Comparison of Formation-Dependent Physicochemical Properties within Self-Assembled Aggregates for an Optimal Drug Carrier. *Colloids Surfaces B* **2017**, *152*, 269-276.

Hoshina, S. Temperature Dependence of Optical Properties of Chlorophyll *a* Incorporated into Phosphatidylcholine Liposomes. *Biochim. Biophys. Acta-Bioenergetics* **1981**, *638*, 334-340.

Hossann, M.; Syunyaeva, Z.; Schmidt R.; Zengerle, A.; Eibl, H.; Issels, R. D.; Lindne, L. H. Proteins and Cholesterol Lipid Vesicles are Mediators of Drug Release from Thermosensitive Liposomes. *J. Controlled Release* **2012**, *162*, 400-406.

Hu, X.; Ritz, T.; Damjanović, A.; Autenrieth, F.; Schulten, K. Photosynthetic Apparatus of Purple Bacteria. *Q. Rev. Biophys.* **2002**, *35*, 1-62.

Huber, V.; Lysetska, M.; Würthner, F. Self-Assembled Single- and Double-Stack π-Aggregates of Chlorophyll Derivatives on Highly Ordered Pyrolytic Graphite. *Small* **2007**, *3*, 1007-1014.

Imura, T.; Otake, K.; Hashimoto, S.; Gotoh, T.; Yuasa, M.; Yokoyama, S.; Sakai, H.; Rathman, J. F.; Abe, M. Preparation and Physicochemical Properties of Various Soybean Lecithin Liposomes Using Supercritical Reverse Phase Evaporation Method. *Coll. Surf. B: Biointerfaces* **2002**, *27*, 133-140.

Ishigami, T.; Kaneko, Y.; Suga, K.; Okamoto, Y.; Umakoshi, H. Homochiral oligomerization of L-Histidine in the Presence of Liposome Membranes. *Coll. Polym. Sci*. **2015**, *293*, 3649-3653.

Ishigami, T.; Suga, K.; Umakoshi, H. Chiral Recognition of L-Amino Acids on Liposomes Prepared with L-Phospholipid. *ACS Appl. Mater. Interfaces* **2015**, *7*, 21065-21072.

Iwasaki, F.; Suga, K.; Umakoshi, H. Pseudo-Interphase of Liposome Promotes 1,3-Dipolar Cycloaddition Reaction of Benzonitrile Oxide and N-Ethylmaleimide in Aqueous Solution. *J. Phys. Chem. B* **2015**, *119*, 9772-9779.

Iwasaki, F.; Luginbühl, S.; Suga, K.; Walde, P.; Umakoshi, H. Fluorescent Probe Study of AOT Vesicle Membranes and Their Alteration upon Addition of Aniline or the Aniline Dimer p-Aminodiphenylamine (PADPA). *Langmuir* **2017**, *33*, 1984-1994.

Iwasaki, F.; Suga, K.; Okamoto, Y.; Umakoshi, H. Enantioselective C-C Bond Formation Enhanced by Self-Assembly of Achiral Surfactants. *ACS Omega* **2017**, 2, 1447-1453.

Jiang, F. Y.; Bouret, Y.; Kindt, J. T. Molecular Dynamics Simulations of the Lipid Bilayer Edge. *Biophysic. J.* **2004**, *87*, 182-192.

Johnson, S. M.; Bangham, A. D.; Hill, M. W.; Korn, E. D. Single Bilayer Liposomes. *Biochim. Biophys. Acta-Biomembranes* **1971**, *233*, 820-826.

Jordan, P.; Fromme, P.; Witt, H. T.; Klukas, O.; Saenger, W.; Krauβ, N. Three-Dimensional Structure of Cyanobacterial Photosystem I at 2.5 Å Resolution. *Nature* **2001**, *411*, 909-917.

Juhaniewicz, J.; Sek, S. Atomic Force Microscopy and Electrochemical Studies of Melittin Action on Lipid Bilayers Supported on Gold Electrodes. *Electrochimica Acta* **2015**, *162*, 53-61.

Kamran, M.; Delgado, J. D.; Friebe, V.; Aartsma, T. J.; Frese, R. N. Photosynthetic Protein Complexes as Bio-photovoltaic Building Blocks Retaining a High Internal Quantum Efficiency. *Biomacromol.* **2014**, *15*, 2833-2838.

Kaneshina, S.; Ichimori, H.; Hata, T.; Matsuki, H. Barotropic Phase Transitions of Dioleoylphosphatidylcholine and Stearoyl-oleoylphosphatidylcholine Bilayer Membranes" *Biochimica Biophysica Acta* **1998**, *1374*, 1-8.

Karamdad, K.; Law, R. V.; Seddon, J. M.; Brooks, N. J.; Ces, O. Preparation and Mechanical Characterization of Giant Unilamellar Vesicles by a Microfluidic Method. *Lab Chip* **2015**, *15*, 557-562.

Kim, D.; Sakimoto, K. K.; Hong, D.; Yang, P. Artificial Photosynthesis for Sustainable Fuel and Chemical Production. *Angew. Chem. Int. Ed*. **2015**, *54*, 3259-3266.

Klymchenko, A. S.; Kreder, R. Fluorescent Probes for Lipid Rafts: From Model Membranes to Living Cells. *Chem. Biol. Rev.* **2014**, *21*, 97-113.

Knight, C.; Rahmani, A.; Morrow, M. R. Effect of an Anionic Lipid on the Barotropic Behavior of a Ternary Bicellar Mixture. *Langmuir* **2016**, *32*, 10259−10267.

Kobayashi, M.; Ohashi, S.; Iwamoto, K.; Shiraiwa, Y.; Kato, Y.; Watanabe, T. Redox Potential of Chlorophyll *d in vitro*. *Biochim. Biophys. Acta – Bioenergetics* **2007**, *1767*, 596-602.

Kolahdouzan, K.; Jackman, J. A.; Yoon, B. K.; Kim, M. C.; Johal, M. S. Cho, N.-J. Optimizing the Formation of Supported Lipid Bilayers from Bicellar Mixtures. *Langmuir* **2017**, *33*, 5052-5064.

Komatsu, H.; Okada, S. Ethanol-Induced Aggregation and Fusion of Small Phosphatidylcholine Liposome: Participation of Interdigitated Membrane Formation in Their Processes. *Biochim. Biophys. Acta - Biomembranes* **1995**, *1235*, 270-280.

Kondo, M.; Ishigure, S.; Maki, Y.; Dewa, T.; Nango, M.; Amao, Y. Photoinduced Hydrogen Production with Photosensitization of Zn Chlorophyll Analog Dimer as a Photosynthetic Special Pair Model. *Int. J. Hydrogen Energy* **2015**, *40*, 5313-5318.

Kremer, J. M. H.; Van der Esker, M. W.; Pathmamanoharan, C.; Wiersema, P. H. Vesicles of variable diameter prepared by a modified injection method. *Biochem.* **1977**, *16* (17), 3932-3935.

Kučerka, N.; Nieh, M.-P.; Katsaras, J. Fluid phase lipid areas and bilayer thicknesses of commonly used phosphatidylcholines as a function of temperature. *Biochim. Biophys. Acta* **2011**, *1808*, 2761-2771.

Kumar, A.; Gupta, M. K.; Kumar, M.; Saxena, D. Micelle Promoted Multicomponent Synthesis of 3-Amino Alkylated Indoles via a Mannich-Type Reaction in Water. *RSC Advances* **2013**, *3*, 1673-1678.

LeBlanc, G.; Gizzie, E.; Yang, S.; Cliffel, D. E.; Jennings, G. K. Photosystem I Protein Films at Electrode Surfaces for Solar Energy Conversion. *Langmuir* **2014**, *30*, 10990-11001.

Lee, A. G. Lipid-protein interactions in biological membranes: A structural perspective. *Biochimica Biophysica Acta - Biomembranes* **2003**, *1612* (1), 1-40.

Lee, A. G. How lipids affect the activities of integral membrane proteins. *Biochimica Biophysica Acta* **2004**, *1666*, 62-87.

Lentz, B. R. Membrane "Fluidity" as Detected by Diphenylhexatriene Probes. *Chem. Phys. Lipids* **1989**, *50*, 171-190.

Li, Y.; To, J.; Verdià-Baguena, C.; Surya, S.; Huang, M.; Paulmichl, M.; Liu, D. X.; Aguilella, V. M.; Torres, J. Inhibition of the Human Respiratory Syncytial Virus Small Hydrophobic Protein and Structural Variations in a Bicelle Environment. *J. Virology* **2014**, *88*, 11899-11914.

Li, L.; Jeffrey, S. W.; Paul, C. R. Continuous Microfluidic Fabrication of Synthetic Asymmetric Vesicles. *Lab Chip* **2015**, *15*, 3591-3599.

Li, Y.; Sasaki, S.; Tamiaki, H. Liu, C. L.; Song, J. Tian, W.; Zheng, E.; Wei, Y. Chen, G.; Fu, X.; Wang, X.-F. Zinc Chlorophyll Aggregates as Hole Transporters for Biocompatible, Natural-Photosynthesis-Inspired Solar Cells. *J. Power Sources* **2015**, *297*, 519-524.

Lingwood D.; Simons, K. Lipid Rafts As a Membrane-Organizing Principle. *Sci.* **2010**, *327*, 46-50.

Loura, L. M. S. Simple Estimation of Förster Resonance Energy Transfer (FRET) Orientation Factor Distribution in Membranes. *Int. J. Mol. Sci.* **2012**, *13*, 15252-15270.

Lu, L.; Schertzer, J. W.; Chiarot, P. R. Continuous Microfluidic Fabrication of Synthetic Asymmetric Vesicles. *Lab Chip* **2015**, *15*, 3591-3599.

Mabrey S.; Sturtevant, J. M. Investigation of Phase Transitions of Lipids and Lipid Mixtures by High Sensitivity Differential Scanning Calorimetry. *Proc. Natl. Acad. Sci*. **1976**, *73* (11), 3862-3866.

Mandal, R. P; Sekh, S.; Mondal, D.; De, S. Multifuntional Role of Liposome-Mimicking Vesicles-Potential Nanoreactors and Effective Storehouses for Hemoglobin. *Coll. Surf. A.* **2018**, *558*, 33-44.

Mary, A. P.; Jane, V. M. Temperature Dependence of 1,6-Diphenyl-1,3,5-hexatriene Fluorescence in Phospholipid Artificial Membranes. *Biochem*. **1976**, *15*, 1257-1261.

Matsui, R.; Ohtani, M.; Yamada, K.; Hikima, T.; Takata, M.; Nakamura, T.; Koshino, H.; Ishida, Y.; Aida, T. Chemically Locked Bicelles with High Thermal and Kinetic Stability. *Angew. Chem. Int. Ed.* **2015**, *54*, 13284-13288.

Matsuzaki, K.; Murase, O; Sugishita, K.; Yoneyama, S.; Akada, K.; Ueha, M.; Nakamura, A.; Kobayashi, K. Optical Characterization of Liposomes by Right Angle Light Scattering and Turbidity Measurement. *Biochimica Biophysica Acta - Biomembrane* **2000**, *1467* (1), 219-226.

Matteo, A. D. Structural, Electronic and Magnetic Properties of Methylviologen in Its Reduced Forms. *Chem. Phys. Lett.* **2007**, *439*, 190-198.

McKibbin, C.; Farmer, N. A.; Jeans, C.; Reeves, P. J.; Khorana, H. G.; Wallace, B. A.; Edwards, P. C. Villa, C.; Booth, P. J. Opsin Stability and Folding: Modulation by Phospholipid Bicelles. *J. Mol. Biol.* **2007**, *374*, 1319-1332.

Mély-Goubert, B.; H. Freedman, M. H. Lipid Fluidity and Membrane Protein Monitoring Using 1,6-Diphenyl-1,3,5-Hexatriene. *Biochimica Biophysica Acta - Biomembranes* **1980**, *601*, 315-327.

Milenkovic, S. M.; Bărbînţă-Pătraşcu, M. E.; Baranga, G.; Markovic, D. Z.; Ţugulea, L. Comparative Spectroscopic Studies on Liposomes Containing Chlorophyll *a* and Chlorophyllide *a*. *General Phys. Biophys.* **2013**, *32*, 559-567.

Mineev, K. S.; Nadezhdin, K. D.; Goncharuk, S. A.; Areseniev, A. S. Characterization of Small Isotropic Bicelles with Various Compositions. *Langmuir* **2016**, *32*, 6624-6637.

Mizushima, T.; Yoshida, A.; Harada, A.; Yoneda, Y.; Minatani, T.; Murata, S. Pyrene-Sensitized Electron Transport Across Vesicle Bilayers: Dependence of Transport Efficiency on Pyrene Substituents. *Org. Biomol. Chem.* **2006**, *4*, 4336-4344.

Morigaki, K.; Kimura, S.; Okada, K. Kawasaki, T.; Kawasaki, K. Formation of Substrate-Supported Membranes from Mixtures of Long- and Short-Chain Phospholipids. *Langmuir* **2012**, *28* (25), 9649-9655.

Mukhopadhyay, A. K.; Bose, S.; Hendler, R. W. Membrane-Mediated Control of the Bacteriorhodopsin Photocycle. *Biochemistry* **1994**, *33*, 10889-10895.

Nacke, C.; Schrader, J. Liposome based Solubilisation of Carotenoid Substrates for Enzymatic Conversion in Aqueous Media. *J. Mol. Catal. B: Enzym.* **2011**, *71*, 133-138.

Nagafuku, M.; Kabayama, K.; Oka, D.; Kato, A.; Tani-ichi, S.; Shimada, Y.; Ohno-Iwashita, Y.; Yamasaki, S.; Saito, T.; Iwabuchi, K.; Hamaoka, T.; Inokuchi, J.; Kosugi, A. Reduction of Glycosphingolipid Levels in Lipid Rafts Affects the Expression State and Function of Glycosylphosphatidylinositol-Anchored Proteins but Does Not Impair Signal Transduction via the T Cell Receptor. *J. Biolog. Chem.* **2003**, *278* (51), 51920-51927.

Nagle, J. F.; Tristram-Nagle, S. Structure of lipid bilayers. *Biochimica Biophysica Acta* **2000**, *1469*, 159-195.

Nakamura, H.; Taguchi, S.; Suga, K.; Hayashi, K. Jung, H.-S.; Umakoshi, H. Characterization of the Physicochemical Properties of Phospholipid Vesicles Prepared in $CO_2$/Water Systems at High Pressure. *Biointerphases* **2015**, *10*, 031005.

Nanga, R. P. R.; Brender, J. R.; Vivekanandan, S.; Ramamoorthy, A. Structure and Membrane Orientation of IAPP in Its Natively Amidated form at Physiological pH in a Membrane Environment. *Biochimica Biophysica Acta* **2011**, *1808*, 2337-2342.

Ngweniform, P.; Kusumoto, Y.; Teshima, T.; Ikeda, M.; Somekawa, S.; Ahmmad, B. Visible-Light Induced Hydrogen Production Using a Polypeptide-Chlorophyll Complex with α-Helix Conformation. *Photochem. Photobiol. Sci.* **2007**, *6*, 165-170.

Niroomand, H.; Mukherjee, D.; Khomami, B. Tuning the Photoexcitation Response of Cyanobacterial Photosystem via Reconstitution into Proteoliposomes. *Sci. Rep.* **2017**, *7*, 2492.

Niroomand, H.; Pamu, R.; Mukherjee, D.; Khomami, B. Microenvironment Alterations Enhance Photocurrents from Photosystem I Confined in Supported Lipid Bilayers. *J. Mater. Chem. A* **2018**, 6 12281-12291.

Niwa, S.; Yu, L.-J.; Takeda, K.; Hirano, Y.; Kawakami, T.; Wang-Otomo, Z.-Y.; Miki, K. Structure of the LH1-RC Complex from *Thermochromatium Tepidum* at 3.0 Å. *Nat.* **2014**, *508*, 228-232.

Opella, S. J.; Marassi, F. M. Structure Determination of Membrane Proteins by NMR Spectroscopy. *Chem. Rev.* **2004**, *104*, 3587-3606.

Ottiger, M.; Bax, A. Characterization of Magnetically Oriented Phospholipid Micelles for Measurement of Dipolar Couplings in Macromolecules. *J. Biomol. NMR* **1998**, *12* (3), 361-372.

Ottova, A. L.; Tien, H. T. Self-Assembled Bilayer Lipid Membranes: from Mimicking Biomembranes to Practical Applications. *Bioelectrochem. Bioenegetics* **1997**, *42*, 141-152.

Parasassi, T.; De Stasio, G.; d'Ubaldo, A.; Gratton, E. Phase Fluctuation in Phospholipid Membranes Revealed by Laurdan Fluorescence. *Biophys. J.* **1990**, *57*, 1179-1186.

Parasassi, T.; Gratton, E. Membrane Lipid Domains and Dynamics as Detected by Laurdan Fluorescence. *J Fluoresc.* **1995**, *5*, 59-69.

Patwardhan, S.; Sengupta, S.; Laurens, D. A.; Siebbeles, L. D. A.; Würthner, F.; Grozema, F. C. Efficient Charge Transport in Semisynthetic Zinc Chlorin Dye Assemblies, *J. Am. Chem. Soc.* **2012**, *134*, 16147-16150.

Peer, D.; Karp, J. M.; Hong, S.; Farokhzad, O. C.; Margalit, R.; Langer, R. Nanocarriers as an Emerging Platform for Cancer Therapy. *Nat. Nanotechnol.* **2007**, *2*, 751-760.

Pons, M.; Foradada M.; Estelrich, J. Liposomes Obtained by the Ethanol Injection Method. *Int. J. Pharmaceutics* **1993**, *95*, 51-56.

Porcar-Castell, A.; Tyystjärvi, E.; Atherton, J.; van der Tol, C.; Flexas, J.; Pfündel, E. E.; Moreno, J.; Frankenberg, C.; Berry, J. A. Linking Chlorophyll *a* Fluorescence to Photosynthesis for Remote Sensing Applications: Mechanisms and Challenges. *J. Exp. Bot.* **2014**, *65*, 4065-4095.

Prosser, R. S.; Evanics, F.; Kitevski, J. L.; Al-Abdul-Wahid, M. S. Current Applications of Bicelles in NMR Studies of Membrane-Associated Amphiphiles and Proteins. *Biochem*. **2006**, *45* (28), 8453-8465.

Ramos, J.; Imaz, A.; Callejas-Fernández, J.; Barbosa-Barros, L.; Estelrich, J.; Quesada-Pérez, M.; Forcada, J. Soft Nanoparticles (Thermos-responsive Nanogels and Bicelles) with Biotechnological Applications: from Synthesis to Simulation Through Colloidal Characterization. *Soft Matter* **2010**, *7*, 5067-5082.

Ringsdorf, H.; Schlarb, B.; Venzmer J. Molecular Architecture and Function of Polymeric Oriented Systems: Models for the Study of Organization, Surface Recognition, and Dynamics of Biomembranes. *Angew. Chem. Int. Ed.* **1988**, *27*, 113-158.

Sabatini, K.; Mattila, J.-P.; Kinnunen, P. K. J. Interfacial Behavior of Cholesterol, Ergosterol, and Lanosterol in Mixtures with DPPC and DMPC. *Biophys. J.* **2008**, *95* (5), 2340-2355.

Saeki, D.; Yamashita, T.; Fujii, A.; Matsuyama, H. Reverse Osmosis Membranes Based on a Supported Lipid Bilayer with Gramicidin A Water Channels. *Desalination* **2015**, *375*, 48-53.

Saleem, Q.; Zhang Z.; Petretic, A.; Gradinaru, C. C.; Macdonald P. M. Single Lipid Bilayer Deposition on Polymer Surfaces Using Bicelles. *Biomacromol.* **2015**, *16* (3), 1032-1039.

Sanders, C. R.; Schwonek, J. P. Characterization of Magnetically Orientable Bilayers in Mixtures of Dihexanoylphosphatidylcholine and Dimyristoylphosphatidylcholine by Solid-State NMR. *Biochemistry* **1992**, *31* (37), 8898-8905.

Sanders, C. R.; Landis, G. C. Reconstitution of Membrane Proteins into Lipid-Rich Bilayered Mixed Micelles for NMR Studies. *Biochemistry* **1995**, *34* (12), 4030-4040.

Santabarbara, S.; Barbato, R.; Zucchelli, G.; Garlaschi, F. M.; Jennings, R. C. The Quenching of Photosystem II Fluorescence Does not Protect the D1 Protein Against Light Induced Degradation in Thylakoids. *FEBS Lett*. **2001**, *505*, 159-162.

Santabarbara, S.; Neverov, K. V.; Garlaschi, F. M.; Zucchelli, G.; Jennings, R. C. Involvement of Uncoupled Antenna Chlorophylls in Photoinhibition in Thylakoids. *FEBS Lett*. **2001**, *491*, 109-113.

Santabarbara, S. Limited Sensitivity of Pigment Photo-Oxidation in Isolated Thylakoids to Singlet Excited State Quenching in Photosystem II Antenna. *Arch. Biochem. Biophys.* **2006**, *455*, 77-88.

Sezgin, E.; Levental, I.; Mayor S.; Eggeling, C. The Mystery of Membrane Organization: Composition, Regulation and Roles of Lipid Rafts. *Nat. Rev.* **2017**, *18*, 361-374.

Shanmugam, S.; Xu, J.; Boyer, C. Utilizing the Electron Transfer Mechanism of Chlorophyll *a* Under Light for Controlled Radical Polymerization. *Chem. Sci.* **2015**, *6*, 1341-1349.

Shibata, Y.; Tateishi, S.; Nakabayashi, S.; Itoh, S. Tamiaki, H. Intensity Borrowing via Excitonic Couplings among Soret and $Q_y$ Transitions of Bacteriochlorophylls in the Pigment Aggregates of Chlorosomes, the Light-Harvesting Antennae of Green Sulfur Bacteria. *Biochem*. **2010**, *49*, 7504-7515.

Shimanouchi, T.; Tasaki, M.; Vu, H. T.; Ishii, H.; Yoshimoto, N.; Umakoshi1, H.; Kuboi, R. Abeta/Cu-Catalyzed Oxidation of Cholesterol in 1,2-Dipalmitoyl Phosphatidylcholine Liposome Membrane. *J. Biosci. Bioeng.* **2010**, *109* (2), 145-148.

Shimizu, T.; Masuda, M.; Minamikawa, H. Supramolecular Nanotube Architectures Based on Amphiphilic Molecules. *Chem. Rev*. **2005**, *105*, 1401-1443.

Shintzky, M.; Barenholz, Y. Fluidity Parameters of Lipid Regions Determined by Fluorescence Polarization. *Biochim. Biophys. Acta* **1978**, *515*, 367-394.

Simons, K.; Toomre, D. Lipid Rafts and Signal Transduction. *Nat. Rev.* **2000**, *1*, 31-41.

Simons, K.; Vaz, W. L. C. Model System, Lipid Rafts, and Cell Membranes. *Annu. Rev. Biophys. Biomol. Struct.* **2004**, *33*, 269-295.

Smith, A. W. Lipid-Protein Interactions in Biological Membranes: A Dynamic Perspective. *Biochimica Biophysica Acta* **2012**, *1818*, 172-177.

Struppe, J.; Vold, R. R. Dilute Bicellar Solutions for Structural NMR Work. *J. Magnetic Resonance* **1998**, *135*, 541-546.

Suga, K.; Umakoshi, H. Detection of Nanosized Ordered Domains in DOPC/DPPC and DOPC/Ch Binary Lipid Mixture Systems of Large Unilamellar Vesicles Using a TEMPO Quenching Method. *Langmuir* **2013**, *29*, 4830-4838.

Suga, K.; Yoshida, T.; Ishii, H.; Okamoto, Y.; Nagao, D.; Konno, M.; Umakoshi, H. Membrane Surface-Enhanced Raman Spectroscopy for Sensitive Detection of Molecular Behavior of Lipid Assemblies. *Anal. Chem.* **2015**, *87*, 4772-4780.

Sugiura, S.; Nakajima, M.; Tong, J.; Nabetani, H.; Sekiy, M. Preparation of Monodispersed Solid Lipid Microspheres Using a Microchannel Emulsification Technique. *J. Colloid Interface Sci*. **2000**, *227*, 95-103.

Sugiura, S.; Kuroiwa, T.; Kagota, T.; Nakajima, M.; Sato, S.; Mukataka, S.; Walde, P.; Ichikawa, S. Novel Method for Obtaining Homogeneous Giant Vesicles from a Monodisperse Water-in-Oil Emulsion Prepared with a Microfluidic Device. *Langmuir* **2008**, *24* (9), 4581-4588.

Sugiyama, N.; Toyoda, M.; Amao, Y. Photoinduced Hydrogen Production with Chlorophyll-Platinum Nano-Conjugated Micellar System. *Colloids Surf. A* **2006**, *284-285*, 384-387.

Sullan, R. M. A.; Li, J. K.; Hao, C.; Walker, G. C.; Zou, S. Cholesterol-Dependent Nanomechanical Stability of Phase-Segregated Multicomponent Lipid Bilayers. *Biophys. J.* **2010**, *99*, 507-516.

Szoka, F. jr.; Papahadjopoulos, D. Procedure for Preparation of Liposomes with Large Internal Aqueous Space and High Capture by Reverse-Phase Evaporation. *Proc. Natl. Acad. Sci.* **1978**, *75*, 4194-4198.

Tabaei, S. R.; Choi, J.-H.; Zan, G. H.; Zhdanov, V. P.; Cho, N.-J. Solvent-Assisted Lipid Bilayer Formation on Silicon Dioxide and Gold. *Langmuir* **2014**, *30*, 10363-10373.

Taguchi, S.; Suga, K.; Hayashi, K.; Yoshimoto, M.; Okamoto, Y.; Nakamura, H.; Umakoshi, H. Characterization of Liposome Membrane Containing Chlorophyll *a* Molecules and Its Photosensitized Functions. *J. Nanosci. Nanotechnol.* **2017**, *17*, 4888-4893.

Takajo, Y.; Matsuki, H.; Matsubara, H.; Tsuchiya, K.; Aratono, M. Yamanaka, M. Structural and Morphological Transition of Long-Chain Phospholipid Vesicles Induced by Mixing with Short-Chain Phospholipid. *Coll. Surf. B: Biointerfaces* **2010**, *76*, 571–576.

Takayama, M.; Itoh, S.; Nagasaki, T.; Tanimizu, I. A New Enzymatic Method for Determination of Serum Choline-Containing Phospholipids. *Clinica Chimica Acta* **1977**, *79*, 93-98.

Tanner, P.; Baumann, P.; Enea, R.; Onaca, O.; Palivan, C.; Meier, W. Polymeric Vesicles: From Drug Carriers to Nanoreactors and Artificial Organelles. *Accounts Chem. Research* **2011**, *44* (10), 1039-1049.

Théry, C. Matias Ostrowski and Elodie Segura, “Membrane vesicles as conveyors of immune responses. *Nat. Rev*. **2009**, *9*, 581-593.

Titorenko, V. I.; Chan, H.; Rachubinski, R.A. Fusion of Small Peroxisomal Vesicles In Vitro Reconstructs an Early Step in the In Vivo Multistep Peroxisome Assembly Pathway of *Yarrowia lipolytica*. *J. Cell Biol.* **2000**, *148*, 30-44.

Tomonou, Y.; Amao, Y. Photoinduced $H_2$ Production with Mg Chlorophyll-*a* from Spirulina and Colloidal Platinum by Visible Light. *Biotechnol. Lett*. **2002**, *24*, 775-778.

Tomonou, Y.; Amao, Y. Effect of Micellar Species on Photoinduced Hydrogen Production with Mg Chlorophyll-*a* from Spirulina and Colloidal Platinum. *Int. J. Hydrogen Energy* **2004**, *29*, 159-162.

Torchilin, V. P. Recent Advances with Liposomes as Pharmaceutical Carriers. *Nat. Rev.* **2005**, *4*, 145-160.

Toyoshima, Y.; Morino, M.; Motoki, H.; Sukigara, M. Photo-oxidaton of Water in Phospholipid Bilayer Membranes Containing Chlorophyll *a*. *Nature* **1977**, *265*, 187-189.

Triba, M. N.; Warschawski, D. E.; Devaux, P. F. Reinvestigation by Phosphorus NMR of Lipid Distribution in Bicelles. *Biophys. J*. **2005**, *88* (3), 1887-1901.

Tsujisho, I.; Toyoda, M.; Amao, Y. Photochemical and Enzymatic Synthesis of Formic Acid from $CO_2$ with Chlorophyll and Dehydrogenase System. *Catal. Commun.* **2006**, *7*, 173-176.

Uchegbu, I. F.; Schätzlein, A. G.; Tetley, L.; Gray, A. I.; Sludden, J.; Siddique, S.; Mosha, E. Polymeric Chitosan-based Vesicles for Drug Delivery. *J. Pharmacy Pharmacology* **1998**, *50*, 453-458.

Ujwal, R.; Bowie J. U. Crystallizing Membrane Proteins Using Lipidic Bicelles. *Methods* **2011**, *55*, 337-341.

Uline, M. J.; Schick, M.; Szleifer, I. Phase Behavior of Lipid Bilayers under Tension. *Biophys. J.* **2012**, *102*, 517–522.

Umakoshi, H.; Morimoto, K.; Ohama, Y.; Nagami, H.; Shimanouchi, T. Kuboi, R. Liposome Modified with Mn-Porphyrin Complex Can Simultaneously Induce Antioxidative Enzyme-like Activity of Both Superoxide Dismutase and Peroxidase. *Langmuir* **2008**, *24*, 4451-4455.

Umakoshi, H.; Suga, K. Use Liposome as a Designable Platform for Molecular Recognition ~from “Statistical Separation” to “Recognitive Separation”~. *Solvent Extr. Res. Dev., Jpn.* **2013**, *20*, 1-13.

Umena, Y.; Kawakami, K.; Jian-Ren Shen, J.-R.; Kamiya, N. Crystal Structure of Oxygen-Evolving Photosystem II at a Resolution of 1.9 Å *Nature* **2011**, *473*, 55-60.

van Dam, L.; Karlsson, G.; Edwards, K. Direct Observation and Characterization of DMPC/DHPC Aggregates under Conditions Relevant for Biological Solution NMR. *Biochim. Biophys. Acta* **2004**, *1664*, 241-256.

van Swaay, D.; DeMello, A. Microfluidic Methods for forming liposomes. *Lab Chip* **2013**, *13*, 752-767.

Vigh, L.; Escribá, P. V.; Sonnleitner, A.; Sonnleitner, M.; Piotto, S.; Maresca, B.; Horváth, I.; Harwood, J. L. The Significance of Lipid Composition for Membrane Activity: New Concepts and Ways of Assessing Function. *Progress Lipid Research* **2005**, *44* (5), 303-344.

Vincent, M.; de Foresta, B.; Gallay, J. Nanosecond Dynamics of a Mimicked Membrane-Water Interface Observed by Time Resolved Stokes Shift of LAURDAN. *Biophys. J.* **2005**, *88*, 4337-4350.

Viseu, M. I.; Correia, R. F.; Fernandes, A. C. Time Evolution of the Thermotropic Behavior of Spontaneous Liposomes and Disks of the DMPC-DTAC Aqueous System. *J. Colloid Interf. Sci.* **2010**, *351*, 156-165.

Vladkova, R. Chlorophyll *a* Self-Assembly in Polar Solvent-Water Mixtures. *Photochem. Photobiol.* **2000**, *71*, 71-83.

Wade, J. H.; Jones, J. D.; Lenov, I. L.; Riordan, C. M.; Sligar, S. G.; Bailey, R. C. Microfluidic Platform for Efficient Nanodisc Assembly, Membrane Protein Incorporation, and Purification. *Lab Chip* **2017**, *17*, 2951-2959.

Walter, A.; Vinson, P. K.; Kaplun, A.; Talmon, Y. Intermediate Structures in the Cholate-Phosphatidylcholine Vesicle-micelle Transition. *Biophys. J.* **1991**, *60*, 1315-1325.

Wang, X.-F.; Kitao, O.; Zhou, H.; Tamiaki, H.; Sasaki, S. Efficient Dye-Sensitized Solar Cell Based on oxo-Bacteriochlorin Sensitized with Broadband Absorption Capability. *J. Phys. Chem. C* **2009**, *113*, 7954-7961.

Watanabe, T.; Honda, K. Measurement of the Extinction Coefficient of the Methyl Viologen Cation Radical and the Efficiency of Its Formation by Semiconductor Photocatalysis. *J. Phys. Chem.* **1982**, *86*, 2617e9.

Watanabe, K.; Moriya, K.; Kouyama, T.; Onoda, A. Minatani, T.; Takizawa, S. Murata, S. Photoinduced Transmembrane Electron Transport in DPPC Vesicles: Mechanism and Application to a Hydrogen Generation System. *J. Photochem. Photobiol. A.* **2011**, *221*, 113-122.

Watts, A. Bacteriorhodopsin: the Mechanism of 2D-Array Formation and the Structure of Retinal in the Protein. *Biophys. Chem.* **1995**, *55*, 137-151.

Wu, H.; Su, K.; Guan, X.; Sublette, M. E.; Stark, R. E. Assessing the Size, Stability, and Utility of Isotropically Tumbling Bicelle Systems for Structural Biology. *Biochim. Biophys. Acta* **2010**, *1798*, 482-488.

Yaghoubi, H.; Lafalce, E.; Jun, D.; Jiang, X.; Beatty, J. T.; Takshi, A. Large Photocurrent Response and External Quantum Efficiency in Biophotoelectrochemical Cells Incorporating Reaction Center Plus Light Harvesting Complexes. *Biomacromol*. **2015**, *16*, 1112−1118.

Yanagi, S. Supramolecularly Engineered Functional π-Assemblies Based on Complementary Hydrogen-Bonding Interactions. *Bull. Chem. Soc. Jpn.* **2015**, *88*, 28-58.

Yang, P.-W.; Lin, T.-L.; Lin, T.-Y.; Yang, C.-H.; Hu, Y.; Jeng, U.-S. Packing DNA with Disc-Shaped Bicelles. *Soft Matter* **2013**, *9*, 11542-11548.

Ye, W.; Lind, J.; Eriksson, J.; Mäler, L. Characterization of the Morphology of Fast-Tumbling Bicelles with Varying Composition. *Langmuir* **2014**, *30*, 5488-5496.

Yoshimoto, M.; Furuya, T.; Kunihiro, N. Temperature-Dependent Permeability of Liposome Membrane Incorporated with Mg-Chlorophyll *a*. *Colloids Surf., A* **2011**, *387*, 65-70.

Zimmermann, T. S.; Lee, A. C. H.; MacLachlan, I. RNAi-Mediated Gene Silencing in Non-Human Primates. *Nature* **2006**, *441*, 111-114.

# List of Publications

**[Papers]**

1. Hidemi Nakamura, Shogo Taguchi, Keishi Suga, Keita Hayashi, Ho-Sup Jung, Hiroshi Umakoshi, Characterization of the Physicochemical Properties of Phospholipid Vesicles Prepared in $CO_2$/Water Systems at High Pressure. *Biointerphases*, **2015**, *10* (3), Article ID 031005 (6 pages)

2. Shogo Taguchi, Keishi Suga, Keita Hayashi, Makoto Yoshimoto, Yukihiro Okamoto, Hidemi Nakamura, Hiroshi Umakoshi, Characterization of Liposome Membrane Containing Chlorophyll *a* Molecules and Its Photosensitized Functions, *J. Nanosci. Nanotechnol.* **2017**, *17*, 4888-4893.

3. Shogo Taguchi, Keishi Suga, Keita Hayashi, Yukihiro Okamoto, Ho-Sup Jung, Hidemi Nakamura, Hiroshi Umakoshi, Systematic Characterization of DMPC/DHPC Self-Assemblies and Their Phase Behaviors in Aqueous Solution, *Coll. Interfaces* **2018**, *2* (4), Article ID 73 (15 pages)

4. Shogo Taguchi, Keishi Suga, Keita Hayashi, Makoto Yoshimoto, Yukihiro Okamoto, Hidemi Nakamura, Hiroshi Umakoshi, Aggregation of Chlorophyll *a* Induced in self-assembled membranes composed of DMPC and DHPC, *Coll. Surface B.* **2019**, *175*, 403-408.

**[Related papers]**

1. Shogo Taguchi, Keishi Suga, Pahn-Shick Chang, Ho-Sup Jung, Hiroshi Umakoshi, Simple Method to Prepare Vesicles from Bicelles by using Flow Device, *Coll. Surf. B.*, **2019**, submitted.
2. Shogo Taguchi, Yuji Seno, Keishi Suga, Ho-Sup Jung, Hiroshi Umakoshi, Bicelle based Preparation of Heterogeneous Supported Lipid Bilayers (SLB): (1) Characterization of Micro-and-Nano Domain, to be submitted.
3. Shogo Taguchi, Yuji Seno, Keishi Suga, Pahn-Shick Chang, Ho-Sup Jung, Hiroshi Umakoshi, Bicelle based Preparation of Heterogeneous Supported Lipid Bilayers (SLB): (2) Continuous Manufacturing of SLB using Flow-Device, to be submitted.

**[International Conferences]**

1. Shogo Taguchi, Keishi Suga, Yukihiro Okamoto, Hiroshi Umakoshi, Keita Hayashi, and Hidemi Nakamura, Physicochemical Properties of Phospholipid Vesicles Prepared Using Supercritical $CO_2$ Reverse-Phase Evaporation Method, *The 10$^{th}$ International Conference on Separation Science and Technology (ICSST14)*, Nara, Japan, Oct. 30-Nov. 1 (2014).

2. Keishi Suga, Shogo Taguchi, Keita Hayashi, Yukihiro Okamoto, Hidemi Nakamura, Hiroshi Umakoshi, Characterization of Physicochemical Properties of Phospholipid Vesicles Prepared in $CO_2$/$H_2O$ System at High Pressure, *2015 International Chemical Congress of Pacific Basin Societies (Pacifichem 2015)*, Honolulu, HI, USA, Dec. 15-20 (2015).

3. Shogo Taguchi, Keishi Suga, Yukihiro Okamoto, Hiroshi Umakoshi, Characterization of Aggregation Behavior of Chlorophyll *a* on Liposome Membrane, *The 10$^{th}$ Conference of Aseanian Membrane Society (AMS10)*, Nara, Japan, Jul. 26-29 (2016).

4. Shogo Taguchi, Keishi Suga, Keita Hayashi, Yukihiro Okamoto, Hidemi Nakamura, Hiroshi Umakoshi, Characterization of Orientation and Photochemical Functions of Chlorophyll *a* Molecules in Self-Assembled Membranes, *2017 AIChE Annual Meeting*, Minneapolis, MN, USA, Oct. 29 - Nov. 3 (2017).

5. Shogo Taguchi, Keishi Suga, Keita Hayashi, Yukihiro Okamoto, Hidemi Nakamura, Hiroshi Umakoshi, Characterization of Chlorophyll *a* Incorporated Liposomes and Bicelles as Photosynthesis Platform, *The 11$^{th}$ International Conference on Separation Science and Technology (ICSST17)*, Haeundae, Korea, Nov. 9 - 11 (2017).

# Acknowledgement

The author is greatly indebted to Prof. Dr. Hiroshi Umakoshi (Division of Chemical Engineering, Graduate School of Engineering Science, Osaka University), for his excellent guidance and helpful advice and supports throughout this work. The author is thankful to Prof. Dr. Nobuyuki Matsubayashi, Prof. Dr. Norikazu Nishiyama (Division of Chemical Engineering, Graduate School of Engineering Science, Osaka University), Prof. Dr. Hidemi Nakamura (Department of Chemical Engineering, Nara National College of Technology) and Prof. Dr. Ho-Sup Jung (School of Mechanical and Aerospace Engineering, Seoul National University) for a number of valuable comments and suggestions during the completion of this thesis. The author would like to offer my special thanks to Assoc. Prof. Dr. Yukihiro Okamoto and Assist. Prof. Dr. Keishi Suga (Division of Chemical Engineering, Graduate School of Engineering Science, Osaka University) for his valuable comments, supports, helpful advices and discussion throughout this work. The author would like to express one's thankfulness to Ms. Keiko Fukumoto for her kind support during this work.

The author is thankful to Prof. Dr. K. Jitsukawa, Prof. Dr. M. Taya, Prof. Dr. Y. Okano, Prof. Dr. M. Nakano, Prof. Dr. T. Hirai, Prof. Dr. S. Sakai, and all the staff of Division of Chemical Engineering, Graduate School of Engineering Science, Osaka University for their kind cooperation during my research.

The author wishes to thank for Prof. Dr. P. Walde (Institute for Polymer, ETH, Zurich), Prof. Dr. B. Higgins (Department of Chemical Engineering and Materials Science, University of California, Davis), Prof. Dr. P. Alexandridis (Department of Chemical Engineering, University at Buffalo), Prof. Dr. S. Ichikawa (Graduate School of Life and Environmental Sciences, University of Tsukuba), Prof. Dr. K. Katakura (Department of Chemical Engineering, Nara National College of Technology), and Prof. Dr. K. Mitsuoka (Research Center for Ultra-High Voltage Electron Microscopy, Osaka University) for their comments and suggestions during this work. The author is grateful for the advice given by Prof. Dr. D. Nagao (Department of Applied Chemistry, Tohoku University), Assoc. Prof. Dr. M. Yoshimoto (Department of Applied Molecular Bioscience, Yamaguchi University), Assoc. Prof. Dr. T. Shimanouchi (Division of Environmental Science, Graduate School of Environmental and Life Science, Okayama University), Assist. Prof. Dr. H. Ishii (Tohoku University), Assoc. Prof. Dr. K. Hayashi (National Institute of Technology), Dr. H. Sugaya (Toray Industries, inc.), Dr. Y. Yamada (Kao corporation), Dr. T. Ishigami (Kao corp.) and Dr. F. Iwasaki (Showa Denko K.K.).

Special thanks are given to following colleagues for their experimental collaboration: M. Hirose, B. T. Tham, N. Watanabe, K. Tanimura, J. Han, A. Tauchi, F. Miftah, M. Chern, B.-S. Kang, R. Ito, R. Kawakami, R. Nishino, T. Wakita, K. Yoshida, Y. Goto, Y. Iimure, K. Kitagawa, Y. Murata, M. Amau, Y. Hasunuma, N. Ikushima, K. Kojima, D. Matsui, S. Matsushita, R. Murazawa, Y. Seno, R. Ueno and all the member in Bio-Inspired Chemical Engineering Laboratory.

The author would like to thank his grandparents Masakuni Taguchi and Setsuko Taguchi and his parents Atsuko Taguchi and Masayuki Taguchi and his sister and brother Kanon Taguchi and Takahiro Taguchi for their continuous encouragements and kind support throughout this work.

The author gratefully acknowledges the financial support of this work by the fellowship of the apan Science Society, (JSS 29-218). I would also like to express my gratitude to the Scholarship from Osaka Univ. "Engineering Science Student Dispatch Program 2014" (School of Mechanical and Aerospace Engineering, Seoul National Univ., Korea).